

# **HiSIM\_HV 2.5.0 User's Manual**

Copyright © 2007–2016 Hiroshima University and STARC  
Copyright © 2016–2019 Hiroshima University

This work is licensed under the Creative Commons Attribution 4.0 International License. To view a copy of this license, visit: <http://creativecommons.org/licenses/by/4.0/> or send a letter to Creative Commons, PO Box 1866, Mountain View, CA 94042, USA.

## **HiSIM\_HV 2.5.0 Developers**

Hiroshima University:

T. Iizuka, H. Kikuchihara, M. Miyake, D. Navarro, H. J. Mattausch,  
M. Miura-Mattausch

Acknowledgement:

Si2/CMC HiSIM\_HV Work Group chair (T. Naito) and its members. Valuable contributions to the development were made by the CMC members.

## **HiSIM\_HV 2.4.0 Developers**

Hiroshima University:

T. Iizuka, H. Kikuchihara, H. Miyamoto, M. Miyake, H. J. Mattausch,  
M. Miura-Mattausch

Acknowledgement:

Si2/CMC HiSIM\_HV Work Group chair (T. Naito) and its members. Valuable contributions to the development were made by the CMC members.

## **HiSIM\_HV 2.3.0 Developers**

Hiroshima University:

H. Kikuchihara, H. Miyamoto, H. J. Mattausch, M. Miura-Mattausch

Acknowledgement:

Si2/CMC HiSIM\_HV Work Group chair (T. Naito) and its members. Valuable contributions to the development were made by the CMC members.

## **HiSIM\_HV 2.2.0 Developers**

Hiroshima University:

T. Umeda, H. Kikuchihara, H. Miyamoto, H. J. Mattausch, M. Miura-Mattausch

Acknowledgement:

CMC HiSIM Subcommittee chairs (E. Seebacher and Y. Mizoguchi) and members.  
Valuable contributions to the development were made by the CMC members.

## **HiSIM\_HV 2.1.0 Developers**

Hiroshima University:

T. Umeda, H. Kikuchihara, M. Miyake, T. Iizuka, U. Feldmann, H. J. Mattausch,  
M. Miura-Mattausch

Semiconductor Technology Academic Research Center:

G. Yokomizo

Acknowledgement:

CMC HiSIM Subcommittee chairs (E. Seebacher and Y. Ueda) and members. Valuable contributions to the development were made by the CMC members.

## **HiSIM\_HV Previous Developers**

Hiroshima University:

A. Tanaka, Y. Oritsuki, M. Yokomichi, T. Kajiwara, N. Sadachika, M. Miyake  
T. Hayashi, K. Nishikawa, T. Saito, A. Oohashi, T. Minami, T. Sakuda, K. Johguchi  
T. Yoshida, T. Murakami, H. Kikuchihara, U. Feldmann H. J. Mattausch,  
M. Miura-Mattausch

Semiconductor Technology Academic Research Center:

T. Ohguro, T. Iizuka, M. Taguchi, S. Miyamoto, R. Inagaki, Y. Furui, G. Yokomizo

Texas Instruments:

Y. Liu, K. Green

# Contents

<b>1 LDMOS/HVMOS Structures</b>	<b>7</b>
<b>2 Basic Concept</b>	<b>11</b>
<b>3 Definition of Device Size</b>	<b>12</b>
<b>4 Charges</b>	<b>14</b>
<b>5 Drain Current</b>	<b>17</b>
<b>6 Threshold Voltage Shift</b>	<b>18</b>
6.1 (I) Short-Channel Effects . . . . .	18
6.2 (II) Reverse-Short-Channel Effects . . . . .	19
<b>7 Short-Channel Effects</b>	<b>23</b>
7.1 Punchthrough Effect . . . . .	23
7.2 Shallow Punchthrough Effect . . . . .	23
7.3 Deep Punchthrough Effect (new model) . . . . .	24
7.4 Channel Conductance . . . . .	25
<b>8 Depletion Effect of the Gate Poly-Si</b>	<b>26</b>
<b>9 Quantum-Mechanical Effects</b>	<b>27</b>
<b>10 Mobility Model</b>	<b>28</b>
<b>11 Channel-Length Modulation</b>	<b>30</b>
<b>12 Narrow-Channel Effects</b>	<b>32</b>
12.1 Threshold Voltage Modification . . . . .	32
12.2 Mobility Change . . . . .	32
12.3 Transistor Leakage due to Shallow Trench Isolation (STI): Hump in $I_{ds}$ . . . . .	33
12.4 Small Geometry . . . . .	34
<b>13 Effects of the Source/Drain Diffusion Length for Shallow Trench Isolation (STI) Technologies</b>	<b>36</b>
<b>14 Temperature Dependences</b>	<b>38</b>
<b>15 Resistances</b>	<b>41</b>
15.1 <b>CORDRIFT=1</b> (default): Diffused Resistor Model . . . . .	42
15.1.1 Drain side . . . . .	42
15.1.2 Source side . . . . .	44
15.2 <b>CORDRIFT=0</b> : old model provided in HiSIM_HV 1 . . . . .	44

15.3 Other resistances . . . . .	47
<b>16 Capacitances</b>	<b>50</b>
16.1 Intrinsic Capacitances . . . . .	50
16.2 Overlap Capacitances . . . . .	50
16.3 Bias-dependent overlap length . . . . .	53
16.4 Extrinsic Capacitances . . . . .	53
16.5 Trench Overlap Capacitance . . . . .	53
<b>17 Leakage Currents</b>	<b>56</b>
17.1 Substrate Current . . . . .	56
17.1.1 Impact-Ionization Induced Bulk Potential Change . . . . .	56
17.2 Gate Current . . . . .	57
17.3 GIDL (Gate-Induced Drain Leakage) . . . . .	60
<b>18 Source/Bulk and Drain/Bulk Diode Models</b>	<b>62</b>
18.1 Diode Current . . . . .	62
18.1.1 Conventional Model ( <b>CODIO</b> = 0) . . . . .	63
18.1.2 Extended Model ( <b>CODIO</b> = 1) . . . . .	63
18.1.3 Common Equations to <b>CODIO</b> Options . . . . .	65
18.2 Diode Capacitance . . . . .	66
18.2.1 Conventional Model ( <b>CODIO</b> = 0) . . . . .	66
18.2.2 Extended Model ( <b>CODIO</b> = 1) . . . . .	66
18.2.3 Common Equations to <b>CODIO</b> Options . . . . .	66
18.3 Diode Recovery Effect . . . . .	67
18.3.1 Anode-Side Carrier Distribution Model . . . . .	68
18.3.2 Cathode-Side Carrier Distribution Model . . . . .	69
18.3.3 Depletion of the Drift Region . . . . .	70
18.3.4 Carrier Injection . . . . .	70
18.3.5 Bias-Independent Part . . . . .	70
<b>19 Break Down Models</b>	<b>74</b>
19.1 Hard Break Down Model . . . . .	74
19.2 Snapback . . . . .	74
<b>20 Noise Models</b>	<b>76</b>
20.1 $1/f$ Noise Model . . . . .	76
20.2 Thermal Noise Model . . . . .	76
20.3 Induced Gate Noise Model . . . . .	77
20.4 Coupling Noise Model . . . . .	77

<b>21 Non-Quasi-Static (NQS) Model</b>	<b>78</b>
21.1 Carrier Formation . . . . .	78
21.2 Delay Mechanisms . . . . .	78
21.3 Time-Domain Analysis . . . . .	78
21.4 AC Analysis . . . . .	79
<b>22 Self-Heating Effect Model</b>	<b>80</b>
<b>23 Multiplication Factor</b>	<b>82</b>
<b>24 DFM Model</b>	<b>83</b>
<b>25 Depletion Mode Model Option</b>	<b>84</b>
25.1 CODEP=1 : old model developed for Version 2.2.0 . . . . .	84
25.2 CODEP=2 : old model . . . . .	88
25.3 CODEP=3 : new model . . . . .	91
25.3.1 Accumulation-mode current $I_{ds,acc}$ . . . . .	91
25.3.2 Resistor current $I_{ds,res}$ . . . . .	93
25.3.3 Channel Length Modulation (CLM) . . . . .	97
25.3.4 Smoothing parameters . . . . .	97
<b>26 Aging Model</b>	<b>101</b>
26.1 (a) The channel region . . . . .	101
26.1.1 (I) HC Aging Model . . . . .	101
26.1.2 (II) N(P)BTI Aging Model: Carrier trapping at interface . . . . .	103
26.2 (b) The drift region . . . . .	104
<b>27 Binning Model</b>	<b>107</b>
<b>28 Exclusion of Modeled Effects and Model Flags</b>	<b>109</b>
<b>29 List of Instance Parameters</b>	<b>114</b>
<b>30 Default Parameters and Limits of the Parameter Values</b>	<b>116</b>
<b>31 Overview of the Parameter-Extraction Procedure</b>	<b>126</b>
31.1 General MOSFET Part . . . . .	126
31.2 HiSIM_HV Specific Part . . . . .	126
<b>References</b>	<b>129</b>

# 1 LDMOS/HVMOS Structures

HiSIM (Hiroshima-university STARC IGFET Model) is the first complete surface-potential-based MOSFET model for circuit simulation based on the drift-diffusion theory [1], which was originally developed by Pao and Sah [2]. The model has been extended for power MOSFETs by considering the resistance effect explicitly, which is named HiSIM\_HV [3].

There are two MOSFET types of structures commonly used for high voltage applications. One is the asymmetrical laterally diffused structure called LDMOS and the other is originally the symmetrical structure, which we distinguish by referring to it as HVMOS. However, the asymmetrical HVMOS structure is also possible. HiSIM\_HV is valid for modeling all these structure types [4, 5].

The most important features of LDMOS/HVMOS devices, different from the conventional MOSFET, are originating from the drift region introduced to achieve the sustainability of high voltages. By varying the length as well as the dopant concentration of the drift region, various devices with various operating biase conditions are realized as shown in Fig. 1 for the LDMOS structure.

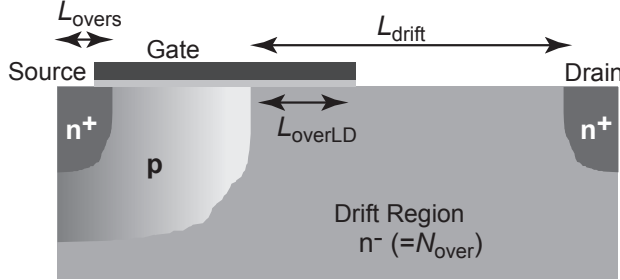


Fig. 1: Schematic of the typical LDMOS structure and device parameters.

A schematic of the general structures for LDMOS and HVMOS are shown in Fig. 2 for the n-channel case.

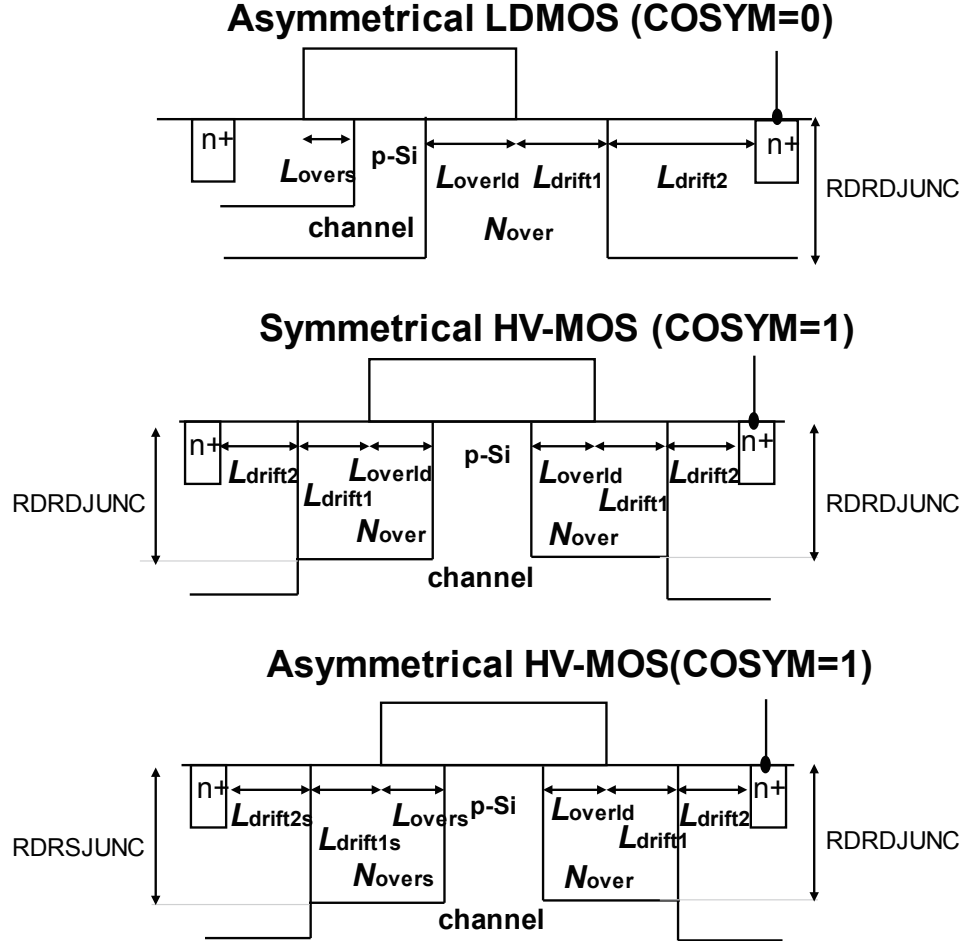


Fig. 2: Device parameters in HiSIM\_HV.

To make the structural definition easy, Flag **COSYM** is introduced as shown in Fig. 3. **COSYM=0** refers to the asymmetrical LDMOS, and all structural parameters have to be determined independently. **COSYM=1** refers to symmetrical/asymmetrical HVMOS. If parameter values of the source side are given, they are activated. If they are not given, parameter values of the drain side are copied to the source side automatically.

HiSIM\_HV 2.5.0 excludes the old resistance model implemented in the HiSIM\_HV1 series.

Table 1 summarizes the structural parameters to be given. In case the overlap length **LOVER** is given instead of **LOVERS**, **LOVER** is taken for **LOVERS**. However, it is recommended to give **LOVERS** but not **LOVER**.

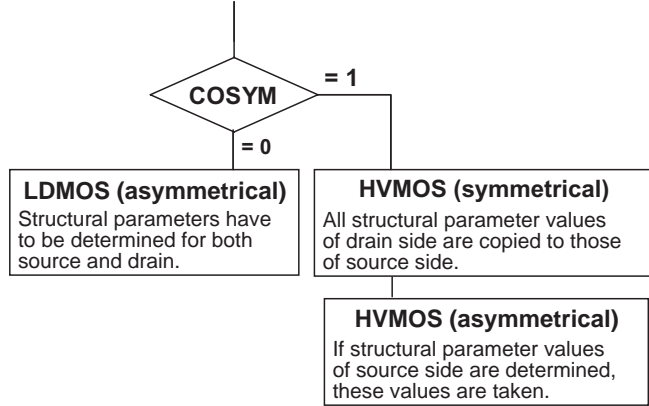


Fig. 3: Device parameters of HiSIM\_HV.

HiSIM\_HV 2.5.0 includes the substrate node  $V_{\text{sub}}$  as schematically shown in Fig. 4, where model parameters **DDRIFT** and **NSUBSUB** are newly introduced for  $D_{\text{drift}}$  and  $N_{\text{subsub}}$ , respectively. The node inclusion is done by selecting Flag **COSUBNODE**=1 as the 5th node.

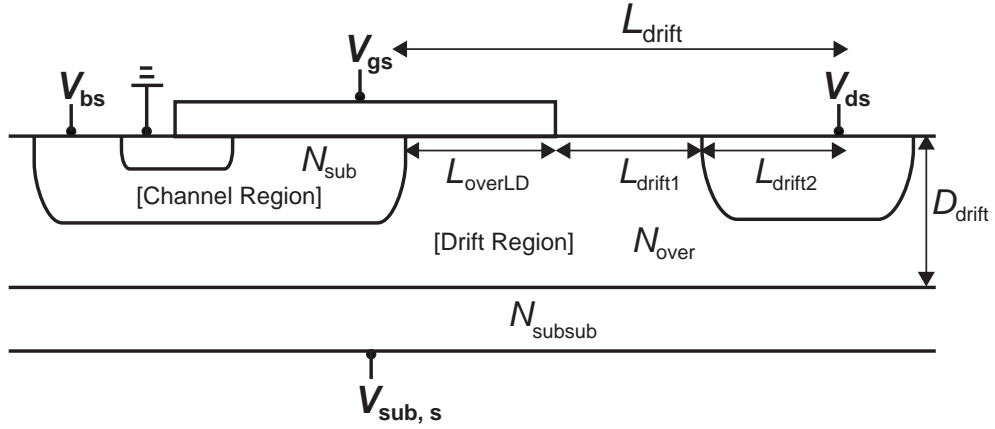


Fig. 4: Schematic of a LDMOS with the substrate node  $V_{\text{sub},s}$ .

Table 1: HiSIM\_HV 2.5.0 model parameters introduced.

	structure	source	drain
<b>COSYM=0</b>	<b>LDMOS</b>	<b>LOVERS</b> <b>RS</b>	<b>LOVERLD</b> <b>LDRIFT1</b> <b>LDRIFT2</b> <b>NOVER</b> <b>RD</b> <b>RDRDJUNC</b>
<b>COSYM=1</b>	<b>symmetrical HVMOS</b>		<b>LOVERLD</b> <b>LDRIFT1</b> <b>LDRIFT2</b> <b>NOVER</b> <b>RD</b> <b>RDRDJUNC</b>
<b>COSYM=1</b>	<b>asymmetrical HVMOS</b>	<b>LOVERS</b> <b>LDRIFT1S</b> <b>LDRIFT2S</b> <b>NOVERS</b> <b>RS</b> <b>RDRSJUNC</b>	<b>LOVERLD</b> <b>LDRIFT1</b> <b>LDRIFT2</b> <b>NOVER</b> <b>RD</b> <b>RDRDJUNC</b>

The HiSIM\_HV model parameters introduced in section 1 are summarized in Table 2.

Table 2: HiSIM\_HV 2.5.0 model parameters introduced in section 1 of this manual.

<b>LOVER</b>	overlap length at source side for <b>LOVERS</b>
<b>LOVERLD</b>	overlap length at drain, and at source, if <b>COSYM=1</b>
<b>LDRIFT1</b>	length of lightly doped drift region at drain, and at source, if <b>COSYM=1</b>
<b>LDRIFT2</b>	length of heavily doped drift region at drain, and at source, if <b>COSYM=1</b>
<b>NOVER</b>	impurity concentration of <b>LOVERLD</b> at drain, and at source, if <b>COSYM=1</b>
<b>LOVERS</b>	overlap length at source
<b>LDRIFT1S</b>	length of lightly doped drift region at source, if <b>COSYM=1</b> and the value is determined
<b>LDRIFT2S</b>	length of heavily doped drift region at source, if <b>COSYM=1</b> and the value is determined
<b>NOVERS</b>	impurity concentration of <b>LOVERS</b> at source, if <b>COSYM=1</b> and the value is determined
<b>VBSMIN</b>	minimum $V_{bs}$ voltage applied: No need and inactivated.
<b>DDRIFT</b>	depth of the drift region
<b>NSUBSUB</b>	impurity concentration of the substrate required for $V_{sub}$ dependence

## 2 Basic Concept

HiSIM\_HV solves the potential distribution along the surface by solving the Poisson equation iteratively including the resistance effect in the drift region, where the bias dependence of the resistance is considered. The HiSIM compact model determines the complete potential distribution along the device including the surface potential at the source side  $\phi_{S0}$ , the potential at the pinch-off point  $\phi_{SL}$ , the potential at the channel/drain junction,  $\phi_S(\Delta L)$ , and the final potential value at the drain contact  $\phi_{S0} + V_{ds}$  as shown in Fig. 5. The potential  $V_{dseff}$  is the potential value which mostly determines the device characteristics. This potential node is considered explicitly in addition to the node potential of  $V_{ds}$ . Advanced version concealing the internal node to speed up the simulation has been developed in parallel [6].

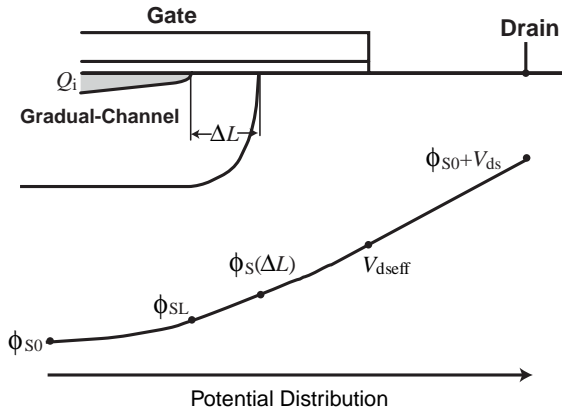


Fig. 5: Schematic of the surface potential distribution in the channel at the drain side of the LDMOS device structure.

### 3 Definition of Device Size

The effective channel length  $L_{\text{eff}}$  and width  $W_{\text{eff}}$  are calculated from the gate length  $L_{\text{gate}}$  and width  $W_{\text{gate}}$ , where  $L_{\text{gate}}$  and width  $W_{\text{gate}}$  deviate from the gate drawn length and width

$$L_{\text{gate}} = L_{\text{drawn}} + \mathbf{XL} \quad (1)$$

$$W_{\text{gate}} = \frac{W_{\text{drawn}}}{\mathbf{NF}} + \mathbf{XW} \quad (2)$$

$$L_{\text{poly}} = L_{\text{gate}} - 2 \cdot \frac{\mathbf{LL}}{(L_{\text{gate}} + \mathbf{LLD})^{\mathbf{LLN}}} \quad (3)$$

$$W_{\text{poly}} = W_{\text{gate}} - 2 \cdot \frac{\mathbf{WL}}{(W_{\text{gate}} + \mathbf{WLD})^{\mathbf{WLN}}} \quad (4)$$

$$L_{\text{eff}} = L_{\text{poly}} - \mathbf{XLD} - \mathbf{XLDLD} \quad (5)$$

$$W_{\text{eff}} = W_{\text{poly}} - 2 \cdot \mathbf{XWD} \quad (6)$$

$$W_{\text{eff,LD}} = W_{\text{poly}} - 2 \cdot \mathbf{XWDLD} \quad (7)$$

$$W_{\text{effc}} = W_{\text{poly}} - 2 \cdot \mathbf{XWDC} \quad (8)$$

$$(9)$$

where **XLD/XLDLD** and **XWD** account for the overlaps of source/drain contact and the gate oxide as shown in Fig. 6. Widening of  $W_{\text{eff}}$  due to the extension of electric-force line of the drift region is considered by **XWDLD**. The model parameter **XWDC** is introduced to describe the different width dependence of capacitances from currents. If the value is not given, the same value as **XWD** is taken. **LL**, **LLD**, **LLN**, **WL**, **WLD**, and **WLN** are further model parameters for including  $L_{\text{gate}}$  or  $W_{\text{gate}}$  dependencies on  $L_{\text{eff}}$  and  $W_{\text{eff}}$ .

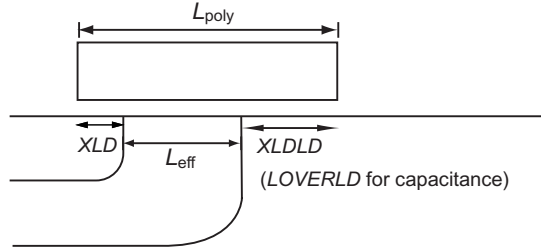


Fig. 6: Cross section of the device.

The HiSIM model parameters introduced in section 3 are summarized in Table 3.

Table 3: HiSIM model parameters introduced in section 3 of this manual. \* and # indicate minor parameters and # an instance parameter, respectively.

<b>#NF</b>	number of gate fingers
<b>XL</b>	difference between real and drawn gate length
<b>XW</b>	difference between real and drawn gate width
<b>XLD</b>	gate-overlap in length at source side
<b>XLDLD</b>	gate-overlap in length at drain side
<b>XWD</b>	gate-overlap in width
<b>XWDLD</b>	widening of drift width
<b>XWDC</b>	gate-overlap in width for capacitance calculation
<b>LL</b>	coefficient of gate length modification
<b>LLD</b>	coefficient of gate length modification
<b>LLN</b>	coefficient of gate length modification
<b>WL</b>	coefficient of gate width modification
<b>WLD</b>	coefficient of gate width modification
<b>WLN</b>	coefficient of gate width modification

## 4 Charges

By applying the Gauss law, the charge density induced in the channel is derived from the Poisson equation [7]:

$$\begin{aligned} -(Q_B + Q_I) &= C_{ox}(V'_G - \phi_S(y)) \\ &= \sqrt{\frac{2\epsilon_{Si}qN_{sub}}{\beta}} \left[ \exp\{-\beta(\phi_S(y) - V_{bs})\} + \beta(\phi_S(y) - V_{bs}) - 1 \right. \\ &\quad \left. + \frac{n_{p0}}{p_{p0}} \left\{ \exp(\beta(\phi_S(y) - \phi_f(y))) - \exp(\beta(V_{bs} - \phi_f(y))) \right\} \right]^{\frac{1}{2}} \end{aligned}$$

$$C_{ox} = \frac{\epsilon_0 \mathbf{KAPPA}}{\mathbf{TOX}} \quad (10)$$

$$V'_G = V_{gs} - \mathbf{VFBC} + \Delta V_{th} \quad (11)$$

$$\beta = \frac{q}{kT} \quad (12)$$

where **VFBC** is the flat-band voltage, **TOX** is the physical gate-oxide thickness, and  $\Delta V_{th}$  is the threshold voltage shift in comparison to the threshold voltage of a long-channel transistor [11].  $\epsilon_0$  and **KAPPA** are permittivities in vacuum and in the gate dielectric, respectively. The electron charge is denoted by  $q$ , and  $\epsilon_{Si}$  and  $N_{sub}$  are the silicon permittivity and the substrate impurity concentration, respectively. The Boltzmann constant and the lattice temperature in Kelvin are  $k$  and  $T$ , respectively. The quasi-Fermi potential  $\phi_f(y)$  preserves the following relationship:

$$\phi_f(L_{eff}) - \phi_f(0) = V_{ds,eff} \quad (13)$$

where  $V_{ds,eff}$  is introduced to fit measured transition characteristics of the channel conductance  $g_{ds}$  between the linear region and the saturation region to compensate for insufficiencies of the charge-sheet approximation as

$$V_{ds,eff} = \frac{V_{ds}}{\left[ 1 + \left( \frac{V_{ds}}{V_{ds,sat}} \right)^{\Delta} \right]^{\frac{1}{\Delta}}} \quad (14)$$

where

**CODDLT=0 :**

$$\Delta = \frac{\mathbf{DDLTMAX} \cdot T1}{\mathbf{DDLTMAX} + T1} + 1 \quad (15)$$

$$T1 = \mathbf{DDLTSLP} \cdot L_{gate} \cdot 10^6 + \mathbf{DDLTICT} \quad (16)$$

**CODDLT=1 ( default ) :**

$$\Delta = \frac{\mathbf{DDLTMAX} \cdot T1}{\mathbf{DDLTMAX} + T1} + \mathbf{DDLTICT} \quad (17)$$

$$T1 = \mathbf{DDLTSLP} \cdot L_{gate} \cdot 10^6 \quad (18)$$

If higher-order derivatives become non-smooth, please increase the **DDLTICT** value. It could be happened for short-channel length, depends on parameter values.

And  $V_{ds,sat}$  is calculated by solving the Poisson equation analytically by neglecting the inversion carrier density [1].

$$V_{ds,sat} = \left[ V'_G + \frac{qN_{sub}\epsilon_{Si}}{C_{ox}^2} \left\{ 1 - \sqrt{1 + 2 \frac{C_{ox}^2}{qN_{sub}\epsilon_{Si}} \left\{ V'_G - \frac{1}{\beta} - V_{bs} \right\} } \right\} \right] \quad (19)$$

The electron concentration at equilibrium condition  $n_{p0}$  is

$$n_{p0} = \frac{n_i^2}{p_{p0}} \quad (20)$$

where the intrinsic carrier concentration  $n_i$  is

$$n_i = n_{i0} T^{\frac{3}{2}} \exp \left( -\frac{E_g}{2q} \beta \right) \quad (21)$$

$p_{p0}$  is approximated to be  $N_{sub}$ , and  $E_g$  describes the temperature dependence of the bandgap (see section 14).

Analytical equations for  $Q_B$  and  $Q_I$  are derived as a function of  $\phi_{S0}$  and  $\phi_{SL}$ . The final equations for  $Q_B$ ,  $Q_I$ , and  $Q_D$  are given in Eqs. (22)- (24).

$$\begin{aligned} Q_B = & - \frac{\mu(W_{eff} \cdot \mathbf{NF})^2}{I_{ds}} \left[ const0 C_{ox} (V_G - \mathbf{VFB}\mathbf{C}) \frac{1}{\beta} \frac{2}{3} \left[ \left\{ \beta(\phi_S - V_{bs}) - 1 \right\}^{\frac{3}{2}} \right]_{\phi_{S0}}^{\phi_{SL}} \right. \\ & - const0 C_{ox} \frac{1}{\beta} \frac{2}{3} \left[ \phi_S \left\{ \beta(\phi_S - V_{bs}) - 1 \right\}^{\frac{3}{2}} \right]_{\phi_{S0}}^{\phi_{SL}} + const0 C_{ox} \frac{1}{\beta} \frac{2}{3} \frac{1}{\beta} \frac{2}{5} \left[ \left\{ \beta(\phi_S - V_{bs}) - 1 \right\}^{\frac{5}{2}} \right]_{\phi_{S0}}^{\phi_{SL}} \\ & - const0^2 \frac{1}{\beta} \frac{1}{2} \left[ \beta^2 (\phi_{SL} - V_{bs})^2 - 2\beta(\phi_{SL} - V_{bs}) + 1 - \beta^2 (\phi_{S0} - V_{bs})^2 + 2\beta(\phi_{S0} - V_{bs}) - 1 \right] \\ & \left. - \frac{1}{\beta} \frac{\mu(W_{eff} \cdot \mathbf{NF})^2}{I_{ds}} \left[ const0 C_{ox} \frac{1}{\beta} \frac{2}{3} \left\{ \beta(\phi_S - V_{bs}) - 1 \right\}^{\frac{3}{2}} + \frac{1}{2} const0^2 \beta \phi_S \right]_{\phi_{S0}}^{\phi_{SL}} \right] \end{aligned} \quad (22)$$

Here  $const0$  is defined as

$$const0 = \sqrt{\frac{2\epsilon_{Si}qN_{sub}}{\beta}}$$

while  $\mu$  and  $I_{ds}$  are the carrier mobility and the drain current, respectively [8, 9].

$$Q_I = - WLC_{ox} (VgVt) \frac{2}{3} \left( \frac{1 + \alpha + \alpha^2}{1 + \alpha} \right) \quad (23)$$

$$Q_D = Q_I \left( \frac{3}{5} - \frac{1}{5} \frac{1 + 2\alpha}{(1 + \alpha)(1 + \alpha + \alpha^2)} \right) \quad (24)$$

where the surface-potential-based description derives

$$\alpha = 1 - \frac{(1 + \delta)(\phi_{SL} - \phi_{S0})}{VgVt} \quad (25)$$

$$VgVt = V_{gs} - \left( \mathbf{VFBC} + \phi_{S0} + \frac{const0}{C_{ox}} BPS0^{\frac{1}{2}} \right) \quad (26)$$

$$\delta = C0Cox \frac{4}{3} \frac{1}{\beta} \frac{(BPSL^{\frac{3}{2}} - BPS0^{\frac{3}{2}})}{(\phi_{SL} - \phi_{S0})^2} - C0Cox \frac{2}{\beta} \frac{(BPSL^{\frac{1}{2}} - BPS0^{\frac{1}{2}})}{(\phi_{SL} - \phi_{S0})^2} - 2C0Cox \frac{BPS0^{\frac{1}{2}}}{(\phi_{SL} - \phi_{S0})} \quad (27)$$

and

$$\begin{aligned} C0Cox &= \frac{const0}{C_{ox}} \\ BPSL^{\frac{1}{2}} &= \sqrt{\beta(\phi_{SL} - V_{bs}) - 1} \\ BPS0^{\frac{1}{2}} &= \sqrt{\beta(\phi_{S0} - V_{bs}) - 1} \\ BPSL^{\frac{3}{2}} &= (BPSL^{\frac{1}{2}})^3 \\ BPS0^{\frac{3}{2}} &= (BPS0^{\frac{1}{2}})^3 \end{aligned} \quad (28)$$

The HiSIM model parameters introduced in section 4 are summarized in Table 4.

Table 4: HiSIM model parameters introduced in section 4 of this manual. \* indicates minor parameters.

<b>VFBC</b>	flat-band voltage
<b>VBI</b>	built-in potential
<b>TOX</b>	physical gate-oxide thickness
<b>KAPPA</b>	dielectric constant of gate dielectric
<b>*DDLTMAX</b>	smoothing coefficient for $V_{ds}$
<b>*DDLTSLP</b>	$L_{gate}$ dependence of smoothing coefficient
<b>*DDLTICT</b>	$L_{gate}$ dependence of smoothing coefficient

## 5 Drain Current

Under the gradual-channel approximation together with approximations of an idealized gate structure and uniform channel doping, the equation for the drain current  $I_{ds}$  is written [7, 10]

$$I_{ds} = \frac{W_{\text{eff}} \cdot \mathbf{NF}}{L_{\text{eff}}} \cdot \mu \cdot \frac{I_{dd}}{\beta} \quad (29)$$

$$\begin{aligned} I_{dd} = & C_{\text{ox}}(\beta V'_G + 1)(\phi_{SL} - \phi_{S0}) - \frac{\beta}{2}C_{\text{ox}}(\phi_{SL}^2 - \phi_{S0}^2) \\ & - \frac{2}{3}const0 \left[ \{\beta(\phi_{SL} - V_{bs}) - 1\}^{\frac{3}{2}} - \{\beta(\phi_{S0} - V_{bs}) - 1\}^{\frac{3}{2}} \right] \\ & + const0 \left[ \{\beta(\phi_{SL} - V_{bs}) - 1\}^{\frac{1}{2}} - \{\beta(\phi_{S0} - V_{bs}) - 1\}^{\frac{1}{2}} \right] \end{aligned} \quad (30)$$

The above description includes the further approximation that the mobility  $\mu$  is independent of position along the channel  $y$ .

## 6 Threshold Voltage Shift

Different from the drift approximation, the drift-diffusion approximation does not require a threshold voltage parameter  $V_{\text{th}}$  for describing device performances. The MOSFET device parameters such as the oxide thickness  $T_{\text{ox}}$  and the substrate doping concentration  $N_{\text{subc}}$  determine the complete MOSFET behavior including the subthreshold characteristics automatically and consistently. However, HiSIM derives many detailed informations on the MOSFET fabrication technology with the  $V_{\text{th}}$  changes from a long-channel transistor ( $\Delta V_{\text{th}}$ ) as a function of gate length ( $L_{\text{gate}}$ ). The modeled  $\Delta V_{\text{th}}$  is incorporated in the  $\phi_S$  iteration as can be seen in Eq. (11), and can be viewed as consisting of two main effects or components:

- (I) the short-channel effect:  $\Delta V_{\text{th,SC}}$
- (II) the reverse-short-channel effect:  $\Delta V_{\text{th,R}}$  and  $\Delta V_{\text{th,P}}$

The separation into these two components ( $\Delta V_{\text{th}} = \Delta V_{\text{th,SC}} + \Delta V_{\text{th,R}}$  (or  $\Delta V_{\text{th,P}}$ )) is schematically shown in Fig. 7.

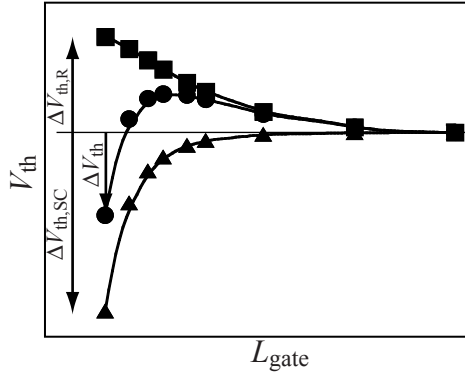


Fig. 7: Schematic plot of the separation of  $V_{\text{th}}$  into the contributions of the short-channel and the reverse-short-channel effect.

### 6.1 (I) Short-Channel Effects

All observed phenomena are caused by the lateral-electric-field contribution in the MOSFET channel, which is important even at threshold condition with small  $V_{\text{ds}}$ . Thus  $\Delta V_{\text{th,SC}}$  can be written as a function of the lateral electric field  $E_y$  by applying the Gauss law. A parabolic potential distribution along the channel is approximated, which results in a position independent gradient of the lateral electric field  $\frac{dE_y}{dy}$  [11]

$$\Delta V_{\text{th,SC}} = \frac{\epsilon_{\text{Si}}}{C_{\text{ox}}} W_{\text{d}} \frac{dE_y}{dy} \quad (31)$$

where  $W_{\text{d}}$  is the depletion-layer thickness written as

$$W_d = \sqrt{\frac{2\epsilon_{Si}(2\Phi_B - V_{bs})}{qN_{sub}}} \quad (32)$$

$$2\Phi_B = \frac{2}{\beta} \ln \left( \frac{N_{sub}}{n_i} \right) \quad (33)$$

where  $n_i$  is the intrinsic carrier density.  $\frac{dE_y}{dy}$  is derived with model parameters in the form

$$\frac{dE_y}{dy} = \frac{2(\mathbf{VBI} - 2\Phi_B)}{(L_{gate} - \mathbf{PARL2})^2} \left( \mathbf{SC1} + \mathbf{SC2} \cdot V_{ds} \cdot \{1 + \mathbf{SC4} \cdot (2\Phi_B - V_{bs})\} + \mathbf{SC3} \cdot \frac{2\Phi_B - V_{bs}}{L_{gate}} \right) \quad (34)$$

**VBI** and **PARL2** represent the built-in potential and the depletion width of the junction vertical to the channel, respectively.  $V'_G$  and *const0* were defined in Eqs. (11) and (23), respectively. The model parameter **SC1** determines the threshold voltage shift for small  $V_{ds}$  and  $V_{bs}$ , and is expected to be unity. If measured  $V_{th}$  is plotted as a function of  $V_{ds}$ , it shows nearly a linear dependence. The gradient is proportional to **SC2**. **SC3** implements a correction of the charge-sheet approximation as well as the impurity-profile gradient along the vertical direction, and is expected to be small. **PTHROU**, describing the increase of the subthreshold swing for short-channel transistors, was deleted and was modeled as the punchthrough effect.

## 6.2 (II) Reverse-Short-Channel Effects

The reverse-short-channel effect is categorized into resulting from two physical MOSFET properties:

- (i) **Impurity concentration inhomogeneity in the direction vertical to the channel (vertical channel inhomogeneity)**  
(obvious in the retrograded implantation):  $\Delta V_{th,R}$
- (ii) **Impurity concentration inhomogeneity in the direction parallel to the channel (lateral channel inhomogeneity)**  
(obvious in the pocket implantation):  $\Delta V_{th,P}$

### (i) Impurity concentration inhomogeneity in the direction vertical to the channel (Retrograded Implantation)

The above model parameters **SC3** and **SCP3** (see in 6.2. (ii)) can be successfully used, if the inhomogeneity is not extremely large.

For cases where the inhomogeneity is large or where positive  $V_{bs}$  is applied, deviation from the linearity of  $V_{th}$  as a function of  $\sqrt{2\Phi_B - V_{bs}}$  is modeled with two fitting parameters **BS1** and **BS2** as

$$Q_{Bmod} = \sqrt{2q \cdot N_{sub} \cdot \epsilon_{Si} \cdot \left( 2\Phi_B - V_{bs} - \frac{\mathbf{BS1}}{\mathbf{BS2} - V_{bs}} \right)} \quad (35)$$

where **BS1** represents the strength of the deviation and **BS2** is the starting value of  $V_{bs}$  where the deviation becomes visible. This  $Q_{Bmod}$  is incorporated into the  $\Delta V_{th}$  description as be seen in Eq. (37).

(ii) Impurity concentration inhomogeneity in the lateral direction parallel to the channel (Pocket Implantation)

The model equations for the  $V_{\text{th}}$  shift due to the pocket implant are:

$$\Delta V_{\text{th,P}} = (V_{\text{th,R}} - V_{\text{th0}}) \frac{\epsilon_{\text{Si}}}{C_{\text{ox}}} W_d \frac{dE_{y,\text{P}}}{dy} \quad (36)$$

$$V_{\text{th,R}} = \mathbf{VFBC} + 2\Phi_B + \frac{Q_{\text{Bmod}}}{C_{\text{ox}}} + \frac{1}{\beta} \log \left( \frac{N_{\text{subb}}}{N_{\text{subc}}} \right) \quad (37)$$

$$V_{\text{th0}} = \mathbf{VFBC} + 2\Phi_{\text{BC}} + \frac{\sqrt{2qN_{\text{subc}}\epsilon_{\text{Si}}(2\Phi_{\text{BC}} - V_{\text{bs}})}}{C_{\text{ox}}} \quad (38)$$

$$\frac{dE_{y,\text{P}}}{dy} = \frac{2(\mathbf{VBI} - 2\Phi_B)}{\mathbf{LP}^2} \left( \mathbf{SCP1} + \mathbf{SCP2} \cdot V_{\text{ds}} + \mathbf{SCP3} \cdot \frac{2\Phi_B - V_{\text{bs}}}{\mathbf{LP}} \right) \quad (39)$$

$$N_{\text{subb}} = 2 \cdot \mathbf{NSUBP} - \frac{(\mathbf{NSUBP} - N_{\text{subc}}) \cdot L_{\text{gate}}}{\mathbf{LP}} - N_{\text{subc}} \quad (40)$$

where  $N_{\text{subc}}$  is the substrate impurity concentration as defined in Eq. (92). The parameters **SCP1** - **SCP3** describe the short-channel effect caused by the potential minimum at the higher impurity concentration of the pocket.  $2\Phi_{\text{BC}}$  is the potential giving threshold condition with  $N_{\text{subc}}$  and  $2\Phi_B$  is the equivalent potential with  $N_{\text{sub}}$

$$\Phi_{\text{BC}} = \frac{2}{\beta} \ln \left( \frac{N_{\text{subc}}}{n_i} \right) \quad (41)$$

$$\Phi_B = \frac{2}{\beta} \ln \left( \frac{N_{\text{sub}}}{n_i} \right) \quad (42)$$

$$N_{\text{sub}} = \frac{N_{\text{subc}}(L_{\text{gate}} - \mathbf{LP}) + \mathbf{NSUBP} \cdot \mathbf{LP}}{L_{\text{gate}}} \quad (43)$$

As defined in Eq. (43),  $N_{\text{sub}}$  is replaced to the averaged impurity concentration in the channel and  $N_{\text{subb}}$  is introduced, beginning from channel lengths where pockets at source and drain start to overlap.

As  $V_{\text{ds}}$  approaches zero, the  $V_{\text{th}}$  dependence on  $V_{\text{ds}}$  deviates from linearity and  $V_{\text{th}}$  increases drastically as shown schematically in Fig. 8. This is modeled with two model parameters **SCP21** and **SCP22** as

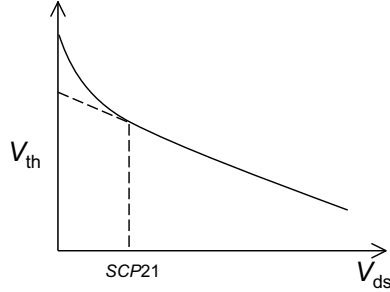


Fig. 8: Threshold voltage as a function of  $V_{\text{ds}}$ . The deviation from linearity for small  $V_{\text{ds}}$  is modeled with parameters **SCP21** and **SCP22**.

$$\Delta V_{\text{th,P}} = \Delta V_{\text{th,P}} - \frac{\mathbf{SCP22}}{(\mathbf{SCP21} + V_{\text{ds}})^2} \quad (44)$$

where **SCP21** determines the  $V_{ds}$  value at which  $V_{th}$  starts to deviate from linearity as a function of  $V_{ds}$ . The parameter **SCP22** determines the gradient of this deviation.

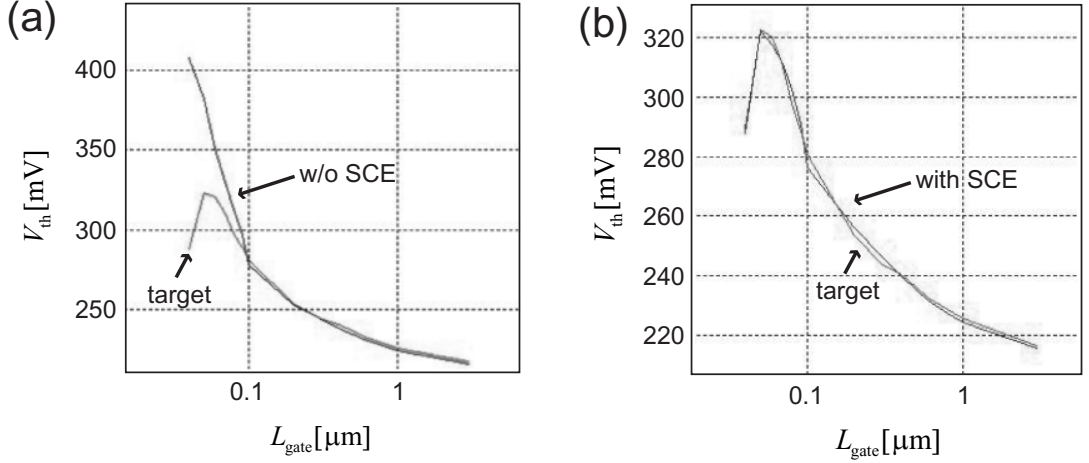


Fig. 9: Comparison of measurements and pocket-implant model for  $V_{th}$  as a function of  $L_{gate}$ . Results (a) with and (b) without short-channel effects (SCE) are shown.

$V_{th,R}$  and  $V_{th0}$ , defined in Eqs. (37) and (38), are the threshold voltages for the cases with and without pocket-implant, respectively. The overlap start of source and drain pockets causes a steep increase of  $V_{th}$  as a function of decreasing  $L_{gate}$ . This effect enables to extract **LP** from measurements. Fig. 9 compares the  $V_{th}$ - $L_{gate}$  characteristics of the developed pocket-implant model with and without inclusion of the short-channel effects (SCE). The steep increase at  $L_{gate}=0.1\mu\text{m}$  in Fig. 9a means the starting of the pocket overlap, where  $\mathbf{LP}=0.05\mu\text{m}$ .

In some cases the pocket profile cannot be described by the single linearly decreasing form, but provides extensive tails as schematically shown in Fig. 10. Therefore, two model parameters **NPEXT** and **LPEXT** are introduced to model the pocket tails as

$$N_{sub} = N_{sub} + \frac{\mathbf{NPEXT} - N_{subc}}{\left(\frac{1}{\mathbf{xx}} + \frac{1}{\mathbf{LPEXT}}\right) L_{gate}} \quad (45)$$

where

$$\mathbf{xx} = 0.5 \cdot L_{gate} - \mathbf{LP} . \quad (46)$$

**NPEXT** is the maximum concentration of the pocket tail and **LPEXT** describes the tail extension characteristics. Usually strong pocket implantation induces a vertical impurity distribution at the same time. For fitting the measured results in such cases it is recommended to use the parameter **SCP3** together with parameters **BS1** and **BS2**.

The HiSIM model parameters introduced in section 6 are summarized in Table 5.

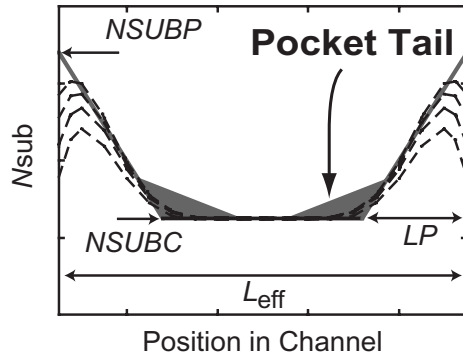


Fig. 10: Modeled pocket tail with **NPEXT** and **LPEXT**.

Table 5: HiSIM model parameters introduced in section 6 of this manual. \* indicates minor parameters.

<b>VBI</b>	built-in potential
<b>PARL2</b>	depletion width of channel/contact junction
<b>SC1</b>	magnitude of short-channel effect
<b>SC2</b>	$V_{ds}$ dependence of short-channel effect
<b>*SC3</b>	$V_{bs}$ dependence of short-channel effect
<b>*SC4</b>	$V_{bs}$ dependence of short-channel effect
<b>NSUBP</b>	maximum pocket concentration
<b>LP</b>	pocket penetration length
<b>*BS1</b>	body-coefficient modification due to impurity profile
<b>*BS2</b>	body-coefficient modification due to impurity profile
<b>SCP1</b>	magnitude of short-channel effect due to pocket
<b>SCP2</b>	$V_{ds}$ dependence of short-channel due to pocket
<b>*SCP3</b>	$V_{bs}$ dependence of short-channel effect due to pocket
<b>*SCP21</b>	short-channel-effect modification for small $V_{ds}$
<b>*SCP22</b>	short-channel-effect modification for small $V_{ds}$
<b>*NPEXT</b>	maximum concentration of pocket tail
<b>*LPEXT</b>	extension length of pocket tail

## 7 Short-Channel Effects

### 7.1 Punchthrough Effect

In idealized MOSFETs, the gate voltage controls carrier concentration at the semiconductor substrate surface. However, this electrostatical control begins to be compromised due to the proximity of source and drain contacts, when MOSFET geometry scales down. Thus, in addition to carriers confined at the surface but also those deep from the surface tend to flow.

Thus the drain current consists of MOSFET intrinsic drain current,  $I_{ds,\text{intrinsic}}$ , and additional leakage types of current, which is punchthrough current  $I_{ds,\text{punch}}$  and pinch-off  $I_{ds,\text{pinchoff}}$ :

$$I_{ds} = I_{ds,\text{intrinsic}} + I_{ds,\text{punch}} + I_{ds,\text{pinchoff}} \quad (47)$$

The origin of the punchthrough effect is the bipolar effect through source, substrate, and drain.

The flag **COPT** is introduced to activate the punchthrough currents with flag **COPSPT** for the solution method:

- **COPT** = 0: without punchthrough effects
- **COPT** = 1: with punchthrough effects
- **COPSPT** = 0: analytical solution (for deep punchthrough effect)
- **COPSPT** = 1: iterative solution (for deep punchthrough effect)

Note. For shallow punchthrough effect, analytical equations are always used, irrespective of **COPSPT**.

Two mechanisms for the punchthrough effect are considered:

$$I_{ds,\text{punch}} = I_{\text{surfacePT}} + I_{\text{deepPT}} \quad (48)$$

### 7.2 Shallow Punchthrough Effect

The effect is described by a power function of the potential difference instead of the exponential function as

$$\text{POTENTIAL} = (\mathbf{VBI} - \phi_{s0})^{\mathbf{PTP}} \quad (49)$$

The final drain current  $I_{ds}$  is written

$$I_{\text{shallowPT}} = \frac{W_{\text{eff}} \cdot \mathbf{NF} \cdot \mu}{L_{\text{eff}}} \cdot \beta \cdot (\phi_{sL} - \phi_{s0}) \\ \left\{ C_{\text{ox}} \cdot \beta \cdot \frac{\mathbf{PTL}}{(L_{\text{gate}} \cdot 10^6)^{\mathbf{PTLP}}} \cdot \text{POTENTIAL} \cdot \left( 1 + \mathbf{PT2} \cdot V_{ds} + \frac{\mathbf{PT4} \cdot (\phi_{s0} - V_{bs})}{(L_{\text{gate}} \cdot 10^6)^{\mathbf{PT4P}}} \right) \right\} \quad (50)$$

where model parameters **PTL**, **PTLP**, **PT2**, **PT4**, and **PT4P** are introduced. Note that surface punchthrough effects can be also turned off by setting **PTL**=0.

### 7.3 Deep Punchthrough Effect (new model)

Apart from the shallow punchthrough current, a direct passage of carriers between source and drain can be formed deep beneath the surface, at the depth comparable to the source and drain junction depth at most.

The deep punchthrough current,  $I_{\text{deepPT}}$ , is written as:

$$I_{\text{PT,deep}} = J_{\text{PT,deep}} \cdot W_{\text{eff}} \cdot \mathbf{NF} \cdot (1 - \exp(-\beta V_{\text{ds}})) \quad (51)$$

A prefactor  $J_{\text{PT,deep}}$  is expressed as:

$$J_{\text{PT,deep}} = \frac{2}{\beta L_{\text{eff}}} \cdot Q_{n0,\text{PT}} \cdot \mathbf{MUPT} \cdot \exp(-\beta \phi_m) \quad (52)$$

**MUPT** represents an effective mobility for deep punchthrough current, and  $Q_{n0,\text{PT}}$  represents an effective charge density per unit area for deep punchthrough current.

$$Q_{n0,\text{PT}} = \sqrt{\frac{2 \cdot q \cdot \mathbf{NJUNC} \cdot \varepsilon_{si}}{\beta}} \sqrt{\beta \phi_{m,gate}} \quad (53)$$

where **NJUNC** is dopant concentration at source and drain junction part.

$\phi_m$  represents an effective potential barrier for carriers to summount from the source to flow into the channel and is regarded as an interplay of electrostatic effects by  $V_{\text{gs}}$  and  $V_{\text{ds}}$ , which will be modeled separately:

$$\phi_m = \phi_{m,gate} + \phi_{m,SD} \quad (54)$$

where and  $\phi_{m,SD}$  is that by  $V_{\text{ds}}$ .

$$\phi_{m,gate} = (\phi_{s,\text{deepPT}} - \phi_{m,SD}) * wfactor \quad (55)$$

$$wfactor = \begin{cases} \left(1 - \frac{\mathbf{XJPT}}{W_{\text{depl,PT}}}\right)^2 & (W_{\text{depl,PT}} \geq \mathbf{XJPT}) \\ 0 & (W_{\text{depl,PT}} < \mathbf{XJPT}) \end{cases} \quad (56)$$

$$W_{\text{depl,PT}} = \begin{cases} \frac{Q_{bu,PT}}{q \cdot N_{\text{subs}}} & (\phi_{s,\text{deepPT}} \geq \phi_{m,SD}) \\ 0 & (\phi_{s,\text{deepPT}} < \phi_{m,SD}) \end{cases} \quad (57)$$

$$Q_{bu,PT} = const0 \cdot \sqrt{\exp(-\beta \cdot (\phi_{s,\text{deepPT}} - \phi_{m,SD})) - 1 + \beta \cdot (\phi_{s,\text{deepPT}} - \phi_{m,SD})} \quad (58)$$

The  $V_{ds}$  controlled part of  $\phi_m$  is expressed as:

$$\phi_{m,SD} = -\frac{1}{4} \frac{(E_{cri} \cdot L_{eff})^2}{(E_{cri} \cdot L_{eff}) + V_{ds}} \quad (59)$$

where  $E_{cri}$  is the critical electric field strength at the junction:

$$E_{cri} = \sqrt{\frac{2q \cdot (V_{bi} - V_{bs})}{\varepsilon_{si}} \frac{N_{sub} \cdot \mathbf{NJUNC}}{N_{sub} + \mathbf{NJUNC}}} \quad (60)$$

where  $V_{bi}$  is built-in potential.

$\phi_{s,deepPT}$  is the potential for the deep region where the deep punchthrough occurs, calculated with use of the Poisson equation with a different flat-band voltage:

$$\mathbf{VFBC} + \mathbf{VFBPT} \quad (61)$$

Additionally, **PSLIMPT** is introduced to limit the  $\phi_{s,deepPT}$ , namely the maximum value.

## 7.4 Channel Conductance

The high field under the saturation condition causes the pinch-off region and the current flows away from the surface. This effect is considered as the lateral-field-induced charge for the capacitacne (see section 16). The simplified formulation is applied to consider the effect as

$$I_{ds} = I_{ds} + \frac{W_{eff} \cdot \mathbf{NF}}{L_{eff}} \frac{\mu}{\beta} \cdot (\phi_{SL} - \phi_{S0}) \cdot CONDUCTANCE$$

$$CONDUCTANCE = C_{ox} \cdot \beta \frac{\mathbf{GDL}}{(L_{gate} \cdot 10^6 + \mathbf{GDLD} \cdot 10^6)^{\mathbf{GDLP}}} \cdot V_{ds} \quad (62)$$

The HiSIM model parameters introduced in section 7 are summarized in Table 6.

Table 6: HiSIM model parameters introduced in section 7 of this manual. \* indicates minor parameters.

<b>COPT</b>	flag for punchthrough effect
<b>COPSPT</b>	selector for solution of deep punchthrough effect
* <b>PTL</b>	strength of shallow punchthrough effect
* <b>PTLP</b>	channel-length dependence of shallow punchthrough effect
* <b>PTP</b>	strength of shallow punchthrough effect
* <b>PT2</b>	$V_{ds}$ dependence of shallow punchthrough effect
* <b>PT4</b>	$V_{bs}$ dependence of shallow punchthrough effect
* <b>PT4P</b>	$V_{bs}$ dependence of shallow punchthrough effect
* <b>GDL</b>	strength of high-field effect
* <b>GDLP</b>	channel-length dependence of high-field effect
* <b>GDD</b>	channel-length dependence of high-field effect
<b>NJUNC</b>	—Deep punchthrough effect—
<b>XJPT</b>	source/drain diffusion dopant concentration
<b>MUPT</b>	effective junction depth for deep punchthrough current calculation
<b>PSLIMPT</b>	effective mobility for deep punchthrough current
<b>VFBPT</b>	potential limiter for deep punchthrough current calculation
	flatband voltage shifter for deep punchthrough current

## 8 Depletion Effect of the Gate Poly-Si

Carrier depletion in the gate poly-Si near the gate-oxide interface starts after the formation of the inversion layer in the substrate as shown in Fig. 11.

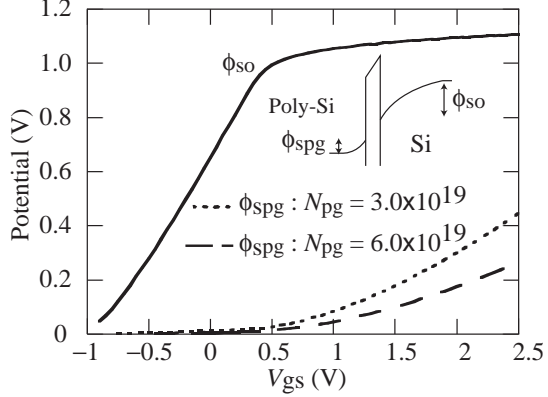


Fig. 11: Simulated surface potential at the source side ( $\phi_{so}$ ) as a function of  $V_{gs}$ . The poly-depletion potential is also shown for two doping concentrations  $N_{pg}$  in the poly-Si.

To eliminate the necessary iteration procedure for the circuit-simulation application, the potential drop within the poly-Si  $\phi_{spg}$  is approximated as a function of  $V_{gs}$  and  $V_{ds}$  by the simple formula of Eq. (63), and is included in the  $\Delta V_{th}$  calculation as a potential drop of  $V_{gs}$ .

$$\phi_{spg} = \mathbf{PGD1} \left( 1 + \frac{1}{L_{gate} \cdot 10^6} \right)^{\mathbf{PGD4}} \exp \left( \frac{V_{gs} - \mathbf{PGD2}}{V} \right) \quad (63)$$

The HiSIM model parameters introduced in section 8 are summarized in Table 7.

Table 7: HiSIM model parameters introduced in section 8 of this manual. \* indicates a minor parameter.

<b>PGD1</b>	strength of poly depletion
<b>PGD2</b>	threshold voltage of poly depletion
<b>*PGD4</b>	$L_{gate}$ dependence of poly depletion

## 9 Quantum-Mechanical Effects

The main quantum-mechanical phenomenon, which has to be included into a MOSFET model for circuit simulation, is the repulsion of the channel's carrier-density peak into the substrate away from the surface. This can be described phenomenologically by an increased effective oxide thickness  $T_{\text{ox}}$  [21, 22]. The calculated  $\Delta T_{\text{ox}}-V_{\text{gs}}$  characteristics is shown in Fig. 12. Equations implemented into HiSIM for the reproduction of quantum mechanical effects are:

$$T_{\text{ox}} = \mathbf{TOX} + \Delta T_{\text{ox}} \quad (64)$$

$$\Delta T_{\text{ox}} = \frac{\mathbf{QME1}}{V_{\text{gs}} - V_{\text{th}}(\mathbf{TOX})} + \mathbf{QME2} + \mathbf{QME3} \quad (65)$$

where **QME1**, **QME2**, and **QME3** are the quantum-effect model parameters. A limiting function is introduced in the source code to avoid unreasonable  $\Delta T_{\text{ox}}$  increase below the threshold voltage.

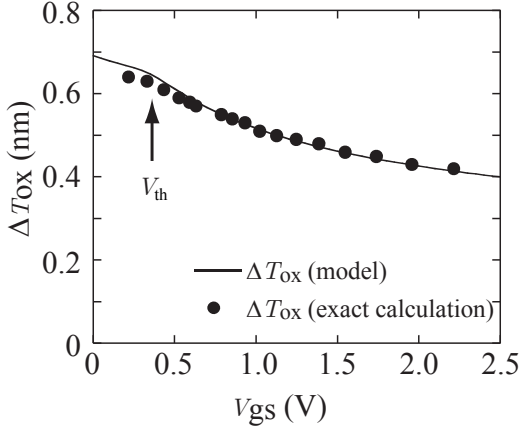


Fig. 12: Calculated  $T_{\text{ox}}$  increase by the quantum mechanical effect. The solid line shows model results with Eqs. (64) and (65). Symbols are exact calculation results by solving the Poisson equation and the Schrödinger equation simultaneously.

The HiSIM model parameters introduced in section 9 are summarized in Table 8.

Table 8: HiSIM model parameters introduced in section 9 of this manual.

<b>QME1</b>	$V_{\text{gs}}$ dependence
<b>QME2</b>	$V_{\text{gs}}$ dependence
<b>QME3</b>	minimum $T_{\text{ox}}$ modification

## 10 Mobility Model

The low-field mobility is described with the following expressions and includes the three independent mechanisms of Coulomb, phonon and surface-roughness scattering [23]:

$$\frac{1}{\mu_0} = \frac{1}{\mu_{CB}} + \frac{1}{\mu_{PH}} + \frac{1}{\mu_{SR}} \quad (66)$$

$$\mu_{CB}(\text{Coulomb}) = \mathbf{MUECB0} + \mathbf{MUECB1} \frac{Q_i}{q \cdot 10^{11}} \quad (67)$$

$$\mu_{PH}(\text{phonon}) = \frac{M_{uephonon}}{E_{eff}^{\mathbf{MUEPH0}}} \quad (68)$$

$$\mu_{SR}(\text{surface roughness}) = \frac{\mathbf{MUESR1}}{E_{eff}^{M_{uesurface}}} \quad (69)$$

where  $\mu_{PH}(\text{phonon})$  is temperature dependent as modeled in section 14.

Here  $E_{eff}$  is the effective field normal to the surface. The field are written as

$$E_{eff} = E_{eff0} \cdot (1 + \mathbf{MUEEFB} \cdot V_{bs}) \quad (70)$$

$$E_{eff0} = \frac{1}{\epsilon_{Si}} (N_{dep} \cdot Q_b + \mathbf{NINV} \cdot Q_i) \cdot f(\phi_S) \quad (71)$$

$$f(\phi_S) = \frac{1}{1 + (\phi_{SL} - \phi_{S0}) \cdot N_{invd}} \quad (72)$$

$$(73)$$

where  $N_{dep}$  and  $N_{invd}$  consider the gate length ( $L_{gate}$ ) dependence as

$$N_{dep} = \frac{\mathbf{NDEP}}{1 + \frac{\mathbf{NDEPL}}{\left(\frac{L_{gate}}{10^{-6}}\right)^{\mathbf{NDEPLP}}}} \quad (74)$$

$$N_{invd} = \mathbf{NINV} \cdot \left( 1 + \frac{\mathbf{NINVDL}}{\left(\frac{L_{gate}}{10^{-6}}\right)^{\mathbf{NINVDLP}}} \right) \quad (75)$$

For the gate width ( $W_{gate}$ ) dependence, see Section 12 Narrow-Channel Effects.

The mobility universality preserves following conditions [24, 25]

$$\mathbf{MUEPH0} \simeq 0.3 \quad (76)$$

$$M_{uesurface} = 2.0 \quad (77)$$

$$\mathbf{NDEP} = 1.0 \quad (78)$$

$$\mathbf{NINV} = 0.5 \quad (79)$$

However, these parameters can be used for fitting purposes [26], if it is necessary.

The  $L_{\text{gate}}$  dependence of the mobility is considered as

$$M_{\text{uephonon}} = \mathbf{MUEPH1} \cdot \left( 1 + \frac{\mathbf{MUEPHL}}{\left( \frac{L_{\text{gate}}}{10^{-6}} \right)^{\mathbf{MUEPLP}}} \right) \quad (80)$$

$$M_{\text{uesurface}} = \mathbf{MUESR0} \cdot \left( 1 + \frac{\mathbf{MUESRL}}{\left( \frac{L_{\text{gate}}}{10^{-6}} \right)^{\mathbf{MUESLP}}} \right) \quad (81)$$

The high-field mobility is modeled as [27]

$$\mu = \frac{\mu_0}{\left( 1 + \left( \frac{\mu_0 E_y}{V_{\text{max}}} \right)^{\mathbf{BB}} \right)^{\frac{1}{\mathbf{BB}}}} \quad (82)$$

The velocity overshoot is included in the mobility model in the following manner

$$V_{\text{max}} = \mathbf{VMAX} \cdot \left( 1 + \frac{\mathbf{VOVER}}{\left( \frac{L_{\text{gate}}}{10^{-6}} \right)^{\mathbf{VOVERP}}} \right) \quad (83)$$

The HiSIM model parameters introduced in section 10 are summarized in Table 9.

Table 9: HiSIM model parameters introduced in section 10 of this manual. \* indicates minor parameters.

<b>MUECB0</b>	Coulomb scattering
<b>MUECB1</b>	Coulomb scattering
<b>MUEPH0</b>	phonon scattering
<b>MUEPH1</b>	phonon scattering
* <b>MUEEFB</b>	Vbs dependence of phonon mobility
* <b>MUEPHL</b>	length dependence of phonon mobility reduction
* <b>MUEPLP</b>	length dependence of phonon mobility reduction
<b>MUESR0</b>	surface-roughness scattering
<b>MUESR1</b>	surface-roughness scattering
* <b>MUESRL</b>	length dependence of surface roughness mobility reduction
* <b>MUESLP</b>	length dependence of surface roughness mobility reduction
<b>NDEP</b>	depletion charge contribution on effective-electric field
* <b>NDEPL</b>	modification of depletion charge contribution for short-channel case
* <b>NDEPLP</b>	modification of depletion charge contribution for short-channel case
<b>NINV</b>	inversion charge contribution on effective-electric field
* <b>NINVD</b>	reduced resistance effect for small $V_{\text{ds}}$
<b>BB</b>	high-field-mobility degradation
<b>VMAX</b>	maximum saturation velocity
<b>VOVER</b>	velocity overshoot effect
<b>VOVERP</b>	$L_{\text{eff}}$ dependence of velocity overshoot

## 11 Channel-Length Modulation

The gradual-channel approximation is applied to derive analytical equations for describing device characteristics. However, this approximation is not valid for large  $V_{ds}$  causing the pinch-off phenomenon in the channel. To include the pinch-off phenomenon in HiSIM, we apply the conventional method of modeling the pinch-off region ( $\Delta L$ ) separately from the rest of the channel as depicted in Fig. 13 [29].

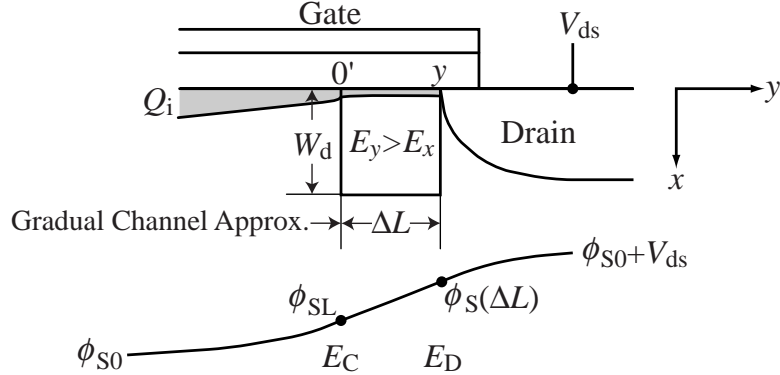


Fig. 13: Schematic showing the correlation among physical quantities in the pinch-off region.

The potential value at the end of the channel ( $\phi_{S(\Delta L)}$ ) lies between  $\phi_{SL}$  and  $\phi_{S0} + V_{ds}$ . The exact value is dependent on the junction profile between the channel and the drain contact. This dependence is modeled with the parameter **CLM1** as

$$\phi_{S(\Delta L)} = (1 - \mathbf{CLM1}) \cdot \phi_{SL} + \mathbf{CLM1} \cdot (\phi_{S0} + V_{ds}) \quad (84)$$

where **CLM1** can be interpreted to represent the hardness of the junction and must be in the range  $0 \leq \mathbf{CLM1} \leq 1$ . Here  $\mathbf{CLM1} = 1$  means that the contact profile is abrupt and the complete potential increase occurs in the  $\Delta L$  region, whereas  $\mathbf{CLM1} = 0$  corresponds to the opposite condition and there is no potential increase in the  $\Delta L$  region.

The final  $\Delta L$  is derived as

$$\begin{aligned} \Delta L = & \frac{1}{2} \left[ -\frac{1}{L_{eff}} \left( 2 \frac{I_{dd}}{\beta Q_i} z + 2 \frac{q N_{sub}}{\epsilon_{Si}} (\phi_s(\Delta L) - \phi_{SL}) z^2 + E_0 z^2 \right) \right. \\ & \left. + \sqrt{\frac{1}{L_{eff}^2} \left( 2 \frac{I_{dd}}{\beta Q_i} z + 2 \frac{q N_{sub}}{\epsilon_{Si}} (\phi_s(\Delta L) - \phi_{SL}) z^2 + E_0 z^2 \right)^2 + 4 \left( 2 \frac{q N_{sub}}{\epsilon_{Si}} (\phi_s(\Delta L) - \phi_{SL}) z^2 + E_0 z^2 \right)} \right] \end{aligned} \quad (85)$$

where  $E_0$  is fixed to  $10^5$  and

$$z = \frac{\epsilon_{Si} \cdot W_d}{\mathbf{CLM2} \cdot Q_b + \mathbf{CLM3} \cdot Q_i} \quad (86)$$

Two model parameters **CLM2** and **CLM3** are introduced to consider the uncertainty of  $Q_i$  in the pinch-off region and to counterbalance the two contributions from  $Q_b$  ( $= q N_{sub} W_d$ ) and  $Q_i$ . It has to be notified that  $\Delta L$  is equal to zero, when **CLM1**=0.

Additional contributions on CLM such as the pocket effect is modeled as

$$\Delta L = \Delta L \left( 1 + \mathbf{CLM6} \cdot (L_{\text{gate}} \cdot 10^6)^{\mathbf{CLM5}} \right) \quad (87)$$

It can be happen that  $L_{\text{eff}} - \Delta L$  becomes negative, if extracted **CLM5** and **CLM6** values are out of acceptable ranges. In this case HiSIM gives "warning" and fixes  $L_{\text{eff}} - \Delta L$  to 1nm.

The HiSIM model parameters introduced in section 11 are summarized in Table 10.

Table 10: HiSIM model parameters introduced in section 11 of this manual.

<b>CLM1</b>	hardness coefficient of channel/contact junction
<b>CLM2</b>	coefficient for $Q_B$ contribution
<b>CLM3</b>	coefficient for $Q_I$ contribution
* <b>CLM5</b>	effect of pocket implantation
* <b>CLM6</b>	effect of pocket implantation

## 12 Narrow-Channel Effects

### 12.1 Threshold Voltage Modification

The fringing capacitances  $C_{\text{ef}}$  at the edge of the isolation is modeled [9] as

$$\Delta V_{\text{th},W} = \left( \frac{1}{C_{\text{ox}}} - \frac{1}{C_{\text{ox}} + 2C_{\text{ef}}/(L_{\text{eff}}W_{\text{eff}})} \right) qN_{\text{sub}}W_{\text{d}} + \frac{\mathbf{WVTH0}}{W_{\text{gate}} \cdot 10^6} \quad (88)$$

where **WVTH0** is the parameter for including the basic width dependence and

$$C_{\text{ef}} = \frac{2\epsilon_{\text{ox}}}{\pi} L_{\text{eff}} \ln \left( \frac{2T_{\text{fox}}}{T_{\text{ox}}} \right) = \frac{\mathbf{WFC}}{2} L_{\text{eff}} \quad (89)$$

Here,  $T_{\text{fox}}$  is the thickness of the oxide at the trench edge, and **WFC** is the model parameter for including the edge-fringing-capacitance effects. The final  $\Delta V_{\text{th}}$  of Eq. (11), under inclusion of the shallow-trench-isolation effects, becomes:

$$\Delta V_{\text{th}} = \Delta V_{\text{th},\text{SC}} + \Delta V_{\text{th},\text{R}} + \Delta V_{\text{th},\text{P}} + \Delta V_{\text{th},\text{W}} - \phi_{\text{Spg}} \quad (90)$$

The width dependence of the pocket impurity concentration is modeled as

$$N_{\text{subp}} = \mathbf{NSUBP0} \cdot \left( 1 + \frac{\mathbf{NSUBP0}}{(W_{\text{gate}} \cdot 10^6)^{\mathbf{NSUBWP}}} \right) \quad (91)$$

The width dependence of the substrate impurity concentration  $N_{\text{subc}}$  is also considered as

$$N_{\text{subc}} = \mathbf{NSUBC} \cdot \left( 1 + \frac{\mathbf{NSUBC}}{(W_{\text{gate}} \cdot 10^6)^{\mathbf{NSUBCWP}}} \right) \quad (92)$$

### 12.2 Mobility Change

A reduction of  $I_{\text{ds,sat}}$  with reduced  $W_{\text{gate}}$  as indicated by curve C1 in Fig. 14 [31] is modeled by a decreasing phonon mobility with two model parameters **MUEPHW** and **MUEPWP** as

$$M_{\text{uephonon}} = M_{\text{uephonon}} \cdot \left( 1 + \frac{\mathbf{MUEPHW}}{(W_{\text{gate}} \cdot 10^6)^{\mathbf{MUEPWP}}} \right) \quad (93)$$

A start to increase for narrower  $W_{\text{gate}}$  as denoted by curve C2 is modeled as a change of the surface-roughness contribution caused by a carrier flow in increasing distance from the surface as

$$M_{\text{uesurface}} = M_{\text{uesurface}} \cdot \left( 1 + \frac{\mathbf{MUESRW}}{(W_{\text{gate}} \cdot 10^6)^{\mathbf{MUESWP}}} \right) \quad (94)$$

Further width dependences are included as

$$N_{\text{invd}} = N_{\text{invd}} \cdot \left( 1 + \frac{\mathbf{NINVDW}}{(W_{\text{gate}} \cdot 10^6)^{\mathbf{NINVDWP}}} \right) \quad (95)$$

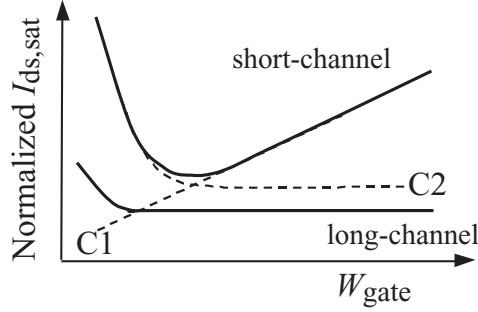


Fig. 14: Schematic of the normalized saturation current  $I_{ds,\text{sat}}$  as a function of the gate width  $W_{\text{gate}}$  for two different gate lengths  $L_{\text{gate}}$ .

### 12.3 Transistor Leakage due to Shallow Trench Isolation (STI): Hump in $I_{ds}$

The surface potential of the leakage regions at the trench edges can be derived analytically as [32]

$$\phi_{S,STI} = V'_{gs,STI} + \frac{\epsilon_{Si} Q_{N,STI}}{C'_{ox}^2} \left[ 1 - \sqrt{1 + \frac{2C'_{ox}^2}{\epsilon_{Si} Q_{N,STI}} \left( V'_{gs,STI} - V_{bs} - \frac{1}{\beta} \right)} \right] \quad (96)$$

where

$$Q_{N,STI} = q \cdot \mathbf{NSTI} \quad (97)$$

$$V'_{gs,STI} = V_{gs} - \mathbf{VFBC} + V_{th,STI} + \Delta V_{th,SCSTI} \quad (98)$$

where

$$V_{th,STI} = \mathbf{VTHSTI} - \mathbf{VDSTI} \cdot V_{ds} \quad (99)$$

and

$$\Delta V_{th,SCSTI} = \frac{\epsilon_{Si}}{C_{ox}} W_{d,STI} \frac{dE_y}{dy} \quad (100)$$

The threshold voltage for the STI effect  $\mathbf{VTHSTI}$  includes features of STI such as  $\mathbf{NSTI}$  which are different from the substrate. The depletion-layer thickness  $W_{d,STI}$  is written as

$$W_{d,STI} = \sqrt{\frac{2\epsilon_{Si}(2\Phi_{B,STI} - V_{bs})}{q\mathbf{NSTI}}} \quad (101)$$

$\frac{dE_y}{dy}$  is described with model parameters in the same form as in section 6.1 on short-channel effects

$$\frac{dE_y}{dy} = \frac{2(\mathbf{VBI} - 2\Phi_{B,STI})}{(L_{gate,sm} - \mathbf{PARL2})^2} (\mathbf{SCSTI1} + \mathbf{SCSTI2} \cdot V_{ds}) \quad (102)$$

where

$$L_{gate,sm} = L_{gate} + \frac{\mathbf{WL1}}{w_l \mathbf{WL1P}} \quad (103)$$

$$wl = (W_{\text{gate}} \cdot 10^6) \times (L_{\text{gate}} \cdot 10^6) \quad (104)$$

The modeling of the transistor leakage for STI technologies is based on the idea that the current in the subthreshold region is governed only by the diffusion term. The carrier concentration  $Q_{i,\text{STI}}$  is calculated analytically for the subthreshold region, where the STI effect is obvious [1]. The final leakage current equation is written as

$$I_{\text{ds,STI}} = 2 \frac{W_{\text{STI}}}{L_{\text{eff}} - \Delta L} \mu \frac{Q_{i,\text{STI}}}{\beta} [1 - \exp(-\beta V_{\text{ds}})] \quad (105)$$

where  $W_{\text{STI}}$  determines the width of the high-field region. The gate length dependence of  $W_{\text{STI}}$  is included as

$$W_{\text{STI}} = \mathbf{WSTI} \left( 1 + \frac{\mathbf{WSTIL}}{(L_{\text{gate,sm}} \cdot 10^6) \mathbf{WSTILP}} \right) \left( 1 + \frac{\mathbf{WSTIW}}{(W_{\text{gate,sm}} \cdot 10^6) \mathbf{WSTIWP}} \right) \quad (106)$$

## 12.4 Small Geometry

Small size devices do not show the same scaling characteristic as long-channel or wide-channel devices, but rather deviate significantly. The reason is mainly due to the resolution inaccuracy of the lithography. The small geometry effects are modeled first as the threshold voltage shift

$$\Delta V_{\text{th}} = \Delta V_{\text{th,SC}} + \Delta V_{\text{th,R}} + \Delta V_{\text{th,P}} + \Delta V_{\text{th,W}} + \Delta V_{\text{th,sm}} - \phi_{\text{Spg}} \quad (107)$$

where

$$\Delta V_{\text{th,sm}} = \frac{\mathbf{WL2}}{wl \mathbf{WL2P}} \quad (108)$$

The mobility modification due to the small device geometry is also modeled in the phonon scattering as

$$M_{\text{uephonon}} = M_{\text{uephonon}} \cdot \left( 1 + \frac{\mathbf{MUEPHS}}{wl \mathbf{MUEPSP}} \right) \quad (109)$$

$$V_{\text{max}} = V_{\text{max}} \cdot \left( 1 + \frac{\mathbf{VOVERS}}{wl \mathbf{VOVERSP}} \right) \quad (110)$$

The HiSIM model parameters introduced in section 12 are summarized in Table 11.

Table 11: HiSIM model parameters introduced in section 12 of this manual. \* indicates minor parameters.

<b>WFC</b>	threshold voltage change due to capacitance change
<b>*WVTH0</b>	threshold voltage shift
<b>NSUBC</b>	substrate-impurity concentration
<b>*NSUBCW</b>	width dependence of substrate-impurity concentration
<b>*NSUBCWP</b>	width dependence of substrate-impurity concentration
<b>*NSUBP0</b>	modification of pocket concentration for narrow width
<b>*NSUBWP</b>	modification of pocket concentration for narrow width
<b>*MUEPHW</b>	phonon related mobility reduction
<b>*MUEPWP</b>	phonon related mobility reduction
<b>*MUESRW</b>	change of surface roughness related mobility
<b>*MUESWP</b>	change of surface roughness related mobility
<b>*NINVDW</b>	width dependence on high field mobility
<b>*NINVDWP</b>	width dependence on high field mobility
<b>*VTHSTI</b>	threshold voltage shift due to STI
<b>*VDSTI</b>	threshold voltage shift dependence on $V_{ds}$ due to STI
<b>*SCSTI1</b>	the same effect as <b>SC1</b> but at STI edge
<b>*SCSTI2</b>	the same effect as <b>SC2</b> but at STI edge
<b>NSTI</b>	substrate-impurity concentration at the STI edge
<b>WSTI</b>	width of the high-field region at STI edge
<b>*WSTIL</b>	channel-length dependence of <b>WSTI</b>
<b>*WSTILP</b>	channel-length dependence of <b>WSTI</b>
<b>*WSTIW</b>	channel-width dependence of <b>WSTI</b>
<b>*WSTIWP</b>	channel-width dependence of <b>WSTI</b>
<b>WL1</b>	threshold volatge shift of STI leakage due to small size effect
<b>WL1P</b>	threshold voltage shift of STI leakage due to small size effect
<b>WL2</b>	threshold volatge shift due to small size effect
<b>WL2P</b>	threshold voltage shift due to small size effect
<b>*MUEPHS</b>	mobility modification due to small size
<b>*MUEPSP</b>	mobility modification due to small size
<b>*VOVERS</b>	modification of maximum velocity due to small size
<b>*VOVERSP</b>	modification of maximum velocity due to small size

## 13 Effects of the Source/Drain Diffusion Length for Shallow Trench Isolation (STI) Technologies

The diffusion length,  $L_{od}$  between MOSFET gate and STI edge affects the MOSFET characteristics.

The influence is observed mainly in  $V_{th}$  and in the saturation current. The  $V_{th}$  change is attributed to a change of the pocket impurity concentration and modeled as

$$N_{\text{substi}} = \frac{1 + T1 \cdot T2}{1 + T1 \cdot T3} \quad (111)$$

where

$$\begin{aligned} T1 &= \frac{1}{1 + \mathbf{NSUBPSTI2}} \\ T2 &= \frac{\mathbf{NSUBPSTI1}^{\mathbf{NSUBPSTI3}}}{L_{od\_half}} \\ T3 &= \frac{\mathbf{NSUBPSTI1}^{\mathbf{NSUBPSTI3}}}{L_{od\_half\_ref}} \end{aligned} \quad (112)$$

which is used to modify the pocket concentration  $N_{\text{subp}}$  as

$$N_{\text{subp}} = N_{\text{subp}} \cdot N_{\text{substi}}. \quad (113)$$

The saturation-current change is attributed to a change of the mobility and modeled as

$$M_{\text{uesti}} = \frac{1 + T1 \cdot T2}{1 + T1 \cdot T3} \quad (114)$$

where

$$\begin{aligned} T1 &= \frac{1}{1 + \mathbf{MUESTI2}} \\ T2 &= \frac{\mathbf{MUESTI1}^{\mathbf{MUESTI3}}}{L_{od\_half}} \\ T3 &= \frac{\mathbf{MUESTI1}^{\mathbf{MUESTI3}}}{L_{od\_half\_eff}} \end{aligned} \quad (115)$$

which is used to modify the phonon mobility parameter  $M_{\text{uephonon}}$  as

$$M_{\text{uephonon}} = M_{\text{uephonon}} \cdot M_{\text{uesti}} \quad (116)$$

where  $L_{od\_half}$  and  $L_{od\_half\_eff}$  are determined in the same way as BSIM4.6.0 with model parameters **SAREF** and **SBREF** and instance parameters **SA**, **SB**, and **SD**.

The HiSIM model parameters introduced in section 13 are summarized in Table 12.

Table 12: HiSIM model parameters introduced in section 13 of this manual. # indicates instance parameters.

<b>NSUBPSTI1</b>	pocket concentration change due to diffusion-region length between gate and STI
<b>NSUBPSTI2</b>	pocket concentration change due to diffusion-region length between gate and STI
<b>NSUBPSTI3</b>	pocket concentration change due to diffusion-region length between gate and STI
<b>MUESTI1</b>	mobility change due to diffusion-region length between gate and STI
<b>MUESTI2</b>	mobility change due to diffusion-region length between gate and STI
<b>MUESTI3</b>	mobility change due to diffusion-region length between gate and STI
<b>SAREF</b>	length of diffusion between gate and STI
<b>SBREF</b>	length of diffusion between gate and STI
<b>#SA</b>	length of diffusion between gate and STI
<b>#SB</b>	length of diffusion between gate and STI
<b>#SD</b>	length of diffusion between gate and gate

## 14 Temperature Dependences

In HiSIM\_HV **TEMP** is treated as a simulation option, and temperature  $T0$  is determined as

$$T0 = \mathbf{TEMP} + \mathbf{DTEMP} \quad (117)$$

where **DTEMP** is an instance parameter describing the temperature increase from **TEMP**, thus  $T0$  is the given temperature. Whereas the temperature including the self heating effect is distinguished by  $T$

$$T = T0 + \delta T \quad (118)$$

where  $\delta T$  is the temperature increase by the self-heating effect. The temperature dependence is included automatically in the surface potentials through  $\beta$ , which is the inverse of the thermal voltage. Additionally the bandgap, the intrinsic carrier concentration, the carrier mobility, and the carrier saturation velocity are also temperature dependent. The temperature dependence of the bandgap determines the temperature dependence of  $V_{th}$  [33] and is modeled as

$$E_g = E_{gnom} - \mathbf{BGTMP1} \cdot (T - \mathbf{TNOM}) - \mathbf{BGTMP2} \cdot (T - \mathbf{TNOM})^2 \quad (119)$$

$$E_{gnom} = \mathbf{EG0} - 90.25 \cdot 10^{-6} \cdot \mathbf{TNOM} - 1.0 \cdot 10^{-7} \cdot \mathbf{TNOM}^2 \quad (120)$$

where  $T$  is the given temperature. The temperature dependence of the intrinsic carrier concentration is given by

$$n_i = n_{i0} \cdot T^{\frac{3}{2}} \cdot \exp\left(-\frac{E_g}{2q}\beta\right) \quad (121)$$

The temperature dependence of the mobility and the temperature dependence of the saturation velocity have a major influence on the temperature dependence of the  $I_{ds}$ - $V_{ds}$  characteristics under the on-current condition. They are modeled as [27]:

$$\mu_{PH}(\text{phonon}) = \frac{M_{uephonon}}{(T/\mathbf{TNOM})^{\mathbf{MUETMP}} \cdot E_{eff}^{\mathbf{MUEPH0}}} \quad (122)$$

$$V_{max} = \frac{\mathbf{VMAX}}{1.8 + 0.4(T/\mathbf{TNOM}) + 0.1(T/\mathbf{TNOM})^2 - \mathbf{VTMP} \cdot (1 - T/\mathbf{TNOM})} \quad (123)$$

$$\mu_{PHdep}(\text{phonon}) = \frac{DEP_{muephonon}}{(T/\mathbf{TNOM})^{\mathbf{DEPMUETMP}} \cdot E_{eff}^{\mathbf{DEPMUEPH0}}} \quad (124)$$

$$DEP_{vmax} = \frac{\mathbf{DEPVMAX}}{1.8 + 0.4(T/\mathbf{TNOM}) + 0.1(T/\mathbf{TNOM})^2 - \mathbf{DEPV TMP} \cdot (1 - T/\mathbf{TNOM})} \quad (125)$$

The temperature dependence of the gate current is modeled by modifying the bandgap specific for the gate current as

$$E_{gp} = E_{g0} + \mathbf{EGIG} + \mathbf{IGTEMP2} \left( \frac{1}{T} - \frac{1}{\mathbf{TNOM}} \right) + \mathbf{IGTEMP3} \left( \frac{1}{T^2} - \frac{1}{\mathbf{TNOM}^2} \right) \quad (126)$$

where  $E_{g0}$  is the bandgap at **TNOM**.

In addition to the temperature dependence of the physical quantities considered, resistances include the temperature dependence, which is modeled with the given temperature to avoid complication in parameter extraction.

#### CORDRIFT=1: default

$$\mu_{\text{drift0,temp}} = \frac{\mathbf{RDRMUE}}{(T/\mathbf{T NOM})^{\mathbf{RDRMUETMP}}} \quad (127)$$

$$V_{\text{max\_drift,temp}} = \frac{\mathbf{RDRVMAX}}{1.8 + 0.4(T/\mathbf{T NOM}) + 0.1(T/\mathbf{T NOM})^2 - \mathbf{RDRV TMP} \cdot (1 - T/\mathbf{T NOM})} \quad (128)$$

where  $V_{\text{max}}$  ( $T$ ),  $V_{\text{over}}$  and  $V_{\text{overp}}$  are temperature dependence of **VMAX**, **VOVER** and **VOVERP** in Section 10.

In addition to the temperature dependence of the physical quantities considered, resistances include the temperature dependence, which is modeled with the given temperature to avoid complication in parameter extraction.

$$\text{tempm} = \frac{1}{(T/\mathbf{T NOM})^{\mathbf{RDRMUETMP}}} \quad (129)$$

$$\mu_{\text{drift0,tempm}} = \text{tempm} \cdot \mathbf{RDRMUE} \quad (130)$$

$$\mu_{\text{source0,temp}} = \text{tempm} \cdot \mathbf{RDRMUES} \quad (131)$$

$$\text{tempv} = \frac{1}{1.8 + 0.4(T/\mathbf{T NOM}) + 0.1(T/\mathbf{T NOM})^2 - \mathbf{RDRV TMP} \cdot (1 - T/\mathbf{T NOM})} \quad (132)$$

$$V_{\text{rmax_drift,temp}} = \text{tempv} \cdot \mathbf{RDRVMAX} \quad (133)$$

$$V_{\text{rmax_source,temp}} = \text{tempv} \cdot \mathbf{RDRVMAXS} \quad (134)$$

$$R_{\text{drbb}} = \mathbf{RDRBB} + \mathbf{RDRBB TMP}(T - \mathbf{T NOM}) \quad (135)$$

#### CORDRIFT=0: old model

$$R_{\text{d0,temp}} = \mathbf{RDTEMP1} \cdot (T_0 - \mathbf{T NOM}) + \mathbf{RDTEMP2} \cdot (T_0^2 - \mathbf{T NOM}^2) \quad (136)$$

$$R_{\text{dvd,temp}} = \mathbf{RDVDTEMP1} \cdot (T_0 - \mathbf{T NOM}) + \mathbf{RDVDTEMP2} \cdot (T_0^2 - \mathbf{T NOM}^2) \quad (137)$$

Additional temperature dependences are also included with the given temperature in case they are needed.

#### CORDRIFT=1,0

$$V_{\text{max}} = V_{\text{MAX}} \cdot (1 + \mathbf{VMAXT1} \cdot (T_0 - \mathbf{T NOM}) + \mathbf{VMAXT2} \cdot (T_0^2 - \mathbf{T NOM}^2)) \quad (138)$$

$$N_{\text{invd}} = N_{\text{invd}} \cdot (1 + \mathbf{NINVDT1} \cdot (T_0 - \mathbf{T NOM}) + \mathbf{NINVDT2} \cdot (T_0^2 - \mathbf{T NOM}^2)) \quad (139)$$

where  $T_0$  in the above four equations can be replaced by  $T$  including the temperature increase due to the self-heating effect by selecting Flag **COTEMP** (see in section 28).

Furthermore, when aging simulation is performed (**CODEG=1**), temperature dependence of the trap density,  $N_{tA}$ , is considered in the following manner:

$$N_{tA}(T) = N_{tA}(\text{TNOM}) \cdot (1 + \text{TRAPTEMP1} \cdot (T_0 - \text{TNOM}) + \text{TRAPTEMP2} \cdot (T_0^2 - \text{TNOM}^2)) \quad (140)$$

The HiSIM model parameters introduced in section 14 are summarized in Table 13.

Table 13: HiSIM model parameters introduced in section 14 of this manual. \* indicates minor parameters. # indicates an instance parameter.

<b>EG0</b>	bandgap
<b>BGTMPI</b>	temperature dependence of bandgap
<b>BGTMPII</b>	temperature dependence of bandgap
<b>MUETMP</b>	temperature dependence of phonon scattering
<b>TNOM</b>	temperature selected as nominal temperature value
<b>#DTEMP</b>	temperature increase from the given temperature
<b>*VTMP</b>	temperature dependence of the saturation velocity
<b>EIG</b>	bandgap of gate current
<b>IGTEMP2</b>	temperature dependence of gate current
<b>IGTEMP3</b>	temperature dependence of gate current
<b>RDRMUE</b>	field dependent mobility in the drift region
<b>RDRMUETMP</b>	temperature dependence of resistance
<b>RDRMUEBS1</b>	1st order coefficient to $V_{bs}$ dependence in the drift region mobility
<b>RDRMUEBS2</b>	2nd order coefficient to $V_{bs}$ dependence in the drift region mobility
<b>RDRV TMP</b>	temperature dependence of resistance
<b>RDRBBT MP</b>	temperature dependence of resistance
<b>RDRV MAX</b>	saturaion velocity in the drift region
<b>RDTEMP1</b>	temperature dependence of resistance for <b>CORDRIFT=0</b>
<b>RDTEMP2</b>	temperature dependence of resistance for <b>CORDRIFT=0</b>
<b>RDVDTEMP1</b>	temperature dependence of resistance
<b>RDVDTEMP2</b>	temperature dependence of resistance
<b>NINVDT1</b>	temperature dependence of univerisal mobility model
<b>NINVDT2</b>	temperature dependence of univerisal mobility model
<b>VMAXT1</b>	temperature dependence of velocity
<b>VMAXT2</b>	temperature dependence of velocity
<b>TRAPTEMP1</b>	temperture dependence of trap density ( <b>CODEG=1</b> )
<b>TRAPTEMP2</b>	temperture dependence of trap density ( <b>CODEG=1</b> )

## 15 Resistances

Specific features of LDMOS/HVMOS originate from its highly resistive source and drift regions, sustaining high voltages applied to the MOSFETs. HiSIM\_HV 2.0.0 provides two options for modeling the drift region resistance  $R_{\text{drift}}$  enabled by the choice of the flag **CORDRIFT**. The resistance model selection is enabled as depicted in Fig. 15. With **CORDRIFT**=0, the legacy resistance model of HiSIM\_HV 1 is activated, and the new model [56] added in HiSIM\_HV 2 is selected by **CORDRIFT**=1. To switch off the resistance effect completely, the flag **CORDRIFT** together with that of **CORSRD** must be set to zero. Alternatively, when **CORDRIFT**=1, the flags **CORS** and/or **CORD** can be set to zero for switching off the resistance model on source and/or drain side respectively. Note **CORSRD** is inactive when **CORDRIFT**=1.

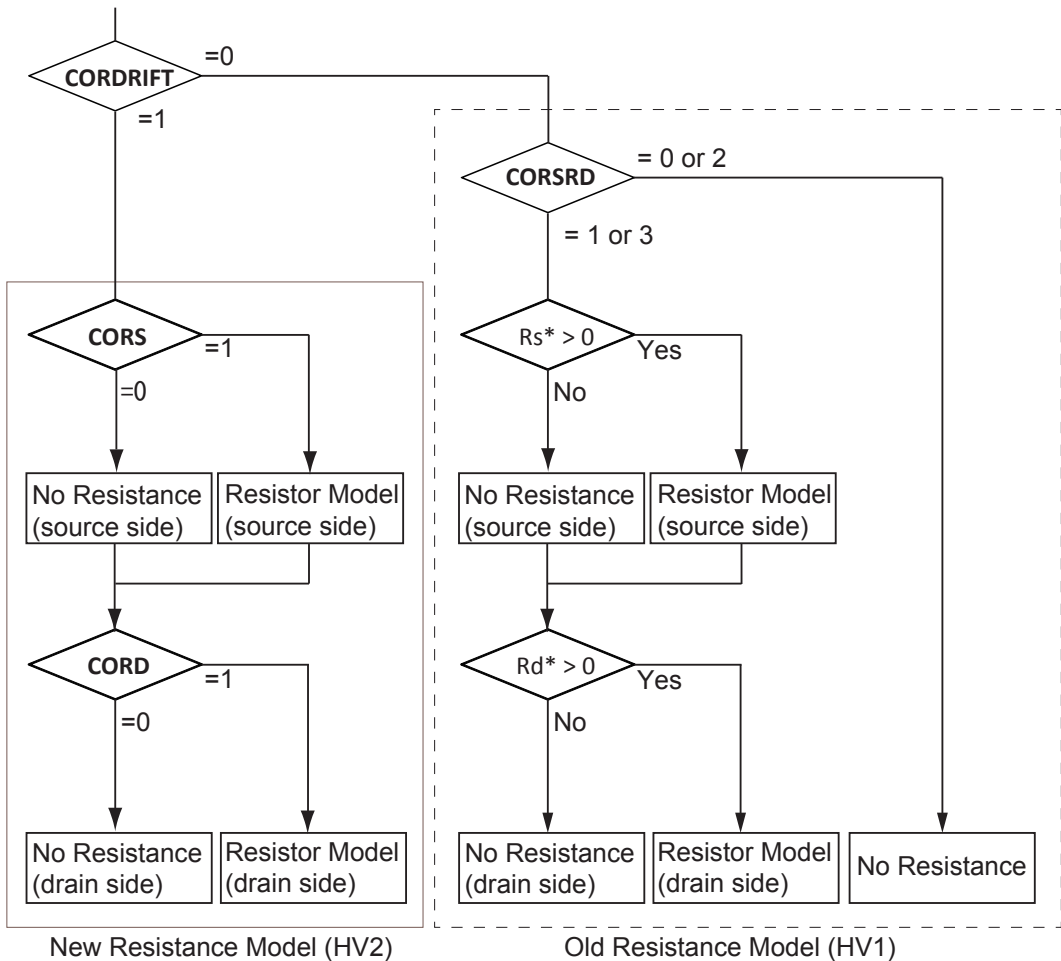


Fig. 15: Resistance model selection. The flag **CORDRIFT** selects either of the legacy HV1 resistance model (**CORDRIFT**=0) or the HV2 resistance model (**CORDRIFT**=1). For **CORDRIFT**=1, the flags **CORS** and **CORD** can be used for activation of the resistance model on source side and drain side respectively. For the use of **CORSRD**, refer to Fig. 17.  $Rd^*$  represents an estimator that consists of bias-independent part of the drain-side resistance expression and reduces to zero when drain resistance becomes zero irrespective of bias and temperature.  $Rs^*$  represents the estimator to this effect for the source-side resistance.

## 15.1 CORDRIFT=1 (default): Diffused Resistor Model

Figure 16 shows a schematic feature of the device. The potential drops  $V_{ssp}$  and  $V_{ddp}$  are calculated by SPICE iteratively.

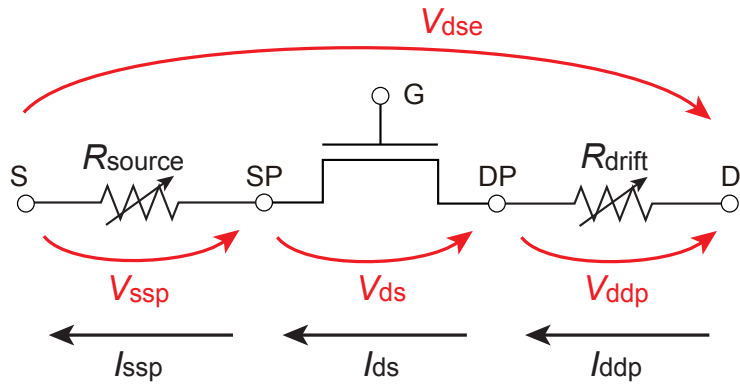


Fig. 16: Model concept

### 15.1.1 Drain side

The drain side resistance  $R_{drift}$  is written with the current flowing in the drift region  $I_{ddp}$  as

$$R_{drift} = \left( \frac{V_{ddp}}{I_{ddp}} \cdot T_{drift} + \mathbf{RSH} \cdot \mathbf{NRD} \right) \quad (141)$$

$$T_{drift} = \begin{cases} \left( \frac{L_{drift}}{\mathbf{DDRIFT} - W_{dep,sub}} \right) & (\text{if substrate terminal is activated}) \\ 1 & (\text{if substrate terminal is not activated}) \end{cases} \quad (142)$$

where **NRD** is an instance parameter describing the number of squares of the drain diffusion, and **RSH** is its the sheet resistance of the square. The first terms of the right hand side of Eq. (141) considers the resistance in the drift region, and the second term is the that in the diffusion region, which are layout dependent.

$$I_{ddp} = W_{eff,LD} \cdot \mathbf{NF} \cdot X_{ov} \cdot q \cdot N_{drift} \cdot \mu_{drift} \frac{V_{ddp}}{L_{drift} + \mathbf{RDRDL1}} \quad (143)$$

$$W_{dep,sub} = \sqrt{\frac{2\epsilon_{Si} (\mathbf{VBISUB} - (\mathbf{RDVDSUB} \cdot V_{ds} + \mathbf{RDVSUB} \cdot V_{sub,s}))}{q}} \cdot \sqrt{\frac{\mathbf{NSUBSUB}}{\mathbf{NOVER} \cdot (\mathbf{NSUBSUB} + \mathbf{NOVER})}} \quad (144)$$

where

$$L_{\text{drift}} = \mathbf{LDRIFT1} + \mathbf{LDRIFT2} \quad (145)$$

$$\mu_{\text{drift}} = \frac{\mu_{\text{drift0}}}{\left[ 1 + \left( \frac{\mu_{\text{drift0}}}{V_{\text{max,drift}}} \cdot \frac{V_{\text{ddp}}}{L_{\text{drift}}} \right)^{R_{\text{drbb}}} \right]^{\frac{1}{R_{\text{drbb}}}}} \quad (146)$$

$$\mu_{\text{drift0}} = \mu_{\text{drift0,temp}} \left( 1 + \frac{\mathbf{RDRMUEL}}{(L_{\text{gate}} \cdot 10^6) \mathbf{RDRMUELP}} \right) \quad (147)$$

$$V_{\text{max-drift}} = V_{\text{max-drift,temp}} \left( 1 + \frac{\mathbf{RDRVMAXL}}{(L_{\text{gate}} \cdot 10^6) \mathbf{RDRVMAXLP}} \right) \left( 1 + \frac{\mathbf{RDRVMAXW}}{(W_{\text{gate}} \cdot 10^6) \mathbf{RDRVMAXWP}} \right) \quad (148)$$

$$X_{\text{ov}} = W_0 - \mathbf{RDRCX} \cdot \left( \frac{W_0}{\mathbf{RDRDJUNC}} W_{\text{dep}} + \frac{W_0}{\mathbf{XLDLD}} W_{\text{junc}} \right) \quad (149)$$

$$W_0 = \sqrt{\mathbf{XLDLD}^2 + \mathbf{RDRDJUNC}^2} \quad (150)$$

$$W_{\text{dep}} = \sqrt{\frac{2\epsilon_{\text{Si}}(-\phi_{\text{s,over}})}{q \cdot \mathbf{NOVER}}} \quad (151)$$

$$W_{\text{junc}} = \sqrt{\frac{2\epsilon_{\text{Si}}(V_{\text{dps}} - V_{\text{bs}} + V_{\text{bi}})}{q} \cdot \frac{N_{\text{sub}}}{\mathbf{NOVER}(N_{\text{sub}} + \mathbf{NOVER})}} \quad (152)$$

$$\begin{aligned} N_{\text{drift}} &= \mathbf{NOVER} \left\{ 1 + \mathbf{RDRCAR} \left( \frac{V_{\text{ddp}}}{L_{\text{drift}} - \mathbf{RDRDL2}} \right) \left( 1 - \frac{1}{1 + \frac{\mu_{\text{drift0}}}{V_{\text{max,drift}}} \cdot \frac{V_{\text{ddp}}}{L_{\text{drift}}}} \right) \right\} \\ &+ \left( \mathbf{RDRQOVER} \frac{-Q'_{\text{over}}}{q} \right) \end{aligned} \quad (153)$$

As in (153),  $N_{\text{drift}}$ , carrier density in the drift region, is primarily governed by **NOVER**, the impurity concentration in the drift region. On top of that, effects of carrier injection from the channel and of carrier accumulation due to the electrostatic control by the overlapping gate are taken into account, through correctional terms accompanying **RDRCAR** and **RDRQOVER**, respectively. These may modulate the conductivity in the drift region. Hence, it modifies a gm roll-off with respect to  $V_{\text{gs}}$ . Users can adjust the gm roll-off through a ceiling of  $N_{\text{drift}}$  where auxiliary parameters such as **NDRILIM**, **NDRIDL**, and **NDRIPW** are available. Through this ceiling mechanism,  $N_{\text{drift}}$  is damped to an upper limit to avoid an unbounded increase. The upper bound can be set by **NOVER**  $\times$  **NDRILIM** where **NDRILIM** is a multiplier to **NOVER**. The damping becomes active in the proximity to that upper bound within the guardband set by **NOVER**  $\times$  **NDRIDL**. The hardness (sharpness) of the damping can be also controlled by a non negative parameter **NDRIPW** where a smaller value of **NDRIPW** results in a more gradual transition to the upper bound. These are intended for a more flexibility in fitting to gm through a fine-tuning of the drift resistance.

The potential value of  $V_{\text{ddp}}$ , the difference between the internal node “d” and the drain node “d” is calculated by circuit simulator.

### 15.1.2 Source side

The source-side resistance  $R_{\text{source}}$  is written with the current flowing in the drift region  $I_{\text{ssp}}$  as

$$R_{\text{source}} = \left( \frac{V_{\text{ssp}}}{I_{\text{ssp}}} \cdot T_{\text{drifts}} + \mathbf{RSH} \cdot \mathbf{NRS} \right) \quad (154)$$

$$T_{\text{drifts}} = \frac{L_{\text{drifts}}}{\mathbf{RDRDJUNC}} \quad (155)$$

where **NRS** is an instance parameter describing the number of squares of the source diffusion, and **RSH** is its sheet resistance of the square. The first terms of the right hand side of Eq. (154) considers the resistance in the source drift region, and the second term is the that in the source diffusion region, which is layout dependent.

$$I_{\text{ssp}} = W_{\text{eff},\text{LD}} \cdot \mathbf{NF} \cdot X_{\text{ov}} \cdot q \cdot \mathbf{NOVERS} \cdot \mu_{\text{source}} \frac{V_{\text{ssp}}}{\mathbf{LDRIFTS}} \quad (156)$$

where

$$\mu_{\text{source}} = \frac{\mu_{\text{source}0}}{\left[ 1 + \left( \frac{\mu_{\text{source}0}}{V_{\text{max\_source}}} \cdot \frac{V_{\text{ssp}}}{\mathbf{LDRIFTS}} \right)^{R_{\text{srbb}}} \right]^{\frac{1}{R_{\text{srbb}}}}} \quad (157)$$

$$\mu_{\text{source}0} = \mu_{\text{drift}0,\text{temp}} \left( 1 + \frac{\mathbf{RDRMUEL}}{(L_{\text{gate}} \cdot 10^6) \mathbf{RDRMUELP}} \right) \quad (158)$$

$$V_{\text{max\_source}} = V_{\text{max\_drift,temp}} \left( 1 + \frac{\mathbf{RDRVMAXL}}{(L_{\text{gate}} \cdot 10^6) \mathbf{RDRVMAXLP}} \right) \left( 1 + \frac{\mathbf{RDRVMAXW}}{(W_{\text{gate}} \cdot 10^6) \mathbf{RDRVMAXWP}} \right) \quad (159)$$

The potential value of  $V_{\text{ssp}}$ , the difference between the internal node  $SP$  and the drain node is calculated by circuit simulator.

## 15.2 CORDRIFT=0: old model provided in HiSIM\_HV 1

The voltage drops are in principle calculated iteratively for applied voltages to keep consistency among all device performances. However, a simple analytical description is also provided. Thus, the parasitic source and drain resistances,  $R_s$  and  $R_{\text{drift}}$ , can be considered by different optional approaches. Flag **CORSRD** is provided for the selection of one of the possible approaches. **CORSRD** = 0, 1, 2, 3 means "no resistance", "external", "analytical", "external + analytical", respectively. Options to be selected by Flag **CORSRD** are summarized in Fig. 17.

The source and the drain resistances  $R_s$  and  $R_d$  cause a voltage drop from the applied voltage biases and the effective voltages are expressed as:

$$V_{\text{gs,eff}} = V_{\text{gs}} - I_{\text{ds}} \cdot R_s \quad (160)$$

$$V_{\text{ds,eff}} = V_{\text{ds}} - I_{\text{ds}} \cdot (R_s + R_{\text{drift}}) \quad (161)$$

$$V_{\text{bs,eff}} = V_{\text{bs}} - I_{\text{ds}} \cdot R_s \quad (162)$$

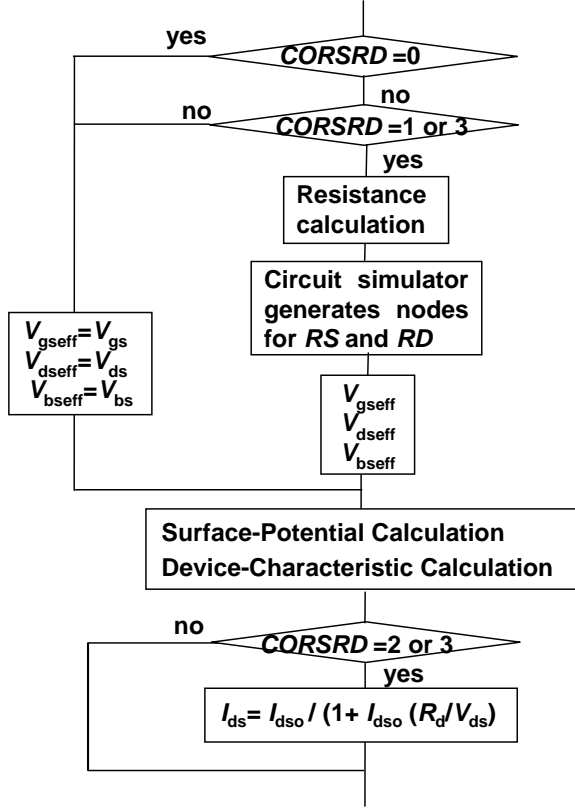


Fig. 17: Model options provided in HiSIM-LDMOS/HV for the resistance models, which are selected by Flag **CORSRD**.

for the DC condition, where the effective voltages are referred as internal node potential  $V_{dp}$ .

The source side resistance is written as

$$R_s = \frac{\mathbf{RS}}{W_{\text{eff},\text{LD}} \cdot \mathbf{NF}} + \mathbf{NRS} \cdot \mathbf{RSH} \quad (163)$$

where **NRS** is an instance parameter describing the number of squares of the source diffusion, and **RSH** is its the sheet resistance of the square. The first term of the right hand side of Eq. (163) considers the resistance in the LDD region, and the second term is that in the diffusion region, which is layout dependent.

**CORSRD=2** considered only the resistance effect on the drain current as

$$I_{ds} = \frac{I_{ds0}}{1 + I_{ds0} \frac{R_d}{V_{ds}}} \quad (164)$$

where  $I_{ds0}$  is the drain current without the resistance effect and

$$R_d = \frac{1}{W_{\text{eff}}} (R'_d \cdot V_{ds}^{\mathbf{RD21}} + V_{bs} \cdot V_{ds}^{\mathbf{RD22D}} \cdot \mathbf{RD22}) \quad (165)$$

$$RD23' \leq R'_d \leq RD23'(1 + \mathbf{RD20}) \quad (166)$$

where

$$RD23' = \mathbf{RD23} \cdot \exp(-\mathbf{RD23L} \cdot (L_{gate} \cdot 10^6)^{\mathbf{RD23LP}}) \left( 1 + \frac{\mathbf{RD23S}}{(W_{gate} \cdot 10^6 \cdot L_{gate} \cdot 10^6)^{\mathbf{RD23SP}}} \right) \quad (167)$$

The  $V_{gs}$  dependence of  $R'_d$  is considered

$$R'_d = \mathbf{RD24} (V_{gs} - \mathbf{RD25}) \quad (168)$$

The resistance effect for the case **CORSRD**=1 is described here. However, in case if it is necessary, both resistance models (internal-node approach and analytical approach) can be applied with **CORSRD**=3.

$$R_{drift} = (R_d + V_{ds} \cdot R_{DVD}) \left( 1 + \frac{\mathbf{RDVG11}}{\mathbf{RDVG12}} \cdot V_{gs} \right) \cdot (1 - V_{bs} \cdot \mathbf{RDVB}) \cdot T_{drift} \quad (169)$$

where  $T_{drift}$  is written in Eq. (142).

$$R_d = \frac{R_{d0}}{W_{eff,LD} \cdot \mathbf{NF}} \left( 1 + \frac{\mathbf{RDS}}{(W_{gate} \cdot 10^6 \cdot L_{gate} \cdot 10^6)^{\mathbf{RDSP}}} \right) \quad (170)$$

$$R_{d0} = (\mathbf{RD} + R_{d0,temp}) f_1 \cdot f_2 \quad (171)$$

$$R_{DVD} = \frac{\mathbf{RDVD} + R_{dvd,temp}}{W_{eff}} \cdot \exp(-\mathbf{RDVDL} \cdot (L_{gate} \cdot 10^6)^{\mathbf{RDVDLP}}) \cdot \left( 1 + \frac{\mathbf{RDVDS}}{(W_{gate} \cdot 10^6 \cdot L_{gate} \cdot 10^6)^{\mathbf{RDVDSP}}} \right) \cdot f_1 \cdot f_2 \cdot f_3 \quad (172)$$

$$f_1(L_{drift1}) = \frac{\mathbf{LDRIFT1}}{1\mu m} \cdot \mathbf{RDSL1} + \mathbf{RDICT1} \quad (173)$$

$$f_2(L_{drift2}) = \frac{\mathbf{LDRIFT2}}{1\mu m} \cdot \mathbf{RDSL2} + \mathbf{RDICT2} \quad (174)$$

$$f_3(L_{over})^* = 1 + \left( \mathbf{RDOV11} - \frac{\mathbf{RDOV11}}{\mathbf{RDOV12}} \right) \cdot \frac{\mathbf{LOVERLD}}{1\mu m} + (1 - \mathbf{RDOV13}) \cdot \frac{\mathbf{LOVERLD}}{1\mu m} \quad (175)$$

**LDRIFT1** and **LDRIFT2** are model parameters denoting lengths of different parts of the drift region. The source resistance in the LDMOS case does not consider a drift region and has therefore no drift length parameters. It is expected that either the second term of Eq. (175) or the third term is selected. For HiSIM.HV1.0 versions, **RDOV13** must be fixed to unity to select the second term. To select the third term **RDOV11** must be zero.

The final drift resistance  $R_{drift}$  is written as

$$R_{drift} = R_{drift} + \mathbf{RSH} \cdot \mathbf{NRD} \quad (176)$$

where **NRD** is an instance parameter describing the number of squares of the drain diffusion, and **RSH** is its the sheet resistance of the square. The first terms of the right hand side of the equation considers the resistance in the drift region, and the second term is the that in the diffusion region, which are layout dependent.

Here summarizes the selection of the resistance model for **CORDRIFT** = 0:

**CORSRD** = 0 : no resistance

**CORSRD** = 1 : solved by circuit simulator with external nodes

All model parameters included in Eq. (163), Eq. (169)–Eq. (175) are used.

Model parameters are:

**RS, NRS, RSH**

**RDVG11, RDVG12, RDVB, RDS, RDSP, NRD**

**RD, RDVD, RDVDL, RDVDLP, RDVDS, RDVDSP**

**RDSLPI, RDICT1, RDSLPII, RDICT2, RDOV11, RDOV12, RDOV13**

**RDVDSUB, RDVSUB, VBISUB, DDRIFT, NSUBSUB**

**CORSRD** = 2 : solved with the analytical equations of Eq. (164)–Eq. (168)

Model parameters are:

**RD21, RD22, RD22D, RD23, RD23L, RD23LP**

**RD23S, RD23SP, RD24, RD25, RD20**

**CORSRD** = 3 : Both **CORSRD** = 1 and **CORSRD** = 2 are considered.

At the starting of the parameter extraction, following model parameters are suggested to set to zero:

**RDVG11, RDVB, RDVD**

**RDTEMP1, RDTEMP2, RDVDTEMP1, RDVDTEMP2**

The above condition refers to the bias independent resistance.

Table 14 summaizes the minimum resistance parameters to be determined.

Table 14: HiSIM\_HV 1.2.0 resistance parameters introduced. If **RS** is not determined for the asymmetrical case, **RD** is taken.

	structure	source	drain
<b>COSYM=0</b>	<b>LDMOS</b>	<b>RS</b> (bias independent)	<b>RD</b>
<b>COSYM=1</b>	<b>symmetrical HVMOS</b>		<b>RD</b>
<b>COSYM=1</b>	<b>asymmetrical HVMOS</b>	<b>RS</b>	<b>RD</b>

### 15.3 Other resistances

The gate resistance becomes large as the gate width becomes large, which is the case for many RF circuits.

The equation for the gate-resistance calculation is taken from the BSIM4 [34] description as

$$R_g = \frac{RSHG \cdot (XGW + \frac{W_{eff}}{3 \cdot NGCON})}{NGCON \cdot (L_{drawn} - XGL) \cdot NF} \quad (177)$$

where **RSHG** is the gate sheet resistance, and others are instance parameters dependent on the layout. The flag **CORG** is provided for the inclusion of gate resistance. **CORG** = 0,1 means "no", "external" gate resistance, respectively.

Model parameters for the same substrate resistance network as BSIM4 (**RPPB**, **RPPD**, **RPPS**) are included in the model parameter list, which are also treated as instance parameters.

The HiSIM model parameters introduced in section 15 are summarized in Table 15.

Table 15: HiSIM model parameters introduced in section 15 of this manual. # indicates instance parameters. \* indicates minor parameters.

<b>RSH</b>	sheet resistance of diffusion region (drain side)
<b>RSHG</b>	gate sheet resistance
<b>RPPB</b>	substrate resistance network
<b>RPPD</b>	substrate resistance network
<b>RPPS</b>	substrate resistance network
<b>#NRS</b>	number of source squares
<b>#NRD</b>	number of drain squares
<b>#XGW</b>	distance from the gate contact to the channel edge
<b>#XGL</b>	offset of the gate length
<b>#NF</b>	number of fingers
<b>#NGCON</b>	number of gate contacts
<b>**CORDRIFT=1**</b>	
<b>RDRDL1</b>	effective $L_{\text{drift}}$ of current in drift region
<b>RDRDL2</b>	pinch-off length in drift region
<b>RDRCX</b>	exude of current flow from $X_{\text{ov}}$
<b>RDRCAR</b>	high field injection in drift region
<b>RDRDJUNC</b>	(recommended to use the same order of the magnitude as the default value) junction depth at channel/drift region (drain side)
<b>RDRBB</b>	high field mobility in drift region (drain side)
<b>RDRBBS</b>	high field mobility in drift region (source side)
<b>RDRMUE</b>	mobility in drift region (drain side)
<b>RDRMUES</b>	mobility in drift region (source side)
<b>RDRVMAX</b>	saturation velocity in drift region (drain side)
<b>RDRVMAXS</b>	saturation velocity in drift region (source side)
<b>RDRVMAXL</b>	saturation velocity $L_{\text{gate}}$ dependence
<b>RDRVMAXLP</b>	saturation velocity $L_{\text{gate}}$ dependence
<b>RDRVMAXW</b>	saturation velocity $W_{\text{gate}}$ dependence
<b>RDRVMAXWP</b>	saturation velocity $W_{\text{gate}}$ dependence
<b>RDRMUEL</b>	mobility in drift region $L_{\text{gate}}$ dependence
<b>RDRMUELP</b>	mobility in drift region $L_{\text{gate}}$ dependence
<b>RDRQOVER</b>	inclusion of the overlap charge into $R_{\text{drift}}$ (drain side)
<b>RDRQOVERS</b>	inclusion of the overlap charge into $R_{\text{drift}}$ (source side)
<b>VBI SUB</b>	built-in potential at the drift/P-substrate junction
<b>RDVDSUB</b>	$V_{\text{ds}}$ dependence of depletion width
<b>RDVSUB</b>	$V_{\text{sub}}$ dependence of depletion width
<b>DDRIFT</b>	depth of the drift region
<b>NSUBSUB</b>	impurity concentration of the substrate required for $V_{\text{sub}}$ dependence

<b>**CORDRIFT=0**</b>	
<b>RD20</b>	<b>RD23</b> boundary for <b>CORSRD=2,3</b>
<b>RD21</b>	$V_{ds}$ dependence of <b>RD</b> for <b>CORSRD=2,3</b>
<b>RD22</b>	$V_{bs}$ dependence of <b>RD</b> for <b>CORSRD=2,3</b>
<b>RD22D</b>	$V_{bs}$ dependence of <b>RD</b> for <b>CORSRD=2,3</b> with large $V_{ds}$
<b>RD23</b>	modification of <b>RD</b> for <b>CORSRD=2,3</b>
<b>*RD23L</b>	$L_{gate}$ dependence of <b>RD23</b> boundary for <b>CORSRD=2,3</b>
<b>*RD23LP</b>	$L_{gate}$ dependence of <b>RD23</b> boundary for <b>CORSRD=2,3</b>
<b>*RD23S</b>	small size dependence of <b>RD23</b> for <b>CORSRD=2,3</b>
<b>*RD23SP</b>	small size dependence of <b>RD23</b> for <b>CORSRD=2,3</b>
<b>*RD24</b>	$V_{gs}$ dependence of <b>RD</b> for <b>CORSRD=2,3</b>
<b>*RD25</b>	$V_{gs}$ dependence of <b>RD</b> for <b>CORSRD=2,3</b>
<b>VBISUB</b>	built-in potential at the drift/substrate junction
<b>RDVDSUB</b>	$V_{ds}$ dependence of depletion width
<b>RDVSUB</b>	$V_{sub}$ dependence of depletion width
<b>DDRIFT</b>	depth of the drift region
<b>NSUBSUB</b>	impurity concentration of the substrate required for $V_{sub}$ dependence

## 16 Capacitances

### 16.1 Intrinsic Capacitances

The intrinsic capacitances are derivatives of the node charges determined as

$$\begin{aligned} C_{jk} &= \delta \frac{\partial Q_j}{\partial V_k} \\ \delta = -1 &\quad \text{for } j \neq k \\ \delta = 1 &\quad \text{for } j = k \end{aligned} \tag{178}$$

HiSiM uses analytical solutions for all 9 independent intrinsic capacitances, derived from the charges as explicit functions of the surface potentials. Therefore, there are no extra model parameters for the intrinsic capacitances except the width reduction parameter **XWDC** different from that of current **XWD**, namely  $W_{\text{effc}}$  for the total capacitance calculation instead of  $W_{\text{eff}}$ , if it is necessary.

The lateral electric field along the channel induces a capacitance  $C_{Q_y}$  which significantly affects the gate capacitance in saturation [35]. The induced charge associated with  $C_{Q_y}$  is described with the surface potential values as

$$Q_y = \epsilon_{\text{Si}} W_{\text{eff}} \cdot \mathbf{NFW}_d \left( \frac{\phi_{S0} + V_{ds} - \phi_S(\Delta L)}{\mathbf{XQY}} \right) + \frac{\mathbf{XQY1}}{L_{\text{gate}}^{\mathbf{XQY2}}} V_{bs} \tag{179}$$

introducing **XQY**, a parameter determining the maximum field at the channel/drain junction independent of  $L_{\text{gate}}$ . For **XQY**=0 the charge  $Q_y$  is fixed to zero.

### 16.2 Overlap Capacitances

The overlap capacitance includes three options as summarized in Fig. 18 for the drain side and Fig. 19 for the source side. If Flags **COOVLP**=**COOVLPS**=0, the overlap capacitances are treated to be constant. If **CGSO** and **CGDO** are determined, these values are taken. If they are not determined, the values are calculated with the overlap length and oxide capacitance.

If Flags **COOVLP**=**COOVLPS**=1, the bias dependent overlap capacitances are considered. Here two models are provided: One is the surface-potential-based model and the other describes with a simple  $V_{gs}$  dependence. If **NOVER** (impurity concentration of the overlap region) is given, the surface-potential-based model is selected. If **NOVER** is set to zero, the simplified bias-dependent model is selected. In addition to the bias-dependent capacitances, **CGSO** and **CGDO** can be also added, if they are determined.

The description is focussed on the drain side. For the source side the same calculation is performed with  $V_{ds}=0$ . Two bias-dependent models are described below.

#### i) Surface-Potential-Based Model

The surface potential  $\phi_{s,over}$  is calculated in the overlap region in the same manner as in the channel region, and only the polarity is inverted from the channel. The final overlap charge equation is written with the calculated  $\phi_{SLD}$

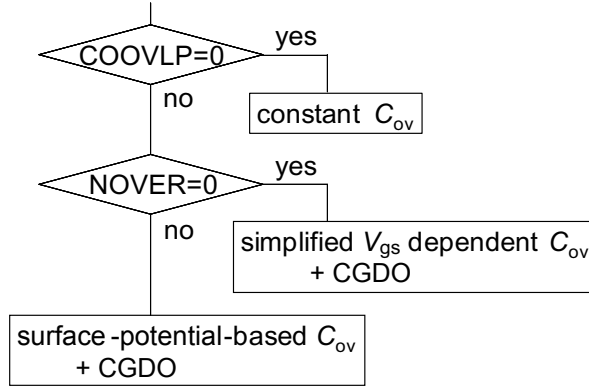


Fig. 18: Model options of the overlap capacitance at the drain side are summarized.

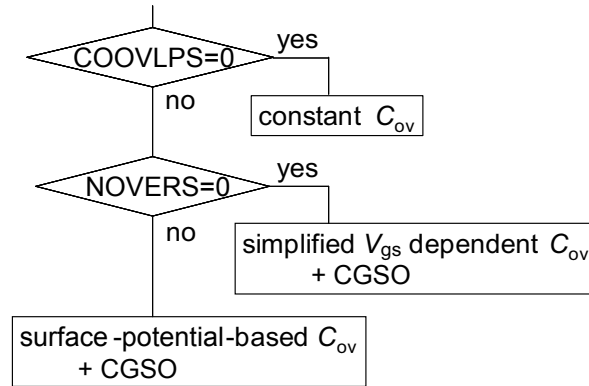


Fig. 19: Model options of the overlap capacitance at the soruce side are summarized.

a) under the depletion and the accumulation conditions

$$Q'_{\text{over}} = \left( \sqrt{\frac{2\epsilon_{\text{Si}}q\text{NOVER}}{\beta}} \sqrt{\beta\phi_{s,\text{over}} - 1} \right)$$

$$Q_{\text{over}} = W_{\text{eff}} \cdot \mathbf{NF} \cdot L_{\text{overLD,mod}} \cdot Q'_{\text{over}} \quad (180)$$

b) under the inversion condition

$$Q_{\text{over}} = W_{\text{eff}} \cdot \mathbf{NF} \cdot L_{\text{overLD,mod}} \cdot C_{\text{ox,b0}}(V_{\text{gs}} - \mathbf{VFBOVER} - \phi_{s,\text{over}}) \quad (181)$$

where  $L_{\text{overLD,mod}}$  is the length of the overlap region of the gate over drain, **NOVER** is the impurity concentration in the drift region, and **VFBOVER** is the flat-band voltage in the overlap region. The gate overlap oxide capacitance on the drain side  $C_{\text{ox,b0}}$  is written as

$$C_{\text{ox,b0}} = \frac{\epsilon_0 \mathbf{KAPPA}}{\mathbf{TOXB}} \quad (182)$$

and that on the source side is  $C_{\text{ox}}$  in Section 4. This model is selected, if **NOVER** is not equal to zero. The potential distribution occurs in the drain side of the drift region underneath the gate overlap before the strong inversion is created. This induces additional charge and the overlap capacitance at the same time. This effect is modeled as

$$Q_{\text{over,d}} = Q_{\text{over}} + W_{\text{eff}} \cdot \mathbf{NF} \cdot \mathbf{QOVADD} \cdot L_{\text{overLD,mod}} \cdot (V_{\text{dp}} - V_{\text{ch}}) \quad (183)$$

$$V_{\text{ch}} = \phi_{\text{SL}} - \phi_{\text{S0}} \quad (184)$$

Three options are provided to calculate  $\phi_s$ , which is selected by the flag **COQOVSM**:

**COQOVSM=0:** with an analytical equation excluding inversion charge

**COQOVSM=1:** with iterative procedure

**COQOVSM=2:** with an analytical equation including inversion charge

The potential value not only at the internal channel/drift junction but also that at the external node can be considered for the overlap capacitance calculation. The model parameter **CVDSOVER** has been introduced to determine the ratio of these two potential contributions as

$$C_{\text{ov}} = (1 - \mathbf{CVDSOVER}) \cdot C_{\text{ov}}(\text{int}) + \mathbf{CVDSOVER} \cdot C_{\text{ov}}(\text{ext}) \quad (185)$$

where  $C_{\text{ov}}(\text{int})$  is the overlap capacitance value calculated with the potential value at the channel/drift junction and  $C_{\text{ov}}(\text{ext})$  is that with the external potential value.

$$D_{\text{DRIFT,mod}} = \mathbf{DDRIFT} - \begin{cases} W_{\text{dep,sub}} & (\text{if substrate terminal is activated}) \\ W_{\text{junc,ov}} & (\text{if substrate terminal is not activated}) \end{cases} \quad (186)$$

$$W_{\text{junc,ov}} = \mathbf{QOVJUNC} \cdot \sqrt{\frac{2\epsilon_{\text{Si}}(-\phi_{\text{s,over}} + V_{\text{bi}})}{q}} \cdot \frac{N_{\text{sub}}}{\mathbf{NOVER}(N_{\text{sub}} + \mathbf{NOVER})} \quad (187)$$

where  $W_{\text{dep,sub}}$  is written in Eq. (144).  $D_{\text{DRIFT,mod}}$  describes the depletion extension from the surface to the bottom within the overlap region. The model parameter **QOVJUNC** is introduced to model the modification of **LOVERLD** (see Fig. 20).

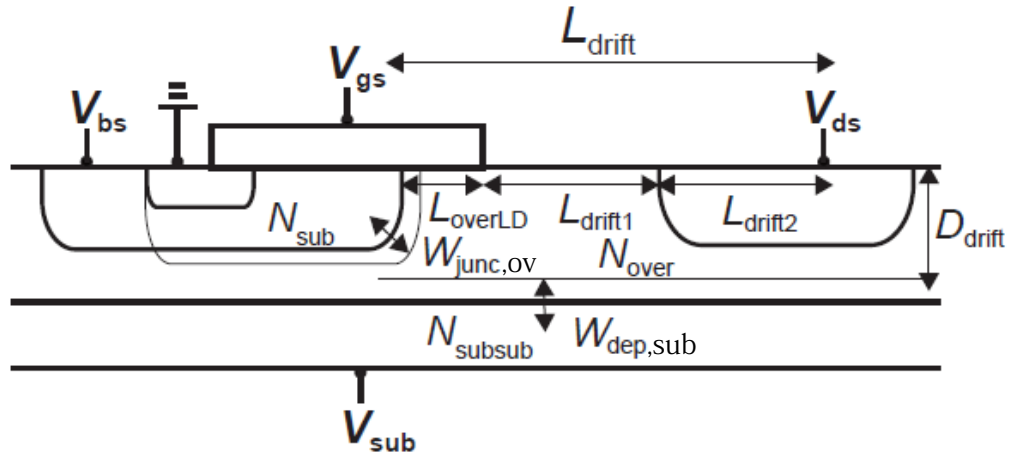


Fig. 20: Schematic of a LDMOS with the substrate node  $V_{\text{sub,s}}$

## ii) Simplified Bias-Dependent Model

If **LOVERLD** > 0 and the flag **COOVLP** = 1, the overlap charge is modeled as

$$Q_{\text{god}} = W_{\text{eff}} \cdot \mathbf{NF} \cdot C_{\text{ox},b0} [(V_{\text{gs}} - V_{\text{ds}}) \mathbf{LOVERLD} - \mathbf{OVSLP} \cdot (1.2 - (\phi_{\text{SL}} - V_{\text{ds}})) \cdot (\mathbf{OVMAG} + (V_{\text{gs}} - V_{\text{ds}}))] \quad (188)$$

The overlap capacitance Flags (**COOVLP** = **COOVLPS** = 0) calculates bias-independent overlap capacitances. User-defined values can be specified using the input parameters **CGDO** and **CGSO**. If these values are not specified, the overlap capacitances are calculated using

$$C_{\text{ov}} = -\frac{\epsilon_{\text{ox}}}{\mathbf{TOXB}} \mathbf{LOVERLD} \cdot W_{\text{eff}} \cdot \mathbf{NF} \quad (189)$$

The gate-to-bulk overlap capacitance  $C_{\text{gbo\_loc}}$  is calculated only with a user-defined value **CGBO** using

$$C_{\text{gbo\_loc}} = -\mathbf{CGBO} \cdot L_{\text{gate}} \quad (190)$$

independent of the model Flags **COOVLP** and **COOVLPS**.

### 16.3 Bias-dependent overlap length

$L_{\text{overLD,mod}}$  in Eqs. (180) and (181) can be bias-dependent due to a lateral extension of the depletion region across the channel and drift-region pn-junction.

$$L_{\text{overLD,mod}} = \mathbf{LOVERLD} - W_{\text{junc,ov}} \quad (191)$$

$$W_{\text{junc,ov}} = \mathbf{QOVJUNC} \cdot \sqrt{\frac{2\epsilon_{\text{Si}}(V_x + V_{\text{bi}})}{q} \cdot \frac{N_{\text{sub}}}{\mathbf{NOVER}(N_{\text{sub}} + \mathbf{NOVER})}} \quad (192)$$

where

$$V_x = \begin{cases} -\phi_{\text{s,over}} & (\mathbf{COOVJUNC}=0 \text{ (default)}) \\ V_{\text{db}} & (\mathbf{COOVJUNC}=1 \text{ (more reasonable implementation)}) \end{cases} \quad (193)$$

This effect can be easily turned off by setting **QOVJUNC**=0. To consider the effect, **COTRENCH** must be set to 0 because the effect conflicts with another effect introduced in Subsection 16.5.

### 16.4 Extrinsic Capacitances

The outer fringing capacitance is modeled as [37]

$$C_f = \frac{\epsilon_{\text{ox}}}{\pi/2} W_{\text{gate}} \cdot \mathbf{NF} \cdot \ln \left( 1 + \frac{\mathbf{TPOLY}}{T_{\text{ox}}} \right) \quad (194)$$

where **TPOLY** is the gate-poly thickness. This capacitance is bias independent.

### 16.5 Trench Overlap Capacitance

The depletion-extension at the channel/overlap junction along the trench overlap region is modeled. To consider the effect, **COTRENCH** must be set to 1. The overlap charge,  $Q_{\text{over}}$  can be calculated in the same way as in (180) and (181), with the remaining overlap length  $L_{\text{overLD,mod}}$  given below.

The modified overlap length along the trench gate is, instead of Eqs. (191) and (192),

$$L_{\text{overLD,mod}} = \mathbf{LOVERLD} + \mathbf{WTRENCH} - W_{\text{junc,ov}} \quad (195)$$

where

$$W_{\text{junc,ov}} = \mathbf{QOVJUNC} \cdot \sqrt{\frac{2\epsilon_{\text{Si}}(V_{\text{xdb}} + \mathbf{VBI})}{q} \cdot \frac{N_{\text{sub}}}{\mathbf{NOVER}(N_{\text{sub}} + \mathbf{NOVER})}} \quad (196)$$

where **QOVJUNC** describes the modification of the depletion-width extension at the junction due to the  $V_{\text{gs}}$  control. To obtain a smooth charge storage at the capacitor,  $V_{\text{xdb}}$  is introduced for an effective voltage difference at the junction calculated by voltage drop  $V_{\text{db}}$  between the drain and the bulk as:

$$V_{\text{xdb}} = \frac{V_{\text{db}}}{\left(1 + \left(\frac{V_{\text{db}}}{V_{\text{dbl}}}\right)^{\frac{1}{\mathbf{OLMDLT}}}\right)^{\frac{1}{\mathbf{OLMDLT}}}} \quad (197)$$

$$V_{\text{dbl}} = \frac{\mathbf{LOVERLD}^2}{k_{\text{junc}}} - \mathbf{VBI} \quad (198)$$

$$k_{\text{junc}} = \frac{2\epsilon_{\text{Si}}}{q} \cdot \frac{N_{\text{sub}}}{\mathbf{NOVER}(N_{\text{sub}} + \mathbf{NOVER})} \quad (199)$$

The overlap length along the trench bottom side could be different from that of  $L_{\text{overLD,mod}}$ . The modification of **WTRENCH** is done by the model parameter **OLMDLT**. The **OLMDLT** value is fixed, but, it could be reduced in case negative capacitance occurs.

For trench-gate structures, **CVDSOVER** must be set to zero.

The HiSIM model parameters introduced in section 16 are summarized in Table 16.

\* indicates minor parameters.

Table 16: HiSIM model parameters introduced in section 16 of this manual.

<b>XQY</b>	distance from drain junction to maximum electric field point
<b>*XQY1</b>	$V_{bs}$ dependence of $Q_y$
<b>*XQY2</b>	$L_{gate}$ dependence of $Q_y$
<b>LOVERLD</b>	overlap length of the drift region
<b>LOVERS</b>	overlap length of the source region
<b>LOVER</b>	overlap length of the source region, if <b>LOVERS</b> is not determined.
<b>VFBOVER</b>	flat-band voltage in overlap region
<b>*QOVADD</b>	additional overlap capacitance
<b>QOVJUNC</b>	$W_{junc}$ coefficient for the $L_{overLD}$ modification
<b>*CVDSOVER</b>	modification of the $C_{gg}$ peak for $V_{ds} \neq 0$ (for <b>COTRENCH</b> =0 only)
<b>OVSLP</b>	coefficient for overlap capacitance
<b>OVMAG</b>	coefficient for overlap capacitance
<b>CGSO</b>	gate-to-source overlap capacitance
<b>CGDO</b>	gate-to-drain overlap capacitance
<b>CGBO</b>	gate-to-bulk overlap capacitance
<b>TPOLY</b>	height of the gate poly-Si
<b>COTRENCH</b>	model flag for trench-gate capacitance
<b>WTRENCH</b>	trench length ( <b>COTRENCH</b> =1)
<b>OLMDLT</b>	smoothing exponent for voltage across channel/drift-region pn junction ( <b>COTRENCH</b> =1)
<b>TOXB</b>	gate overlap oxide thickness on the drain side

## 17 Leakage Currents

### 17.1 Substrate Current

The substrate current is modeled as

$$I_{\text{sub}} = X_{\text{sub}1} \cdot P_{\text{sisubsat}} \cdot I_{\text{ds}} \cdot \exp\left(-\frac{X_{\text{sub}2}}{P_{\text{sisubsat}}}\right) \quad (200)$$

where

$$X_{\text{sub}1} = \mathbf{SUB1} \cdot \left(1 + \frac{\mathbf{SUB1L}}{L_{\text{gate}}^{\mathbf{SUB1LP}}}\right) \cdot X_{\text{subTmp}} \quad (201)$$

$$X_{\text{sub}2} = \mathbf{SUB2} \cdot \left(1 + \frac{\mathbf{SUB2L}}{L_{\text{gate}}}\right) \cdot \frac{1}{X_{\text{subTmp}}} \quad (202)$$

$$P_{\text{sisubsat}} = \mathbf{SVDS} \cdot V_{\text{ds}} + \phi_{\text{S0}} - \frac{L_{\text{gate}} \cdot P_{\text{sislsat}}}{X_{\text{gate}} + L_{\text{gate}}} \quad (203)$$

$$X_{\text{gate}} = \mathbf{SLG} \cdot \left(1 + \frac{\mathbf{SLGL}}{L_{\text{gate}}^{\mathbf{SLGLP}}}\right) \quad (204)$$

$$P_{\text{sislsat}} = V_{\text{g2}} + \frac{q \cdot \epsilon_{\text{Si}} \cdot N_{\text{sub}}}{C_{\text{ox}}^2} \cdot \left\{ 1 - \sqrt{1 + \frac{2C_{\text{ox}}^2}{q \cdot \epsilon_{\text{Si}} \cdot N_{\text{sub}}} \cdot \left(V_{\text{g2}} - \frac{1}{\beta} - X_{\text{vbs}} \cdot V_{\text{bs}}\right)} \right\} \quad (205)$$

$$X_{\text{vbs}} = \mathbf{SVBS} \cdot \left(1 + \frac{\mathbf{SVBLS}}{L_{\text{gate}}^{\mathbf{SVBSLP}}}\right) \quad (206)$$

$$V_{\text{g2}} = \mathbf{SVGS} \cdot \left(1 + \frac{\mathbf{SVGSL}}{L_{\text{gate}}^{\mathbf{SVGSLP}}}\right) \cdot \frac{W_{\text{gate}}^{\mathbf{SVGSWP}}}{W_{\text{gate}}^{\mathbf{SVGSWP}} + \mathbf{SVGSW}} \cdot V'_{\text{G}} \quad (207)$$

$X_{\text{subTmp}}$  is temperature dependent as following equation

$$X_{\text{subTmp}} = 1.0 + \mathbf{SUBTMP} \cdot (T - \mathbf{TNOM}) \quad (208)$$

#### 17.1.1 Impact-Ionization Induced Bulk Potential Change

The impact ionization induces electron and hole pairs, which is the origin of the substrate current. However, not only the leakage current but also the charge distribution in the bulk is changed. This induced charge redistribution affects as the bulk potential change. This is modeled in a simple way as

$$\begin{aligned} \Delta I_{ds} = & \frac{2}{3} \sqrt{\frac{2\epsilon_{Si}qN_{sub}}{\beta}} \left[ \left\{ \beta(\phi_{SL} - V_{bs}) - 1 \right\}^{\frac{3}{2}} \frac{3}{2} \frac{\beta\Delta V_{bulk}}{\beta(\phi_{SL} - V_{bs}) - 1} \right. \\ & \left. - \left\{ \beta(\phi_{S0} - V_{bs}) - 1 \right\}^{\frac{3}{2}} \frac{3}{2} \frac{\beta\Delta V_{bulk}}{\beta(\phi_{S0} - V_{bs}) - 1} \right] \\ & - \sqrt{\frac{2\epsilon_{Si}qN_{sub}}{\beta}} \left[ \left\{ \beta(\phi_{SL} - V_{bs}) - 1 \right\}^{\frac{1}{2}} \frac{1}{2} \frac{\beta\Delta V_{bulk}}{\beta(\phi_{SL} - V_{bs}) - 1} \right. \\ & \left. - \left\{ \beta(\phi_{S0} - V_{bs}) - 1 \right\}^{\frac{1}{2}} \frac{1}{2} \frac{\beta\Delta V_{bulk}}{\beta(\phi_{S0} - V_{bs}) - 1} \right] \end{aligned} \quad (209)$$

where

$$\Delta V_{bulk} = IBPC1 \cdot (1 + \mathbf{IBPC2} \cdot \Delta V_{th}) \cdot I_{sub} \quad (210)$$

where

$$IBPC1 = \mathbf{IBPC1} \cdot \left( 1 + \frac{\mathbf{IBPC1L}}{(L_{gate} \cdot 10^6)^{\mathbf{IBPC1LP}}} \right) \quad (211)$$

and **IBPC1**, **IBPC1L**, **IBPC1LP** and **IBPC2** are model parameters.

### Impact-Ionization in Drift Region

With increased  $V_{gs}$  the impact ionization occurs in the drift region, which shows exponential characteristics as a function of  $V_{gs}$ . This type of impact-ionization induced current is modeled as

$$\begin{aligned} I_{subLD} = & I_{ds} \cdot SUBLD1 \cdot E_y \cdot L_{drift} \\ & \cdot \exp \left( \frac{-\mathbf{SUBLD2}}{E_y \cdot f(V_g V_t)} \right) \end{aligned} \quad (212)$$

$$E_y = \frac{V_{ddp} - \Delta V}{L_{drift}} \quad (213)$$

$$f(V_g V_t) = \sqrt{Q_I/q} \quad (214)$$

$$L_{drift} = \mathbf{LDRIFT1} + \mathbf{LDRIFT2} \quad (215)$$

where  $\Delta V$  is the potential change due to the stored generated carriers in the overlap region, and is modeled as

$$\Delta V = \mathbf{XPDV} \cdot T0 \cdot \mathbf{XLDLD} \cdot \exp \left( -\frac{a}{T0} \right) \quad (216)$$

$$T0 = V_{ddp} - \mathbf{XPVDTH} \cdot (1 + \mathbf{XPVDTHG} \cdot V_{gs}) \quad (217)$$

where  $a$  is unity with voltage dimension. This  $I_{subLD}$  is added to the conventional  $I_{sub}$ . The potential change  $\Delta V$  is the origin of the expansion effect [57]. The parameter  $SUBLD1$  provides the  $L_{gate}$  dependence

$$SUBLD1 = \mathbf{SUBLD1} \cdot \left( 1 + \frac{\mathbf{SUBLD1L}}{(L_{gate} \cdot 10^6)^{\mathbf{SUBLD1LP}}} \right) \quad (218)$$

## 17.2 Gate Current

All possible gate leakage currents are schematically shown in Fig. 21.

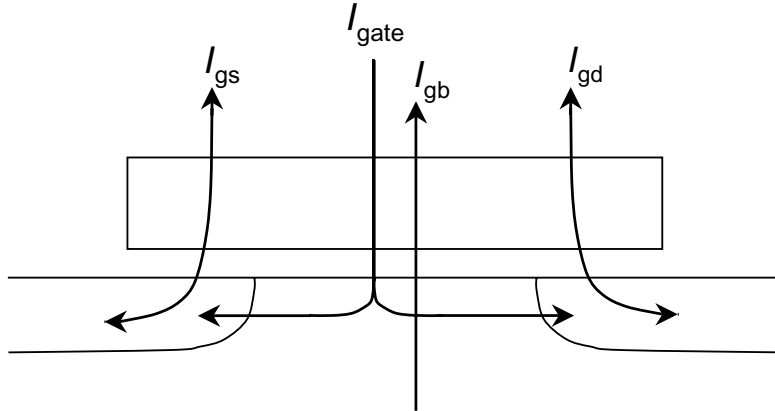


Fig. 21: Gate leakage currents considered.

### (i) Between Gate and Channel, $I_{\text{gate}}$

As for the current between gate and channel, ( $I_{\text{gate}}$ ) the direct-tunneling mechanism is considered [39]. Since measured  $I_{\text{gate}}$  shows nearly linear  $L_{\text{gate}}$  dependence, the tunneling is assumed to occur along the whole channel length. Thus the final description implemented in HiSIM is [40, 41]

$$I_{\text{gate}} = q \cdot \mathbf{GLEAK1} \cdot \frac{E^2}{E_{\text{gp}}^{\frac{1}{2}}} \cdot \exp\left(-\frac{E_{\text{gp}}^{\frac{3}{2}} \cdot \mathbf{GLEAK2}}{E}\right) \cdot \sqrt{\frac{Q_i}{\text{const0}}} \cdot W_{\text{eff}} \cdot \mathbf{NF} \cdot L_{\text{eff}} \\ \cdot \frac{\mathbf{GLEAK6}}{\mathbf{GLEAK6} + V_{\text{ds}}} \cdot \frac{\mathbf{GLEAK7}}{\mathbf{GLEAK7} + W_{\text{eff}} \cdot \mathbf{NF} \cdot L_{\text{eff}}} \quad (219)$$

where

$$E = \frac{\{V_G - \mathbf{GLEAK3} \cdot \phi_S(\Delta L)\}^2}{T_{\text{ox}}} \cdot \left(1 + \frac{E_y}{\mathbf{GLEAK5}}\right) \quad (220)$$

$$V_G = V_{\text{gs}} - \mathbf{VFBC} + \mathbf{GLEAK4} \cdot \Delta V_{\text{th}} \cdot L_{\text{eff}} \quad (221)$$

$$\Delta V_{\text{th}} = \Delta V_{\text{th,SC}} + \Delta V_{\text{th,P}} + \Delta V_{\text{th,W}} - \phi_{\text{Spg}} \quad (222)$$

**GLEAK1 – 7** are model parameters, and  $E_{\text{gp}}$  describes the temperature dependent bandgap for the gate current. The gate-channel current  $I_{\text{gate}}$  is partitioned into two terminal currents with one model parameter in the following manner.

$$I_{\text{gate}} = I_{\text{gate,s}} + I_{\text{gate,d}} \quad (223)$$

where

$$I_{\text{gate,s}} = (1 - P_{\text{partition}} \cdot I_{\text{gate}}) \quad (224)$$

$$I_{\text{gate,d}} = P_{\text{partition}} \cdot I_{\text{gate}} \quad (225)$$

where analytical description of  $P_{\text{partition}}$  is obtained by integrating the following equation

$$I_{\text{gate,d}} = \int_0^{L_{\text{eff}}} \frac{y}{L_{\text{eff}}} I_{\text{gate}}(y) dy = P_{\text{partition}} I_{\text{gate}} \quad (226)$$

The straightforward simulation result is shown in Fig. 22.

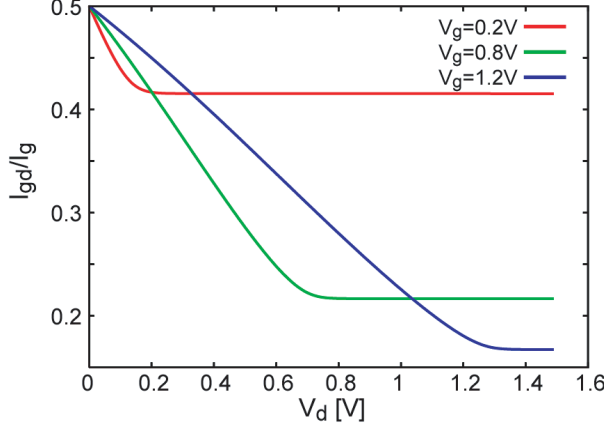


Fig. 22: Exact results of gate partitioning.

### (ii) Between Gate and Bulk, $I_{gb}$

The  $I_{gb}$  current under the accumulation condition is modeled as

$$I_{gb} = \mathbf{GLKB1} \cdot E_{gb}^2 \cdot \exp\left(-\frac{\mathbf{GLKB2}}{E_{gb}}\right) W_{\text{eff}} \cdot \mathbf{NF} \cdot L_{\text{eff}} \quad (227)$$

$$E_{gb} = -\frac{V_{gs} - \mathbf{VFBC} + \mathbf{GLKB3}}{T_{\text{ox}}} \quad (228)$$

The Fowler-Nordheim tunneling mechanism is also considered

$$I_{FN} = \frac{q \cdot \mathbf{FN1} \cdot E_{FN}^2}{E_{g12}} \cdot \exp\left(-\frac{\mathbf{FN2} \cdot E_{g32}}{E_{FN}}\right) \cdot W_{\text{eff}} \cdot \mathbf{NF} \cdot L_{\text{eff}} \quad (229)$$

where

$$E_{FN} = -\frac{\mathbf{FVBS} \cdot V_{bs} - (V_{gs} - \Delta V_{\text{th,SC}} - \Delta V_{\text{th,P}}) - \mathbf{FN3}}{T_{\text{ox}}} \quad (230)$$

$$E_{g32} = E_g \cdot E_{g12} \quad (231)$$

$$E_{g12} = \sqrt{E_g} \quad (232)$$

Total substrate current is the sum of the two components as

$$I_{gb} = I_{gb} + I_{FN} \quad (233)$$

### (iii) Between Gate and Source/Drain, $I_{gs}/I_{gd}$

The tunneling current between the gate and the source/drain overlap region is modeled as

$$I_{gs} = \text{sign} \mathbf{GLKSD1} \cdot E_{gs}^2 \exp(T_{\text{ox}}(-\mathbf{GLKSD2} \cdot V_{gs} + \mathbf{GLKSD3})) W_{\text{eff}} \cdot \mathbf{NF} \quad (234)$$

$$E_{gs} = \frac{V_{gs}}{T_{\text{ox}}} \quad (235)$$

$$I_{\text{gd}} = \text{sign} \mathbf{GLKSD1} \cdot E_{\text{gd}}^2 \exp(T_{\text{ox}}(\mathbf{GLKSD2} \cdot (-V_{\text{gs}} + V_{\text{ds}}) + \mathbf{GLKSD3})) W_{\text{eff}} \cdot \mathbf{NF} \quad (236)$$

$$E_{\text{gd}} = \frac{V_{\text{gs}} - V_{\text{ds}}}{T_{\text{ox}}} \quad (237)$$

$$\text{sign} = +1 \quad \text{for } E \leq 0$$

$$\text{sign} = -1 \quad \text{for } E \geq 0$$

### 17.3 GIDL (Gate-Induced Drain Leakage)

The GIDL current is generated at the drain junction under the accumulation condition. The  $V_{\text{ds}}$  increase induces a very narrow potential well in the drain just under the gate, causing carrier generation. Therefore, the GIDL current is strongly dependent on  $V_{\text{ds}}$ . At further reduced  $V_{\text{gs}}$  values the direct gate tunneling starts to dominate the  $I_{\text{GIDL}}$  measurements, resulting in  $V_{\text{ds}}$  independence. The  $V_{\text{ds}}$  dependent  $I_{\text{GIDL}}$  is modeled here. The generation mechanism is considered to be the direct tunneling between the above mentioned narrow potential well of length  $\Delta Y$  and the ordinary drain region.

$$I_{\text{GIDL}} = \alpha I_{\text{ds}} \Delta Y \quad (238)$$

The generation occurs only in this  $\Delta Y$  region at the drain. The final equation is

$$I_{\text{GIDL}} = q \cdot \mathbf{GIDL1} \cdot \frac{E^2}{E_g^{\frac{1}{2}}} \cdot \exp\left(-\mathbf{GIDL2} \cdot \frac{E_g^{\frac{3}{2}}}{E}\right) \cdot W_{\text{eff}} \cdot \mathbf{NF} \cdot A \quad (239)$$

where

$$E = \frac{\mathbf{GIDL3} \cdot (V_{\text{ds}} + \mathbf{GIDL4}) - V'_G}{T_{\text{ox}}} \quad (240)$$

$$V'_G = V_{\text{gs}} + \Delta V_{\text{th}} \cdot \mathbf{GIDL5} \quad (241)$$

and  $A$  is introduced after BSIM4 as

$$A = \left( \frac{V_{\text{db}}^3}{V_{\text{db}}^3 + 0.5} \right) \quad (242)$$

$$V_{\text{db}} = V_{\text{ds}} - V_{\text{bs}} \quad (243)$$

Here  $\Delta V_{\text{th}}$  is defined as

$$\Delta V_{\text{th}} = \Delta V_{\text{th,SC}} + \Delta V_{\text{th,P}} \quad (244)$$

The GISL current is calculated with the same equation as the GIDL current described above. The selection either  $I_{\text{GIDL}}$  or  $I_{\text{GISL}}$  is done by the polarity of the current flow.

The HiSIM model parameters introduced in section 17 are summarized in Table 17.

Table 17: HiSIM model parameters introduced in section 17 of this manual. \* indicates minor parameters.

<b>SUB1</b>	substrate current coefficient of magnitude
<b>SUB1L</b>	$L_{\text{gate}}$ dependence <b>SUB1</b>
<b>SUB1LP</b>	$L_{\text{gate}}$ dependence <b>SUB1</b>
<b>SUB2</b>	substrate current coefficient of exponential term
<b>SUB2L</b>	$L_{\text{gate}}$ dependence of <b>SUB2</b>
<b>SUBTMP</b>	temperature dependence of $I_{\text{sub}}$
<b>SVDS</b>	substrate current dependence on $V_{\text{ds}}$
<b>SLG</b>	substrate current dependence on $L_{\text{gate}}$
<b>SLGL</b>	substrate current dependence on $L_{\text{gate}}$
<b>SLGLP</b>	substrate current dependence on $L_{\text{gate}}$
<b>SVBS</b>	substrate current dependence on $V_{\text{bs}}$
<b>SVBSL</b>	$L_{\text{gate}}$ dependence of <b>SVBS</b>
<b>SVBSP</b>	$L_{\text{gate}}$ dependence of <b>SVBS</b>
<b>SVGS</b>	substrate current dependence on $V_{\text{gs}}$
<b>SVGSL</b>	$L_{\text{gate}}$ dependence of <b>SVGS</b>
<b>SVGSLP</b>	$L_{\text{gate}}$ dependence of <b>SVGS</b>
<b>SVGSW</b>	$W_{\text{gate}}$ dependence of <b>SVGS</b>
<b>SVGSWP</b>	$W_{\text{gate}}$ dependence of <b>SVGS</b>
<b>IBPC1</b>	impact-ionization induced bulk potential change
<b>IBPC1L</b>	$L_{\text{gate}}$ length dependence of impact-ionization induced bulk potential change
<b>IBPC1LP</b>	$L_{\text{gate}}$ length dependence of impact-ionization induced bulk potential change
<b>IBPC2</b>	impact-ionization induced bulk potential change
<b>SUBLD1</b>	substrate current induced in $L_{\text{drift}}$
<b>SUBLD1L</b>	$L_{\text{gate}}$ length dependence of substrate current induced in $L_{\text{drift}}$
<b>SUBLD1LP</b>	$L_{\text{gate}}$ length dependence of substrate current induced in $L_{\text{drift}}$
<b>SUBLD2</b>	substrate current induced in $L_{\text{drift}}$
<b>XPDV</b>	potential change for expansion effect
<b>XPVDTH</b>	potential change for expansion effect
<b>XPVDTHG</b>	potential change for expansion effect
<b>GLEAK1</b>	gate to channel current coefficient
<b>GLEAK2</b>	gate to channel current coefficient
<b>GLEAK3</b>	gate to channel current coefficient
<b>GLEAK4</b>	gate to channel current coefficient
<b>*GLEAK5</b>	gate to channel current coefficient ( short channel correction )
<b>*GLEAK6</b>	gate to channel current coefficient ( $V_{\text{ds}}$ dependence correction )
<b>*GLEAK7</b>	gate to channel current coefficient ( gate length and width dependence correction )
<b>*EGIG</b>	bandgap of gate leakage
<b>*IGTEMP2</b>	temperature dependence of gate leakage
<b>*IGTEMP3</b>	temperature dependence of gate leakage
<b>GLKB1</b>	gate to bulk current coefficient
<b>GLKB2</b>	gate to bulk current coefficient
<b>GLKB3</b>	flat-band shift for gate to bulk current
<b>GLKSD1</b>	gate to source/drain current coefficient
<b>GLKSD2</b>	gate to source/drain current coefficient
<b>GLKSD3</b>	gate to source/drain current coefficient
<b>GLPART1</b>	partitioning ratio of gate leakage current
<b>FN1</b>	coefficient of Fowler-Nordheim-current contribution
<b>FN2</b>	coefficient of Fowler-Nordheim-current contribution
<b>FN3</b>	coefficient of Fowler-Nordheim-current contribution
<b>FVBS</b>	$V_{\text{bs}}$ dependence of Fowler-Nordheim current
<b>GIDL1</b>	magnitude of the GIDL
<b>GIDL2</b>	field dependence of the GIDL
<b>GIDL3</b>	$V_{\text{ds}}$ dependence of the GIDL
<b>*GIDL4</b>	threshold of $V_{\text{ds}}$ dependence
<b>*GIDL5</b>	correction of high-field contribution

## 18 Source/Bulk and Drain/Bulk Diode Models

Four P/N junctions are available within the MOSFET structure and corresponding input voltages across the junctions are followings:

$$V_{bd} = V(DB,D) \quad (245)$$

$$V_{bdi} = V(BP,DP) \quad (246)$$

$$V_{bs} = V(SB,S) \quad (247)$$

$$V_{bsi} = V(BP,SP) \quad (248)$$

where the branch (DB,D) handles the drain-side outer diode, (BP,DP) the drain-side inner diode, (SB,S) the source-side outer diode, (BP,SP) the source-side inner diode.

### 18.1 Diode Current

The model equations for the source/bulk and drain/bulk diode currents are based on the concepts of BSIM3v3 [43], but include a number of modifications. The two regions denoted (a) and (b) in the schematic diagram of Fig. 23, are distinguished in the modeling and are treated separately.

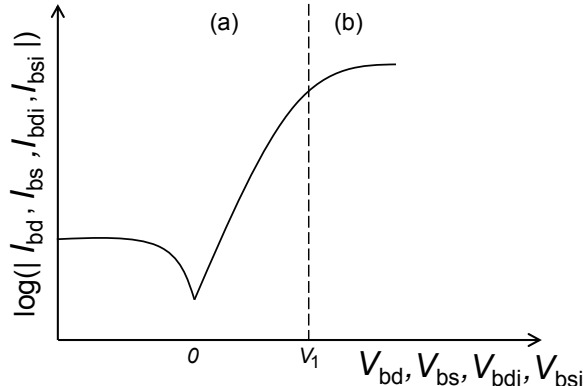


Fig. 23: The four  $I_{\text{diode}}$  currents ( $I_{bd}$ ,  $I_{bs}$ ,  $I_{bdi}$  and  $I_{bsi}$ ) are modeled separately in the two different operating regions (a) and (b). Border of the two regions is  $V_1$  which is written in (271).

Two model options: Conventional model (**CODIO** = 0) and the extended model (**CODIO** = 1) are available in the versions 2.4.0 and later.

The notations  $\Theta = S$ ,  $\theta = s$  (for source/bulk junction) and  $\Theta = D$ ,  $\theta = d$  (for drain/bulk junction) apply.

For instance, **JS0Θ** denotes **JS0S** or **JS0D**. In addition, the default values of **JS0S** and **JS0D** are **JS0** if those parameters are not given in the netlist.

### 18.1.1 Conventional Model (CODIO = 0)

$I_{bd}$  contributes to the drain-side outer branch (DB,D) and  $I_{bs}$  contributes to the source-side outer branch (SB,S). In this conventional option, the inner diode branches (BP,DP) and (BP,SP) are missing:  $I_{bdi} = 0$  and  $I_{bsi} = 0$ . The resulting diode current equations for the outer diode branches (DB,D) and (SB,S) are derived separately in the 2 regions (a) and (b) as follows.

#### a) $V_{b\theta} < V_1$ (Original Equation)

$$\begin{aligned} I_{b\theta} = & I_{sb\theta} \left\{ \exp \left( \frac{V_{b\theta}}{N_{vtm}} \right) - 1 \right\} \\ & + I_{sb\theta 2} \cdot C_{isb} \left\{ \exp \left( -\frac{V_{b\theta} \cdot \mathbf{CVB}\Theta}{N_{vtm}} \right) - 1 \right\} \\ & + \mathbf{CISBK}\Theta \left\{ \exp \left( -\frac{V_{b\theta} \cdot \mathbf{CVB}\Theta}{N_{vtm}} \right) - 1 \right\} \\ & + \mathbf{DIVX}\Theta \cdot I_{sb\theta 2} \cdot V_{b\theta} \end{aligned} \quad (249)$$

#### b) $V_{b\theta} \geq V_1$ (Linearized Equation)

$$\begin{aligned} I_{b\theta} = & I_{sb\theta} \left\{ \exp \left( \frac{V_1}{N_{vtm}} \right) - 1 \right\} + \frac{I_{sb\theta}}{N_{vtm}} \exp \left( \frac{V_1}{N_{vtm}} \right) (V_{b\theta} - V_1) \\ & + I_{sb\theta 2} \cdot C_{isb} \left\{ \exp \left( -\frac{V_{b\theta} \cdot \mathbf{CVB}\Theta}{N_{vtm}} \right) - 1 \right\} \\ & + \mathbf{CISBK}\Theta \left\{ \exp \left( -\frac{V_{b\theta} \cdot \mathbf{CVB}\Theta}{N_{vtm}} \right) - 1 \right\} \\ & + \mathbf{DIVX}\Theta \cdot I_{sb\theta 2} \cdot V_{b\theta} \end{aligned} \quad (250)$$

where  $I_{sb\theta}$  and  $I_{sb\theta 2}$  are written as

$$I_{sb\theta} = A\Theta \cdot j_s + P\Theta \cdot j_{ssw} \quad (251)$$

$$I_{sb\theta 2} = A\Theta \cdot j_{s2} + P\Theta \cdot j_{ssw2} \quad (252)$$

where  $A\Theta$  is the area parameter and  $P\Theta$  is the perimeter parameter of the drain or source region.

### 18.1.2 Extended Model (CODIO = 1)

$$I_{bd} = I_{bd,btm} + I_{bd,sws} \quad \text{contributed to the outer branch (DB,D)} \quad (253)$$

$$I_{bdi} = I_{bd,swg} \quad \text{contributed to the inner branch (BP,DP)} \quad (254)$$

$$I_{bs} = I_{bs,btm} + I_{bs,sws} \quad \text{contributed to the outer branch (SB,S)} \quad (255)$$

$$I_{bsi} = I_{bs,swg} \quad \text{contributed to the inner branch (BP,SP)} \quad (256)$$

#### a) $V_{b\theta} < V_1$ (Original Equations)

$$\begin{aligned} I_{b\theta,btm} = & I_{sb\theta,btm} \left\{ \exp \left( \frac{V_{b\theta}}{N_{vtm}} \right) - 1 \right\} \\ & + I_{sb\theta 2,btm} \cdot C_{isb} \left\{ \exp \left( -\frac{V_{b\theta} \cdot \mathbf{CVB}\Theta}{N_{vtm}} \right) - 1 \right\} \\ & + \mathbf{CISBK}\Theta \left\{ \exp \left( -\frac{V_{b\theta} \cdot \mathbf{CVB}\Theta}{N_{vtm}} \right) - 1 \right\} \\ & + \mathbf{DIVX}\Theta \cdot I_{sb\theta 2,btm} \cdot V_{b\theta} \end{aligned} \quad (257)$$

$$\begin{aligned}
I_{b\theta,sws} = & I_{sb\theta,sws} \left\{ \exp \left( \frac{V_{b\theta}}{N_{vtm}} \right) - 1 \right\} \\
& + I_{sb\theta 2,sws} \cdot C_{isb} \cdot \left\{ \exp \left( -\frac{V_{b\theta} \cdot \mathbf{CVB}\Theta}{N_{vtm}} \right) - 1 \right\} \\
& + \mathbf{CISBK}\Theta \cdot \left\{ \exp \left( -\frac{V_{b\theta} \cdot \mathbf{CVB}\Theta}{N_{vtm}} \right) - 1 \right\} \\
& + \mathbf{DIVX}\Theta \cdot I_{sb\theta 2,sws} \cdot V_{b\theta}
\end{aligned} \tag{258}$$

$$\begin{aligned}
I_{b\theta,swg} = & I_{sb\theta,swg} \left\{ \exp \left( \frac{V_{b\theta i}}{N_{vtm}} \right) - 1 \right\} \\
& + I_{sb\theta 2,swg} \cdot C_{isb} \cdot \left\{ \exp \left( -\frac{V_{b\theta i} \cdot \mathbf{CVB}\Theta}{N_{vtm}} \right) - 1 \right\} \\
& + \mathbf{CISBK}\Theta \cdot \left\{ \exp \left( -\frac{V_{b\theta i} \cdot \mathbf{CVB}\Theta}{N_{vtm}} \right) - 1 \right\} \\
& + \mathbf{DIVX}\Theta \cdot I_{sb\theta 2,swg} \cdot V_{b\theta i}
\end{aligned} \tag{259}$$

b)  $V_{b\theta} \geq V_1$  (Linearized Equations)

$$\begin{aligned}
I_{b\theta,btm} = & I_{sb\theta,btm} \left\{ \exp \left( \frac{V_1}{N_{vtm}} \right) - 1 \right\} + \frac{I_{sb\theta,btm}}{N_{vtm}} \exp \left( \frac{V_1}{N_{vtm}} \right) (V_{b\theta} - V_1) \\
& + I_{sb\theta 2,btm} \cdot C_{isb} \left\{ \exp \left( -\frac{V_{b\theta} \cdot \mathbf{CVB}\Theta}{N_{vtm}} \right) - 1 \right\} \\
& + \mathbf{CISBK}\Theta \left\{ \exp \left( -\frac{V_{b\theta} \cdot \mathbf{CVB}\Theta}{N_{vtm}} \right) - 1 \right\} \\
& + \mathbf{DIVX}\Theta \cdot I_{sb\theta 2,btm} \cdot V_{b\theta}
\end{aligned} \tag{260}$$

$$\begin{aligned}
I_{b\theta,sws} = & I_{sb\theta,sws} \left\{ \exp \left( \frac{V_1}{N_{vtm}} \right) - 1 \right\} + \frac{I_{sb\theta,sws}}{N_{vtm}} \exp \left( \frac{V_1}{N_{vtm}} \right) (V_{b\theta} - V_1) \\
& + I_{sb\theta 2,sws} \cdot C_{isb} \left\{ \exp \left( -\frac{V_{b\theta} \cdot \mathbf{CVB}\Theta}{N_{vtm}} \right) - 1 \right\} \\
& + \mathbf{CISBK}\Theta \left\{ \exp \left( -\frac{V_{b\theta} \cdot \mathbf{CVB}\Theta}{N_{vtm}} \right) - 1 \right\} \\
& + \mathbf{DIVX}\Theta \cdot I_{sb\theta 2,sws} \cdot V_{b\theta}
\end{aligned} \tag{261}$$

$$\begin{aligned}
I_{b\theta,swg} = & I_{sb\theta,swg} \left\{ \exp \left( \frac{V_1}{N_{vtm}} \right) - 1 \right\} + \frac{I_{sb\theta,swg}}{N_{vtm}} \exp \left( \frac{V_1}{N_{vtm}} \right) (V_{b\theta i} - V_1) \\
& + I_{sb\theta 2,swg} \cdot C_{isb} \left\{ \exp \left( -\frac{V_{b\theta i} \cdot \mathbf{CVB}\Theta}{N_{vtm}} \right) - 1 \right\} \\
& + \mathbf{CISBK}\Theta \left\{ \exp \left( -\frac{V_{b\theta i} \cdot \mathbf{CVB}\Theta}{N_{vtm}} \right) - 1 \right\} \\
& + \mathbf{DIVX}\Theta \cdot I_{sb\theta 2,swg} \cdot V_{b\theta i}
\end{aligned} \tag{262}$$

where

$$I_{sb\theta} = I_{sb\theta,btm} + I_{sb\theta,sws} + I_{sb\theta,swg} \tag{263}$$

where

$$I_{\text{sb}\theta,\text{btm}} = A\Theta \cdot j_s \quad (264)$$

$$I_{\text{sb}\theta,\text{sww}} = \begin{cases} (P\Theta - W_{\text{eff}} \cdot \mathbf{NF}) \cdot j_{\text{sww}} & (P\Theta > W_{\text{eff}} \cdot \mathbf{NF}) \\ 0 & (P\Theta \leq W_{\text{eff}} \cdot \mathbf{NF}) \end{cases} \quad (265)$$

$$I_{\text{sb}\theta,\text{swg}} = \begin{cases} W_{\text{eff}} \cdot \mathbf{NF} \cdot j_{\text{swwg}} & (P\Theta > W_{\text{eff}} \cdot \mathbf{NF}) \\ P\Theta \cdot j_{\text{swwg}} & (P\Theta \leq W_{\text{eff}} \cdot \mathbf{NF}) \end{cases} \quad (266)$$

$$I_{\text{sb}\theta 2,\text{btm}} = A\Theta \cdot j_{s2} \quad (267)$$

$$I_{\text{sb}\theta 2,\text{sww}} = \begin{cases} (P\Theta - W_{\text{eff}} \cdot \mathbf{NF}) \cdot j_{\text{sww2}} & (P\Theta > W_{\text{eff}} \cdot \mathbf{NF}) \\ 0 & (P\Theta \leq W_{\text{eff}} \cdot \mathbf{NF}) \end{cases} \quad (268)$$

$$I_{\text{sb}\theta 2,\text{swg}} = \begin{cases} W_{\text{eff}} \cdot \mathbf{NF} \cdot j_{\text{swwg2}} & (P\Theta > W_{\text{eff}} \cdot \mathbf{NF}) \\ P\Theta \cdot j_{\text{swwg2}} & (P\Theta \leq W_{\text{eff}} \cdot \mathbf{NF}) \end{cases} \quad (269)$$

### 18.1.3 Common Equations to CODIO Options

$$N_{\text{vtm}} = \frac{\mathbf{NJ}\Theta}{\beta} \quad (270)$$

$$V_1 = N_{\text{vtm}} \cdot \log \left( \frac{V_{\text{diffj}}}{I_{\text{sb}\theta}} + 1 \right) \quad (271)$$

$$V_{\text{diffj}} = \mathbf{VDIFFJ}\Theta \cdot (T_{\text{tnom}})^2 \quad (272)$$

$$C_{\text{isb}} = \mathbf{CISB}\Theta \cdot \exp((T_{\text{tnom}} - 1) \cdot \mathbf{CTEMP}\Theta) \quad (273)$$

The models for forward-biased current densities, describing the area and sidewall components of the source/drain regions, are given in Eqs. (275) and (276), respectively. The corresponding backward-biased current densities are given in Eqs. (278) and (279).

$$T_{\text{tnom}} = \frac{T}{\mathbf{TNOM}} \quad (274)$$

$$j_s = \mathbf{JS0}\Theta \cdot \exp \left( \frac{(E_g(T = \mathbf{TNOM}) \cdot \beta(T = \mathbf{TNOM}) - E_g\beta + \mathbf{XTI}\Theta \cdot \log(T_{\text{tnom}}))}{\mathbf{NJ}\Theta} \right) \quad (275)$$

$$j_{\text{sww}} = \mathbf{JS0SW}\Theta \cdot \exp \left( \frac{(E_g(T = \mathbf{TNOM}) \cdot \beta(T = \mathbf{TNOM}) - E_g\beta + \mathbf{XTI}\Theta \cdot \log(T_{\text{tnom}}))}{\mathbf{NJSW}\Theta} \right) \quad (276)$$

$$j_{\text{swwg}} = \mathbf{JS0SWG}\Theta \cdot \exp \left( \frac{(E_g(T = \mathbf{TNOM}) \cdot \beta(T = \mathbf{TNOM}) - E_g\beta + \mathbf{XTI}\Theta \cdot \log(T_{\text{tnom}}))}{\mathbf{NJSWG}\Theta} \right) \quad (277)$$

$$j_{s2} = \mathbf{JS0}\Theta \cdot \exp \left( \frac{(E_g(T = \mathbf{TNOM}) \cdot \beta(T = \mathbf{TNOM}) - E_g\beta + \mathbf{XTI2}\Theta \cdot \log(T_{\text{tnom}}))}{\mathbf{NJ}\Theta} \right) \quad (278)$$

$$j_{\text{ssw2}} = \mathbf{JS0SW}\Theta \cdot \exp\left(\frac{(E_g(T = \mathbf{T NOM}) \cdot \beta(T = \mathbf{T NOM}) - E_g\beta + \mathbf{XTI2}\Theta \cdot \log(T_{\text{tnom}}))}{\mathbf{NJSW}\Theta}\right) \quad (279)$$

$$j_{\text{sswg2}} = \mathbf{JS0SWG}\Theta \cdot \exp\left(\frac{(E_g(T = \mathbf{T NOM}) \cdot \beta(T = \mathbf{T NOM}) - E_g\beta + \mathbf{XTI2}\Theta \cdot \log(T_{\text{tnom}}))}{\mathbf{NJSWG}\Theta}\right) \quad (280)$$

## 18.2 Diode Capacitance

The diode capacitances of the source/bulk junction  $C_{\text{apbs}}$  and of the drain/bulk junction  $C_{\text{apbd}}$  are given by the following equations. These equations have the same basis as those used in BSIM3v3 [43], but include a number of minor modifications.

### 18.2.1 Conventional Model (CODIO = 0)

$$Q_{\text{bd}} = Q_{\text{bd,btm}}(V_{\text{bd}}) + Q_{\text{bd,sws}}(V_{\text{bd}}) + Q_{\text{bd,swg}}(V_{\text{bd}}) + Q_{\text{bd,recovery}}(V_{\text{bd}}) \quad \text{to the branch (DB,D)} \quad (281)$$

$$Q_{\text{bdi}} = 0 \quad \text{to the branch (BP,DP)} \quad (282)$$

$$Q_{\text{bs}} = Q_{\text{bs,btm}}(V_{\text{bs}}) + Q_{\text{bs,sws}}(V_{\text{bs}}) + Q_{\text{bs,swg}}(V_{\text{bs}}) \quad \text{to the branch (SB,S)} \quad (283)$$

$$Q_{\text{bsi}} = 0 \quad \text{to the branch (BP,SP)} \quad (284)$$

where the argument for each charge expression is referred to as  $V_{\text{arg}}$  in Subsubsection 18.2.3 and  $Q_{\text{bd,recovery}}$  is defined in Subsection 18.3.

### 18.2.2 Extended Model (CODIO = 1)

$$Q_{\text{bd}} = Q_{\text{bd,btm}}(V_{\text{bd}}) + Q_{\text{bd,sws}}(V_{\text{bd}}) + Q_{\text{bd,recovery}}(V_{\text{bd}}) \quad \text{to the branch (DB,D)} \quad (285)$$

$$Q_{\text{bdi}} = Q_{\text{bd,swg}}(V_{\text{bdi}}) \quad \text{to the branch (BP,DP)} \quad (286)$$

$$Q_{\text{bs}} = Q_{\text{bs,btm}}(V_{\text{bs}}) + Q_{\text{bs,sws}}(V_{\text{bs}}) \quad \text{to the branch (SB,S)} \quad (287)$$

$$Q_{\text{bsi}} = Q_{\text{bs,swg}}(V_{\text{bsi}}) \quad \text{to the branch (BP,SP)} \quad (288)$$

where the argument for each charge expression is referred to as  $V_{\text{arg}}$  in Subsubsection 18.2.3 and  $Q_{\text{bd,recovery}}$  is defined in Subsection 18.3.

### 18.2.3 Common Equations to CODIO Options

The notations  $\Theta = S, \theta = s$  (for source/bulk junction) and  
 $\Theta = D, \theta = d$  (for drain/bulk junction) apply.

For instance, **CJ** $\Theta$  denotes **CJS** or **CJD**. In addition, the default values of **CJS** and **CJD** are **CJ** if those parameters are not given in the netlist.

(i)  $V_{\text{arg}} < 0$

$$Q_{\text{b}\theta,\text{btm}}(V_{\text{arg}}) = \frac{\phi_{\text{b}\theta} \cdot c_{\text{zb}\theta} \left\{ 1 - (1 - \frac{V_{\text{arg}}}{\phi_{\text{b}\theta}})^{1-\mathbf{MJ}\Theta} \right\}}{1 - \mathbf{MJ}\Theta} \quad (289)$$

$$Q_{\text{b}\theta,\text{sww}}(V_{\text{arg}}) = \frac{\phi_{\text{b}\theta\text{sw}} \cdot c_{\text{zb}\theta\text{sw}} \left\{ 1 - (1 - \frac{V_{\text{arg}}}{\phi_{\text{b}\theta\text{sw}}} )^{1.0-\mathbf{MJSW}\Theta} \right\}}{1.0 - \mathbf{MJSW}\Theta} \quad (290)$$

$$Q_{\text{b}\theta,\text{swg}}(V_{\text{arg}}) = \frac{\phi_{\text{b}\theta\text{swg}} \cdot c_{\text{zb}\theta\text{swg}} \left\{ 1 - (1 - \frac{V_{\text{arg}}}{\phi_{\text{b}\theta\text{swg}}})^{1-\mathbf{MJSWG}\Theta} \right\}}{1 - \mathbf{MJSWG}\Theta} \quad (291)$$

(ii)  $V_{\text{arg}} \geq 0$

$$Q_{\text{b}\theta,\text{btm}}(V_{\text{arg}}) = c_{\text{zb}\theta} \cdot V_{\text{arg}} + \frac{1}{2} \frac{c_{\text{zb}\theta} \cdot \mathbf{MJ}\Theta}{\phi_{\text{b}\theta}} \cdot V_{\text{arg}}^2 \quad (292)$$

$$Q_{\text{b}\theta,\text{sww}}(V_{\text{arg}}) = c_{\text{zb}\theta\text{sw}} \cdot V_{\text{arg}} + \frac{1}{2} \frac{c_{\text{zb}\theta\text{sw}} \cdot \mathbf{MJSW}\Theta}{\phi_{\text{b}\theta\text{sw}}} \cdot V_{\text{arg}}^2 \quad (293)$$

$$Q_{\text{b}\theta,\text{swg}}(V_{\text{arg}}) = c_{\text{zb}\theta\text{swg}} \cdot V_{\text{arg}} + \frac{1}{2} \frac{c_{\text{zb}\theta\text{swg}} \cdot \mathbf{MJSWG}\Theta}{\phi_{\text{b}\theta\text{swg}}} \cdot V_{\text{arg}}^2 \quad (294)$$

where

$$c_{\text{zb}\theta} = c_{\text{j}\theta} \cdot A\Theta \quad (295)$$

$$c_{\text{zb}\theta\text{sw}} = \begin{cases} c_{\text{j}\theta\text{sw}} \cdot (P\Theta - W_{\text{eff}} \cdot \mathbf{NF}) & (P\Theta > W_{\text{eff}} \cdot \mathbf{NF}) \\ 0 & (P\Theta \leq W_{\text{eff}} \cdot \mathbf{NF}) \end{cases} \quad (296)$$

$$c_{\text{zb}\theta\text{swg}} = \begin{cases} c_{\text{j}\theta\text{swg}} \cdot W_{\text{eff}} \cdot \mathbf{NF} & (P\Theta > W_{\text{eff}} \cdot \mathbf{NF}) \\ c_{\text{j}\theta\text{swg}} \cdot P\Theta & (P\Theta \leq W_{\text{eff}} \cdot \mathbf{NF}) \end{cases} \quad (297)$$

and

$$c_{\text{j}\theta} = \mathbf{CJ}\Theta \cdot (1 + \mathbf{TCJB}\Theta \cdot (T - \mathbf{TNOM})) \quad (298)$$

$$c_{\text{j}\theta\text{sw}} = \mathbf{CJSW}\Theta \cdot (1 + \mathbf{TCJB}\Theta\mathbf{SW} \cdot (T - \mathbf{TNOM})) \quad (299)$$

$$c_{\text{j}\theta\text{swg}} = \mathbf{CJSWG}\Theta \cdot (1 + \mathbf{TCJB}\Theta\mathbf{SWG} \cdot (T - \mathbf{TNOM})) \quad (300)$$

and

$$\phi_{\text{b}\theta} = \mathbf{PB}\Theta - \mathbf{TPBB}\Theta \cdot (T - \mathbf{TNOM}) \quad (301)$$

$$\phi_{\text{b}\theta\text{sw}} = \mathbf{PBSW}\Theta - \mathbf{TPBB}\Theta\mathbf{SW} \cdot (T - \mathbf{TNOM}) \quad (302)$$

$$\phi_{\text{b}\theta\text{swg}} = \mathbf{PBSWG}\Theta - \mathbf{TPBB}\Theta\mathbf{SWG} \cdot (T - \mathbf{TNOM}) \quad (303)$$

### 18.3 Diode Recovery Effect

The recovery model introduced in "HiSIM\_HV 2.5.0" is basically compatible with "Diode\_CMC 2.0.0" and based on the dynamic carrier distribution within the N<sup>-</sup> drift layer [65, 64].

The total body-to-drain current  $I_{\text{bd},\text{total}}(t)$  including the recovery effect is written as

$$I_{\text{bd},\text{total}}(t) = I_{\text{bd}} + \frac{dQ_{\text{bd}}}{dt} \quad (304)$$

where the steady-state current term  $I_{bd}$  is defined in Subsection 18.1 and the displacement current term  $dQ_{bd}/dt$  including the recovery current originates from the total body-to-drain diode charge  $Q_{bd}$  in Subsection 18.2.

### i) Dynamic Carrier Distribution

$(W_{dep,A,NQS} \leq x \leq \mathbf{WI})$ :

$$q_{n,ex,A,NQS}(x, t) = q_{n,ex,A,NQS}(t) \cdot \exp\left(-\frac{x}{L_a}\right) \quad (305)$$

$$q_{n,ex,K,NQS}(x, t) = q_{n,ex,K,NQS}(t) \cdot \exp\left(-\frac{\mathbf{WI} - x}{L_a}\right) \quad (306)$$

### ii) Total Recovery Charge in the Drain-Side Drift Region

The total body-to-drain diode charge  $Q_{bd}$  in Subsection 18.2, includes the total body-to-drain diode recovery charge  $Q_{bd,recovery}$  written as

$$Q_{bd,recovery} = -Q_{n0} - Q_{n,ex,A,NQS}(t) - Q_{n,ex,K,NQS}(t) \quad (307)$$

where

$$\begin{aligned} Q_{n0} &= \int_0^{\mathbf{WI}} (\mathbf{AD} \cdot q \cdot \mathbf{NDIBOT}) dx \\ &= \mathbf{AD} \cdot q \cdot \mathbf{NDIBOT} \cdot \mathbf{WI} \end{aligned} \quad (308)$$

$$\begin{aligned} Q_{n,ex,A,NQS}(t) &= \int_{W_{dep,A,NQS}}^{\mathbf{WI}} q_{n,ex,A,NQS}(x, t) dx \\ &= -L_a \cdot q_{p,ex,A,NQS} \cdot \left[ \exp\left(-\frac{x}{L_a}\right) \right]_{W_{dep,A,NQS}}^{\mathbf{WI}} \\ &= -L_a \cdot q_{p,ex,A,NQS} \cdot \left[ \exp\left(-\frac{\mathbf{WI}}{L_a}\right) - \exp\left(-\frac{W_{dep,A,NQS}}{L_a}\right) \right] \end{aligned} \quad (309)$$

$$\begin{aligned} Q_{n,ex,K,NQS}(t) &= \int_{W_{dep,A,NQS}}^{\mathbf{WI}} q_{n,ex,K,NQS}(x, t) dx \\ &= L_a \cdot q_{p,ex,K,NQS} \cdot \left[ \exp\left(-\frac{(\mathbf{WI} - x)}{L_a}\right) \right]_{W_{dep,A,NQS}}^{\mathbf{WI}} \\ &= L_a \cdot q_{p,ex,K,NQS} \cdot \left[ 1 - \exp\left(-\frac{(\mathbf{WI} - W_{dep,A,NQS})}{L_a}\right) \right] \end{aligned} \quad (310)$$

#### 18.3.1 Anode-Side Carrier Distribution Model

### i) Excess Charge Density at the P<sup>+</sup>/i Junction

In the high-injection condition ( $V_{bd} \geq V_{H,A}$ ), the excess charge density shows saturated characteristic as a function of the current density. Therefore,  $exp_A$  for the DC diode current is modified as

$$exp_{A2} = exp_A \cdot \mathbf{INJ1} \exp\left(-\mathbf{INJ2} \cdot \exp(\mathbf{INJT} \cdot \ln(\frac{T_{nom}}{T})) \cdot (V_{bd} - V_{H,A})^2\right) \quad (311)$$

while in the low-injection condition ( $V_{bd} < V_{H,A}$ ), those are the same.

$$exp_{A2} = exp_A \cdot \mathbf{INJ1} \quad (312)$$

$$p_{n,A} = p_{n0} \cdot exp_{A2} \quad (313)$$

The excess charge density is written as

$$q_{n,ex,A}(V_{bd}) = q_{p,ex,A}(V_{bd}) = \mathbf{AD} \cdot q \cdot (p_{n,A} - p_{n0}) \quad (314)$$

## ii) Nonquasi-Static (NQS) Effect

The most important development in this modeling is to describe the remaining carriers after the anode-to-cathode voltage  $V_{bd}(t)$  turns down to reverse-biased condition, which is written as

$$\begin{aligned} q_{n,ex,A,NQS}(t) = q_{n,ex,A,NQS}(t - \Delta t) + \frac{\Delta t}{\mathbf{NQS} + \Delta t} \cdot \\ \left[ q_{n,ex,A} - q_{n,ex,A,NQS}(t - \Delta t) \right] \end{aligned} \quad (315)$$

where  $\tau_{NQS}$  is the time constant required for the stored charge to move out. This modeling approach originates from the carrier-transit-delay-based nonquasi-static (NQS) effect model for advanced MOS-FETs [52]. Equation (315) is transformed into a nonlinear circuit equation, and the nonlinear equation is implemented as a  $RC$  network with an internal node “charge\_A” and its node voltage is expressed as  $q_{n,ex,A,NQS}(t)$ .

### 18.3.2 Cathode-Side Carrier Distribution Model

In high-injection conditions, carriers are injected also from the cathode side.

## i) Excess Charge Density at the i/ $N^+$ Junction

In the high-injection condition ( $V_{bd} \geq V_{H,K}$ ),

$$exp_{K2} = exp_K \cdot \mathbf{INJ1} \exp \left( -\mathbf{INJ2} \cdot \exp(\mathbf{INJT} \cdot \ln(\frac{T_{nom}}{T})) \cdot (V_{bd} - V_{H,K})^2 \right) \quad (316)$$

while in the low-injection condition ( $V_{bd} < V_{H,K}$ ),

$$exp_{K2} = exp_K \cdot \mathbf{INJ1} \quad (317)$$

$$p_{n,K} = p_{n0} \cdot exp_{K2} \quad (318)$$

$$q_{n,ex,K}(V_{bd}) = q_{p,ex,K}(V_{bd}) = \mathbf{AD} \cdot q \cdot (p_{n,K} - p_{n0}) \quad (319)$$

## ii) Nonquasi-Static (NQS) Effect

$$\begin{aligned} q_{n,ex,K,NQS}(t) = q_{n,ex,K,NQS}(t - \Delta t) + \frac{\Delta t}{\mathbf{NQS} + \Delta t} \cdot \\ \left[ q_{n,ex,K} - q_{n,ex,K,NQS}(t - \Delta t) \right] \end{aligned} \quad (320)$$

where  $q_{n,ex,K,NQS}(t)$  is expressed by the node voltage of an internal node “charge\_K” of a  $RC$  network which represents the above equation.

### 18.3.3 Depletion of the Drift Region

#### i) Depletion Width

$$V_{\text{junc},A} = \mathbf{PBD} - V_{\text{bd}} \quad (321)$$

where  $V_{\text{junc},A}$  is smoothly limited to have a positive value.

$$W_{\text{dep},A} = \sqrt{\frac{2 \cdot \epsilon_S \cdot V_{\text{junc},A}}{q \cdot \mathbf{NDIBOT}}} \quad (322)$$

where  $W_{\text{dep},A}$  is smoothly limited to have a value shorter than  $\mathbf{WI}$ .

#### ii) Nonquasi-Static (NQS) Effect

In this model, dynamic suppression of the depletion width due to the recovery current is simply modelled by the NQS modeling technique as

$$\begin{aligned} W_{\text{dep},A,\text{NQS}}(t) &= W_{\text{dep},A,\text{NQS}}(t - \Delta t) + \frac{\Delta t}{\mathbf{DEPNQS} + \Delta t} \cdot \\ &\quad [W_{\text{dep},A} - W_{\text{dep},A,\text{NQS}}(t - \Delta t)] \end{aligned} \quad (323)$$

where  $\mathbf{DEPNQS}$  is the time constant for the dynamic suppression.

### 18.3.4 Carrier Injection

#### i) $P^+/\text{i}$ Junction on the Anode Side:

$$\exp_A = \exp\left(\frac{V_{\text{bd}}}{N_{\text{vtm}}}\right) \quad (324)$$

#### ii) $\text{i}/N^+$ Junction on the Cathode Side:

$$\exp_K = \exp\left(\frac{V_{\text{bd}} - (V_{\text{H,K}} - V_{\text{H,A}})}{N_{\text{vtm}}}\right) \quad (325)$$

### 18.3.5 Bias-Independent Part

#### i) Diffusion Length and the Related Quantities

Diffusion coefficients in the drift region are written as

$$D_n = \frac{kT}{q} \cdot \mathbf{MUEN} \cdot \left(\frac{T}{T_{\text{nom}}}\right)^{-1.5} \quad (326)$$

$$D_p = \frac{kT}{q} \cdot \mathbf{MUEP} \cdot \left(\frac{T}{T_{\text{nom}}}\right)^{-1.5} \quad (327)$$

$$D_a = 2 \cdot \frac{D_n \cdot D_p}{D_n + D_p} \quad (328)$$

Carrier lifetime is written as

$$\tau_{\text{HL}} = \mathbf{TAU} \cdot \left(\frac{T}{T_{\text{nom}}}\right)^{\mathbf{TAUT}} \quad (329)$$

Diffusion length in the drift region is modelled as

$$L_a = \sqrt{D_a \cdot \tau_{\text{HL}}} \quad (330)$$

## ii) Definition of the High-Injection Condition

Intrinsic carrier density in the drift region:

$$n_{i,\text{dio}} = n_{i0d} \cdot \exp \left( \frac{(E_g(T = \text{TNOM}) \cdot \beta(T = \text{TNOM}) - E_g\beta + \text{XTID} \cdot \log(T_{tnom}))}{\text{NJD}} \right) \quad (331)$$

Minority carrier density in the drift region:

$$p_{n0} = \frac{n_{i,\text{dio}}^2}{\text{NDIBOT}} \quad (332)$$

Anode-side high-injection threshold voltage:

$$V_{H,A} = \frac{\text{NJD}}{\beta} \ln \left( \frac{\text{NDIBOT}}{p_{n0}} \right) \quad (333)$$

Cathode-side high-injection threshold voltage:

$$V_{H,K} = \frac{\text{NJD}}{\beta} \cdot \left\{ \ln \left( \frac{\text{NDIBOT}}{p_{n0}} \right) + \frac{\text{WI}}{L_a} \right\} \quad (334)$$

The HiSIM model parameters introduced in section 18 are summarized in Table 18.

Table 18: HiSIM model parameters introduced in section 18 of this manual. # indicates instance parameters.

<b>JS0</b>	saturation current density
<b>JS0D</b>	saturation current density for drain junction
<b>JS0S</b>	saturation current density for source junction
<b>JS0SW</b>	sidewall saturation current density
<b>JS0SWD</b>	sidewall saturation current density for drain junction
<b>JS0SWS</b>	sidewall saturation current density for source junction
<b>JS0SWG</b>	gate-side saturation current density ( <b>CODIO</b> =1)
<b>JS0SWGD</b>	gate-side saturation current density for drain junction ( <b>CODIO</b> =1)
<b>JS0SWGS</b>	gate-side saturation current density for source junction ( <b>CODIO</b> =1)
<b>NJ</b>	emission coefficient
<b>NJD</b>	emission coefficient for drain junction
<b>NJS</b>	emission coefficient for source junction
<b>NJSW</b>	sidewall emission coefficient
<b>NJSWD</b>	sidewall emission coefficient for drain junction
<b>NJSWS</b>	sidewall emission coefficient for source junction
<b>NJSWG</b>	gate sidewall emission coefficient
<b>NJSWGD</b>	gate sidewall emission coefficient for drain junction
<b>NJSWGS</b>	gate sidewall emission coefficient for source junction
<b>XTI</b>	temperature coefficient for forward-current densities
<b>XTID</b>	temperature coefficient for forward-current densities for drain junction
<b>XTIS</b>	temperature coefficient for forward-current densities for source junction
<b>XTI2</b>	temperature coefficient for reverse-current densities
<b>XTI2D</b>	temperature coefficient for reverse-current densities for drain junction
<b>XTI2S</b>	temperature coefficient for reverse-current densities for source junction
<b>DIVX</b>	reverse current coefficient
<b>DIVXD</b>	reverse current coefficient for drain junction
<b>DIVXS</b>	reverse current coefficient for source junction
<b>CISB</b>	reverse biased saturation current
<b>CISBD</b>	reverse biased saturation current for drain junction
<b>CISBS</b>	reverse biased saturation current for source junction
<b>CVB</b>	bias dependence coefficient of <b>CISB</b>
<b>CVBD</b>	bias dependence coefficient of <b>CISB</b> for drain junction
<b>CVBS</b>	bias dependence coefficient of <b>CISB</b> for source junction
<b>CTEMP</b>	temperature coefficient of reverse currents
<b>CISBK</b>	reverse biased saturation current ( at low temperature )
<b>CISBKD</b>	reverse biased saturation current ( at low temperature ) for drain junction
<b>CISBKS</b>	reverse biased saturation current ( at low temperature ) for source junction
<b>VDIFFJ</b>	diode threshold voltage between source/drain and substrate
<b>VDIFFJD</b>	diode threshold voltage between drain and substrate
<b>VDIFFJS</b>	diode threshold voltage between source and substrate

<b>CJ</b>	bottom junction capacitance per unit area at zero bias
<b>CJD</b>	bottom junction capacitance per unit area at zero bias for drain junction
<b>CJS</b>	bottom junction capacitance per unit area at zero bias for source junction
<b>CJSW</b>	source/drain sidewall junction cap. grading coefficient per unit length at zero bias
<b>CJSWD</b>	drain sidewall junction cap. grading coefficient per unit length at zero bias
<b>CJSWS</b>	source sidewall junction cap. grading coefficient per unit length at zero bias
<b>CJSWG</b>	source/drain sidewall junction capacitance per unit length at zero bias
<b>CJSWGD</b>	drain sidewall junction capacitance per unit length at zero bias
<b>CJSWGS</b>	source sidewall junction capacitance per unit length at zero bias
<b>MJ</b>	bottom junction capacitance grading coefficient
<b>MJD</b>	bottom junction capacitance grading coefficient for drain junction
<b>MJS</b>	bottom junction capacitance grading coefficient for source junction
<b>MJSW</b>	source/drain sidewall junction capacitance grading coefficient
<b>MJSWD</b>	drain sidewall junction capacitance grading coefficient
<b>MJSWS</b>	source sidewall junction capacitance grading coefficient
<b>MJSWG</b>	source/drain gate sidewall junction capacitance grading coefficient
<b>MJSWGD</b>	drain gate sidewall junction capacitance grading coefficient
<b>MJSWGS</b>	source gate sidewall junction capacitance grading coefficient
<b>PB</b>	bottom junction build-in potential
<b>PBD</b>	bottom junction build-in potential for drain junction
<b>PBS</b>	bottom junction build-in potential for source junction
<b>PBSW</b>	source/drain sidewall junction build-in potential
<b>PBSWD</b>	drain sidewall junction build-in potential
<b>PBSWS</b>	source sidewall junction build-in potential
<b>PBSWG</b>	source/drain gate sidewall junction build-in potential
<b>PBSWGD</b>	drain gate sidewall junction build-in potential
<b>PBSWGS</b>	source gate sidewall junction build-in potential
<b>TCJB</b>	temperature dependence of drain-side diode capacitance
<b>TCJBDSW</b>	temperature dependence of drain-side diode capacitance
<b>TCJBDSWG</b>	temperature dependence of drain-side diode capacitance
<b>TCJBSS</b>	temperature dependence of source-side diode capacitance
<b>TCJBSSW</b>	temperature dependence of source-side diode capacitance
<b>TCJBSSWG</b>	temperature dependence of source-side diode capacitance
<b>TPBBD</b>	temperature dependence of drain-side diode capacitance
<b>TPBBDSW</b>	temperature dependence of drain-side diode capacitance
<b>TPBBDSWG</b>	temperature dependence of drain-side diode capacitance
<b>TPBBS</b>	temperature dependence of source-side diode capacitance
<b>TPBBSSW</b>	temperature dependence of source-side diode capacitance
<b>TPBBSSWG</b>	temperature dependence of source-side diode capacitance
<b>NDIBOT</b>	Doping concentration of drift region
<b>INJ1</b>	For carrier density
<b>INJ2</b>	For carrier density in high-injection condition
<b>NQS</b>	Carrier delay time
<b>TAU</b>	Carrier lifetime
<b>WI</b>	Length of drift region
<b>DEPNQS</b>	Depletion delay time
<b>TAUT</b>	Temp. co of carrier lifetime
<b>INJT</b>	Temp. co of carrier density in high-injection condition
<b>#AD</b>	junction area of the drain contact
<b>#PD</b>	junction periphery of the drain contact
<b>#AS</b>	junction area of the source contact
<b>#PS</b>	junction periphery of the source contact

## 19 Break Down Models

### 19.1 Hard Break Down Model

This model accounts for junction avalanche breakdown at drain.

$$I_{\text{hbbreak}} = \mathbf{HBDF} \cdot \exp(\beta \cdot (V_{\text{dse}} - HB_{\text{dv}})) \quad (335)$$

**COHBD=1:** refers to the monotonous increasing breakdown voltage with increased Vgs

$$HB_{\text{dv}} = HBDC_{\text{eff}} \quad (\text{if } V_{\text{gs}} < \mathbf{HBDB}) \quad (336)$$

$$HB_{\text{dv}} = HB_{\text{dv,base}} \quad (\text{if } V_{\text{gs}} \geq \mathbf{HBDB}) \quad (337)$$

**COHBD=-1:** refers to the monotonous decresing breakdown voltage with increased Vgs

$$HB_{\text{dv}} = HB_{\text{dv,base}} \quad (\text{if } V_{\text{gs}} \leq \mathbf{HBDB}) \quad (338)$$

$$HB_{\text{dv}} = HBDC_{\text{eff}} \quad (\text{if } V_{\text{gs}} > \mathbf{HBDB}) \quad (339)$$

$$HB_{\text{dv,base}} = \mathbf{HBDA} \cdot (V_{\text{gs}} - \mathbf{HBDB})^2 + HBDC_{\text{eff}} \quad (340)$$

where  $HB_{\text{dv}}$  means hard break down voltage and **HBDA**, **HBDB**, and **HBDC** are model parameters.

When **COHBD=0**, hard break down current is not calculated.

Tempetature dependence is considered in  $HBDC_{\text{eff}}$  in the following way as

$$HBDC_{\text{eff}} = \mathbf{HBDC} + \mathbf{HBDCTMP} \cdot (T - \mathbf{T NOM}) \quad (341)$$

### 19.2 Snapback

As impact ionization in the channel-drain region intensifies with increased Vds, large amount of carriers flow to the substrate contact. This causes the potential build-up within the substrate. At the source junction, the potential build-up works as foward biasing of the pn junction and carrier injection to the source starts. This is observed as the parasitic bipolar current. The same amount of carriers flow to the drain-substrate junction, which experience again multiplication phenomenon. These behaviors are captured in the current-driven mode rather than the voltage-driven mode of simulation and/or measurement.

To simulate snapback, set the following flags: **COSNP** = 1 (mandatory), **COISUB** = 1 (mandatory), **CORBNET** = 1 and set an appropriate value to **RBPB**. Otherwise, supply an external resistor to the bulk terminal so that the bulk potential can rise toward forward biasing of the source junction.

The parasitic bipolar current,  $I_{\text{bjt}}$ , which flows the substrate, is expressed as:

$$I_{\text{bjt}} = \left( 1 + X_{\text{sub1SNP}} \cdot P_{\text{sisubsatSNP}} \cdot \exp \left( -\frac{X_{\text{sub2SNP}}}{P_{\text{sisubsatSNP}}} \right) \right) \cdot I_{\text{bs}} \quad (342)$$

where  $I_{bs}$  represents the source/bulk junction diode current (Section 18.1).

In the above expression, the same equations for impact ionization (Section 17.1) are used except for the new parameters (**SUB1SNP**, **SUB2SNP**, and **SVDSSNP**) distinct from **SUB1**, **SUB2**, and **SVDS**, respectively, as follows:

$$X_{\text{sub1SNP}} = \mathbf{SUB1SNP} \cdot \left( 1 + \frac{\mathbf{SUB1L}}{L_{\text{gate}}^{\mathbf{SUB1LP}}} \right) \cdot X_{\text{subTmp}} \quad (343)$$

$$X_{\text{sub2SNP}} = \mathbf{SUB2SNP} \cdot \left( 1 + \frac{\mathbf{SUB2L}}{L_{\text{gate}}} \right) \cdot \frac{1}{X_{\text{subTmp}}} \quad (344)$$

$$P_{\text{sislsatSNP}} = \mathbf{SVDSSNP} \cdot V_{ds} + \phi_{s0} - \frac{L_{\text{gate}} \cdot P_{\text{sislsat}}}{X_{\text{gate}} + L_{\text{gate}}} \quad (345)$$

Those new parameters can be used for fitting a folded part of I-V characteristics during the current-driven measurement.

The HiSIM model parameters introduced in section 18 are summarized in Table 19.

Table 19: HiSIM model parameters introduced in section 19 of this manual. # indicates instance parameters.

<b>HBDA</b>	coeff. for hard break down voltage
<b>HBDB</b>	coeff. for hard break down voltage
<b>HBDC</b>	coeff. for hard break down voltage
<b>HBDF</b>	coeff. for hard break down voltage
<b>HBDCTMP</b>	temperature dependence of <b>HBDC</b>
<b>SUB1SNP</b>	impact ionization parameter for snapback
<b>SUB2SNP</b>	impact ionization parameter for snapback
<b>SVDSSNP</b>	impact ionization parameter for snapback

## 20 Noise Models

### 20.1 $1/f$ Noise Model

The  $1/f$  noise is caused by both the carrier fluctuation and the mobility fluctuation. The final description for the drift-diffusion model is [44]

$$S_{I_{ds}} = \frac{I_{ds}^2 \mathbf{NFTRP}}{\beta f(L_{\text{eff}} - \Delta L) W_{\text{eff}} \cdot \mathbf{NF}} \left[ \frac{1}{(N_0 + N^*)(N_L + N^*)} + \frac{2\mu E_y \mathbf{NFALP}}{N_L - N_0} \ln \left( \frac{N_L + N^*}{N_0 + N^*} \right) + (\mu E_y \mathbf{NFALP})^2 \right] \quad (346)$$

where the parameters **NFALP** and **NFTP** represent the contribution of the mobility fluctuation and the ratio of trap density to attenuation coefficient, respectively.  $N_0$  and  $N_L$  are carrier densities at source side and drain side or pinch-off point, respectively, as calculated in HiSIM.  $N^*$  is written as

$$N^* = \frac{C_{\text{ox}} + C_{\text{dep}} + \mathbf{CIT}}{q\beta} \quad (347)$$

where  $C_{\text{dep}}$  is the depletion capacitance calculated with  $\phi_s$ . **CIT** is the capacitance caused by the interface-trapped carriers and is normally fixed to be zero.

$$N_{\text{flick}} = S_{I_{ds}} \cdot f^{\mathbf{FALPH}} \quad (348)$$

is calculated in HiSIM, where **FALPH** has been introduced to model the deviation from the exact  $1/f$  characteristic.

### 20.2 Thermal Noise Model

Van der Ziel derived the equation for the spectral density of the thermal drain-noise current at temperature  $T$  by integrating the transconductance along the channel direction  $y$  based on the Nyquist theorem [45]

$$S_{\text{id}} = \frac{4kT}{L_{\text{eff}}^2} \int g_{\text{ds}}(y) dy = 4kT g_{\text{ds}0} \gamma \quad (349)$$

Here  $k$ ,  $I_{\text{ds}}$ ,  $g_{\text{ds}}(y)$ ,  $g_{\text{ds}0}$ ,  $\gamma$  are Boltzmann's constant, drain current, position-dependent channel conductance, channel conductance at  $V_{\text{ds}} = 0$ , and drain-noise coefficient, respectively. In HiSIM the integration is performed with the surface potential  $\phi_s$  instead of the channel position as [46, 47]

$$S_{\text{id}} = \frac{4kT}{L_{\text{eff}}^2 I_{\text{ds}}} \int g_{\text{ds}}^2(\phi_s) d\phi_s \quad (350)$$

$$g_{\text{ds}}(\phi_s) = \frac{W_{\text{eff}} \cdot \mathbf{NF}}{L_{\text{eff}}} \beta \frac{d(\mu(\phi_s) f(\phi_s))}{d\phi_s} \quad (351)$$

Here  $f(\phi_s)$  is a characteristic function of HiSIM related to the carrier concentration [48]. The final equations for  $S_{\text{id}}$  in our compact-modeling approach, obtained after solving the integral of Eq. (350), become functions of the self-consistent surface potentials as well as the surface-potential derivatives at source and drain.

$$S_{\text{id}} = 4kT \frac{W_{\text{eff}} \cdot \mathbf{NFC}_{\text{ox}} V g V t \mu}{(L_{\text{eff}} - \Delta L)} \frac{(1 + 3\eta + 6\eta^2)\mu_d^2 + (3 + 4\eta + 3\eta^2)\mu_d\mu_s + (6 + 3\eta + \eta^2)\mu_s}{15(1 + \eta)\mu_{\text{av}}^2} \quad (352)$$

where  $\mu_s$ ,  $\mu_d$  and  $\mu_{av}$  are mobilities at the source side, the drain side, and averaged, respectively.

$$\eta = 1 - \frac{(\phi_{SL} - \phi_{S0}) + \chi(\phi_{SL} - \phi_{S0})}{V_g V_t} \quad (353)$$

$$\chi = 2 \frac{cnst0}{C_{ox}} \left[ \left[ \frac{2}{3} \frac{1}{\beta} \frac{\{\beta(\phi_{SL} - V_{bs}) - 1\}^{\frac{3}{2}} - \{\beta(\phi_{S0} - V_{bs}) - 1\}^{\frac{3}{2}}}{\phi_{SL} - \phi_{S0}} \right] - \sqrt{\beta(\phi_{S0} - V_{bs}) - 1} \right] \quad (354)$$

$V_g V_t$  is equal to the carrier density at the source side divided by the oxide capacitance.

Thus no additional model parameters are required for the thermal noise model.

$$N_{thrm1} = S_{id}/4kT \quad (355)$$

is calculated in HiSIM.

### 20.3 Induced Gate Noise Model

No additional model parameters are required for the induced gate noise model.

$$N_{igate} = S_{igate}/f^2 \quad (356)$$

is calculated in HiSIM. Explicit model equation were presented at SISPAD in 2006 [49].

### 20.4 Coupling Noise Model

No additional model parameters are required for the coupling noise model.

$$N_{cross} = \frac{S_{igid}}{\sqrt{S_{igate} \cdot S_{id}}} \quad (357)$$

is calculated in HiSIM. Explicit model equation were presented at SISPAD in 2006 [49].

The HiSIM model parameters introduced in section 20 are summarized in Table 20.

Table 20: HiSIM model parameters introduced in section 20 of this manual. \* indicates a minor parameter.

<b>NFTRP</b>	ratio of trap density to attenuation coefficient
<b>NFALP</b>	contribution of the mobility fluctuation
<b>*CIT</b>	capacitance caused by the interface trapped carriers
<b>FALPH</b>	power of $f$ describing deviation of $1/f$

## 21 Non-Quasi-Static (NQS) Model

### 21.1 Carrier Formation

To consider the carrier transit delay in HiSIM, the carrier formation is modeled as [50, 51, 52]

$$q(t_i) = \frac{q(t_{i-1}) + \frac{\Delta t}{\tau} Q(t_i)}{1 + \frac{\Delta t}{\tau}} \quad (358)$$

where  $q(t_i)$  and  $Q(t_i)$  represent the non-quasi-static and the quasi-static carrier density at time  $t_i$ , respectively, and  $\Delta t = t_i - t_{i-1}$  is valid. The delay is determined by the carrier transit delay  $\tau$  and the time interval in the circuit simulation  $\Delta t$ .

### 21.2 Delay Mechanisms

Up to weak inversion:

$$\tau_{\text{diff}} = \mathbf{DLY1} \quad (359)$$

At strong inversion:

$$\tau_{\text{cond}} = \mathbf{DLY2} \cdot \frac{Q_i}{I_{\text{ds}}} \quad (360)$$

$$\frac{1}{\tau} = \frac{1}{\tau_{\text{diff}}} + \frac{1}{\tau_{\text{cond}}} \quad (361)$$

For the formation of bulk carriers:

$$\tau_B = \mathbf{DLY3} \cdot C_{\text{ox}} \quad (362)$$

where **DLY3** is a constant coefficient and  $C_{\text{ox}}$  is the oxide capacitance. From the HiSIM\_HV 1.1.0 version this NQS model is implemented in the newwork form as shown in Fig. 24.

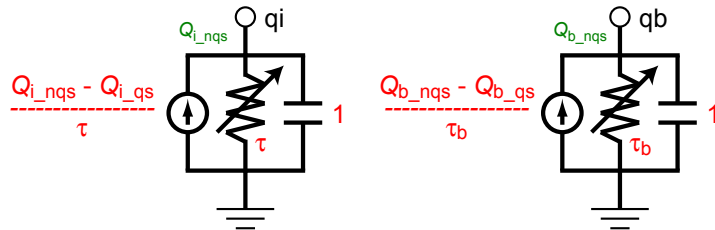


Fig. 24: NQS model implementation into circuit simulator.

### 21.3 Time-Domain Analysis

The total drain/source/bulk terminal currents are derived from the superposition of the transport current and the charging current. The transport current is a function of the instantaneous terminal voltages and is approximated by the steady-state solution. The source/drain/bulk charging currents are the time derivatives of the associated non-quasi-static charges,  $q_S$ ,  $q_D$ , and  $q_B$ , respectively.

For LDMOS/HVMOS, carrier transit delay effect in the drift region is included as the *RC* delay. The resistance  $R$  and the capacitance  $C$  contributing the delay are taken calculated in HiSIM\_HV. If the resistance in the drift region is large, the delay becomes automatically large.

The formation delay of the overlap charge  $Q_{\text{over}}$  is also modeled as

$$\tau_{\text{LD}} = \mathbf{DLYOV} \cdot C_{\text{ox0}} \cdot \phi_{s,\text{LD}} \quad (363)$$

where  $\phi_{s,\text{LD}}$  represents the surface potential in the overlap region.

## 21.4 AC Analysis

The load file is rewritten from the HiSIM\_HV 1.1.0 version so that the internal node is seen explicitly. Thus, the calculation procedure becomes different from the older versions, however, the formulae used for the calculation are the same.

The HiSIM model parameters introduced in section 21 are summarized in Table 21.

Table 21: HiSIM model parameters introduced in section 21 of this manual.

<b>DLY1</b>	coefficient for delay due to diffusion of carriers
<b>DLY2</b>	coefficient for delay due to conduction of carriers
<b>DLY3</b>	coefficient for RC delay of bulk carriers
<b>DLYOV</b>	coefficient for RC delay of overlap charge ( <b>CONQSOV=1</b> )

## 22 Self-Heating Effect Model

The self-heating effect is modeled with the thermal network shown in Fig. 25. The flag **COSELFHEAT** must be equal to one and **RTH0** must not be equal to zero to activate the model. The temperature node must not be zero, if the self-heating effect is switched on. The self-heating effect should be switched on/off only with the model flag **COSELFHEAT**. To avoid unrealistic temperature increase during circuit simulation, clipping has been introduced. The clipping method can be also selected by the model flag **COSELFHEAT**:

- =0 : no self-heating effect (default)
- =1 : power clipping
- =2 : temperature clipping

**COSELFHEAT**=2 is newly added from the present version. **COSELFHEAT**=2 is recommended.

The temperature node is automatically generated in circuit simulator for each device as other bias nodes. First, the model core (HiSIMhv.eval) is called to evaluate device characteristics without heating. Then, the temperature is updated considering the self-heating effect by creating the temperature node. The model core is called again to update the device characteristics with the calculated temperature  $T$ . Under the DC condition the temperature increase is calculated analytically as

$$T = T + R_{\text{th}} \cdot I_{\text{ds}} \cdot V_{\text{ds}} \quad (364)$$

where  $R_{\text{th}}$  as well as  $C_{\text{th}}$  are a function of  $W_{\text{eff}}$  as

$$R_{\text{th}} = \frac{R_{\text{th}0}}{W_{\text{eff}}} \cdot \left( \frac{1}{\text{NF}^{\text{RTH0NF}}} \right) \left( 1 + \frac{\text{RTHOL}}{(L_{\text{gate}}/10^{-6})^{\text{RTHOLP}}} \right) \left( 1 + \frac{\text{RTHOW}}{(W_{\text{gate}}/10^{-6})^{\text{RTHOWP}}} \right) \quad (365)$$

$$R_{\text{th}0} = \text{RTH0} + \text{RTHTEMP1} \cdot (T_0 - \text{TNOM}) + \text{RTHTEMP2} \cdot (T_0^2 - \text{TNOM}^2) \quad (366)$$

$$C_{\text{th}} = \text{CTH0} \cdot W_{\text{eff}} \quad (367)$$

where  $(L_{\text{gate}}/10^{-6})$  and  $(W_{\text{gate}}/10^{-6})$  or equivalently,  $(L_{\text{gate}} \cdot 10^6)$  and  $(W_{\text{gate}} \cdot 10^6)$  intend normalization to a unitless quantity, the magnitude of which stays around the unity (=1).

The model parameter **RTH0** is fitted to measured DC data, and the model parameter **CTH0** is introduced for AC fitting.

The thermal dissipation is modeled as [55]

$$T = T + R_{\text{th}} \cdot I_{\text{ds}} \cdot V'_{\text{ds}} \quad (368)$$

$$V'_{\text{ds}} = V_{\text{dsi}} + \text{POWRAT}_{\text{ratio}}(V_{\text{ds}} - V_{\text{dsi}}) \quad (369)$$

$$\text{POWRAT}_{\text{ratio}} = \text{POWRAT} + \text{PRATTEMP1} \cdot (T_0 - \text{TNOM}) + \text{PRATTEMP2} \cdot (T_0^2 - \text{TNOM}^2) \quad (370)$$

where **POWRAT** is a model parameter. The external node potential is represented by  $V_{\text{ds}}$  and the internal node potential within the drift region at the channel/drift junction is by  $V_{\text{dsi}}$ , which is calculated during the SPICE simulation.

A limiter for the temperature increase due to the self-heating effect **SHEMAX** is introduced to avoid drastic artificial temperature increase during circuit simulations.

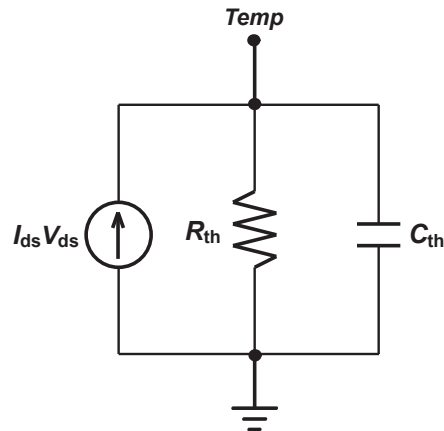


Fig. 25: Thermal Network applied for the self-heating effect.

Table 22: HiSIM model parameters introduced in section 22 of this manual.

<b>RTH0</b>	thermal resistance
<b>RTHTEMP1</b>	temperature dependence of thermal resistance
<b>RTHTEMP2</b>	temperature dependence of thermal resistance
<b>CTH0</b>	thermal capacitance
<b>RTH0L</b>	length dependence of thermal resistance
<b>RTH0LP</b>	length dependence of thermal resistance
<b>RTH0W</b>	width dependence of thermal resistance
<b>RTH0WP</b>	width dependence of thermal resistance
<b>RTH0NF</b>	number of finger dependence of thermal resistance
<b>POWRAT</b>	thermal dissipation
<b>PRATTEMP1</b>	tenperature dependence of thermal dissipation
<b>PRATTEMP2</b>	tenperature dependence of thermal dissipation
<b>SHEMAX</b>	maximum temperature increase

The HiSIM model parameters introduced in section 22 are summarized in Table 22.

## 23 Multiplication Factor

For the case of a multiple device construction the multiple factor **M** is introduced as an instance parameter. All device features such as currents and capacitances are multiplied by **M**. Noises are also multiplied by **M**.

The HiSIM model parameters introduced in section 23 are summarized in Table 23.

Table 23: HiSIM model parameters introduced in section 23 of this manual. # indicates an instance parameter.

# M	multiplication factor
-----	-----------------------

## 24 DFM Model

To support design for manufacturability (DFM) HiSIM introduces an option for considering the variation of device parameters.

Accurate prediction of device performance for a wide range of the substrate-impurity-concentration variations is secured by introducing an impurity concentration dependent mobility due to the phonon scattering as

$$M_{\text{uephonon}} = \mathbf{MUEPH1} [\mathbf{MPHDFM} \{\ln(\mathbf{NSUBCDFM}) - \ln(N_{\text{subc}})\} + 1] \\ \mathbf{NSUBP} = \mathbf{NSUBP} + (N_{\text{SUBCDFM}} - N_{\text{subc}}) \quad (371)$$

$$\mathbf{NEXT} = \mathbf{NEXT} + (\mathbf{NSUBCDFM} - N_{\text{subc}}) \quad (372)$$

where **NSUBCDFM** is an instance parameter and **MPHDFM** is a model parameter describing the mobility reduction due to the increase of the substrate impurity concentration. This model is activated if the model flag **CODFM** = 1, and NSUBCDFM is also given.

The HiSIM model parameters introduced in section 24 are summarized in Table 24.

Table 24: HiSIM model parameters introduced in section 24 of this manual. # indicates an instance parameter.

# <b>NSUBCDFM</b>	substrate impurity concentration
<b>MPHDFM</b>	mobility dependence of $N_{\text{subc}}$ due to $\mu_{\text{phonon}}$

## 25 Depletion Mode Model Option

To support depletion mode MOSFET devices, an option for considering the structural feature is introduced in HiSIM. Modeling is done for the p-Si substrate, however, it is applicable for the n-Si substrate as well. This is done automatically by determining the device “type” in netlist.

In the depletion mode MOSFET, an n layer is constructed at the channel surface of conventional MOSFET devices as shown Fig. 26 where  $N_{\text{dep}}$  denotes the carrier concentration of the n layer, and  $T_{\text{dep}}$  denotes the thickness of the n layer.

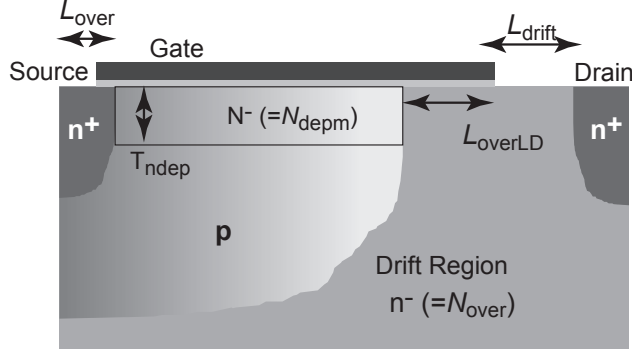


Fig. 26: Schematic of the typical depletion mode MOSFET structure and device parameters.

Fig. 27 depicts the potential and the electron carrier density distribution along the depth direction of a depletion mode device. The Poisson equation including all charges induced within the device is solved for calculating the accurate distributions under any bias conditions.  $N_{\text{dep}}^m$  takes the impurity concentration as

$$N_{\text{dep}}^m = \mathbf{NDEPM} \cdot \left( 1 + \frac{\mathbf{NDEPML}}{(L_{\text{gate}} \cdot 10^6)^{\mathbf{NDEPMLP}}} \right) \quad (373)$$

This model is activated if the model flag **CODEP** = 1 (old depletion model), 2 (old depletion model) and **CODEP** = 3 (new depletion mode). ( default = 0 : no depletion mode )

Three model options are explained in the following. To use **CODEP**=3 is suggested for better derivative characteristics.

### i) CODEP=1 : old model developed for Version 2.2.0

#### 25.1 CODEP=1 : old model developed for Version 2.2.0

In the depletion mode MOSFET model, the quasi-Fermi potential( $V_{ds,\text{eff}}$ ) for the majority carrier is written in the same way as that of the minority carrier.

$$V_{ds,\text{eff}} = \frac{V_{ds}}{\left[ 1 + \left( \frac{V_{ds}}{V_{ds,\text{sat}}} \right)^\Delta \right]^{\frac{1}{\Delta}}} \quad (374)$$

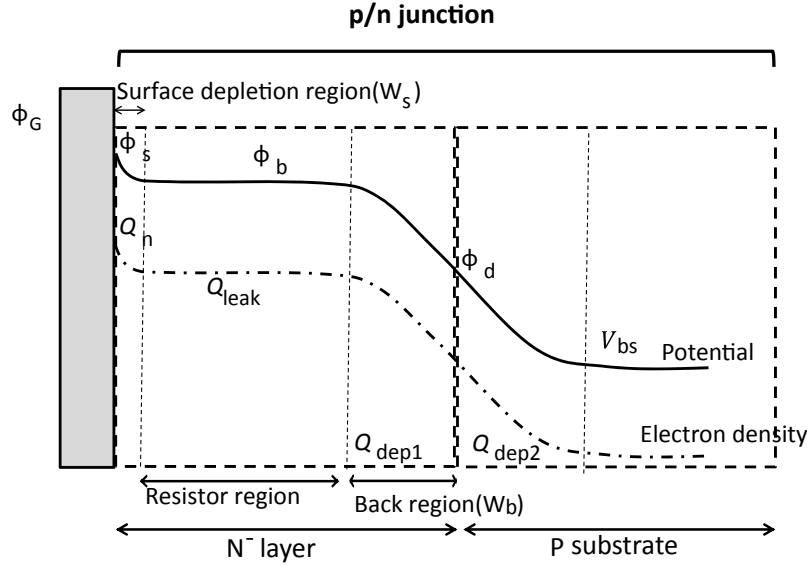


Fig. 27: Potential and electron carrier density distribution along the channel cross section of the depletion mode MOSFET.

where

**CODDLT=0 :**

$$\Delta = \frac{\text{DDLTMAX} \cdot T1}{\text{DDLTMAX} + T1} + 1 \quad (375)$$

$$T1 = \text{DDLTSLP} \cdot L_{\text{gate}} \cdot 10^6 + \text{DDLTICT} \quad (376)$$

**CODDLT=1 (defualt) :**

$$\Delta = \frac{\text{DDLTMAX} \cdot T1}{\text{DDLTMAX} + T1} + \text{DDLTICT} \quad (377)$$

$$T1 = \text{DDLTSLP} \cdot L_{\text{gate}} \cdot 10^6 \quad (378)$$

The saturation voltage is defined as

$$V_{ds,\text{sat}} = V'_G + \frac{qN_{\text{depm}}\epsilon_{\text{Si}}}{C_{\text{ox}}^2} \left\{ 1 - \sqrt{1 + 2 \frac{C_{\text{ox}}^2}{qN_{\text{depm}}\epsilon_{\text{Si}}} \left( V'_G + 2 - \frac{1}{\beta} - V_{\text{bs}} \right)} \right\} \quad (379)$$

The total drain current  $I_{ds}$  is the sum of the accumulation current  $I_{dd}$  and that flowing in the resistor region  $I_{\text{res}}$  and that flowing in the back region  $I_{\text{back}}$  written as

$$I_{ds} = \frac{W_{\text{eff,nf}}}{L_{\text{ch}}} \cdot \frac{1}{\beta} (\mu \cdot I_{dd}) + I_{ds,\text{res}} + I_{ds,\text{back}} \quad (380)$$

where,

$$I_{dd} = -\beta \frac{(Q_{n0} + Q_{nl})}{2} \cdot (\phi_{SL} - \phi_{S0}) - Q_{n0} + Q_{nl} \quad (381)$$

$Q_{n0}$  and  $Q_{nl}$  denote the accumulation charge in the n layer at the source side and the drain side, respectively. The threshold voltage shift  $\Delta V_{th}$  due to the short-channel effect (see Sec. 7) is modified by adding  $V_{ds}$  into the depletion width equation (see Eq. (32)) as

$$W_d = \sqrt{\epsilon_{Si} \cdot (2\Phi_B - V_{bs} - \mathbf{DEPETA} \cdot V_{ds})} \quad (382)$$

In the same way as for the inversion carrier, the carrier mobility model for  $I_{dd}$  is written as

$$\mu = \frac{\mu_0}{\left(1 + \left(\frac{\mu_0 E_y}{V_{max}}\right)^{\frac{1}{BB}}\right)^{\frac{1}{BB}}} \quad (383)$$

where

$$\frac{1}{\mu_0} = \frac{1}{\mu_{CB}} + \frac{1}{\mu_{PH}} + \frac{1}{\mu_{SR}} \quad (384)$$

$$\mu_{SR} = \frac{\mathbf{MUESR1}}{E_{eff}^{M_{uesurface}}} \quad (385)$$

$$\mu_{PH} = \frac{M_{uephonon}}{E_{eff}^{\mathbf{MUEPH0}}} \quad (386)$$

$$\mu_{CB} = \mathbf{MUECB0} + \mathbf{MUECB1} \cdot \frac{-Q_{n0}}{q \cdot 10^{11}} \quad (387)$$

$$E_{eff} = \frac{\left(\frac{\mathbf{NINV}}{\epsilon_{Si}}\right) \cdot (-Q_{n0})}{1 + (\phi_{SL} - \phi_{S0}) \cdot N_{invde}} \quad (388)$$

The resistor current and the back current are written as

$$I_{ds,res} = W_{eff,nf} \cdot Q_{leak,resistor0} \cdot \mu_{leak,res} \cdot \frac{V_{ds,eff}}{L_{ch}} \quad (389)$$

$$I_{ds,back} = W_{eff,nf} \cdot Q_{leak,back0} \cdot \mu_{leak,back} \cdot \frac{V_{ds,eff}}{L_{ch}} \quad (390)$$

$Q_{leak,resistor0}$  denotes the charge in the resistor part at the source side. Furthermore,  $Q_{leak,back0}$  denotes the charge in the back part at the source side.

$$Q_{leak,resistor0} = -q \cdot N_{depm} \cdot (\mathbf{TND}EP - W_s - W_b) \quad (391)$$

$$Q_{leak,back0} = -q \cdot N_{depm} \cdot \exp\{\beta(\phi_{b0} - V_{ds,eff})\} \cdot W_b \quad (392)$$

$$W_b = \sqrt{\frac{2\epsilon_{Si}\epsilon_0 N_{subc}}{qN_{depm}(N_{depm} + N_{subc})} \cdot (\phi_{bi} - V_{bs})} \quad (393)$$

$$W_s = \sqrt{\frac{2\epsilon_{Si}\epsilon_0}{q \cdot N_{depm}} (-\phi_s)} \quad (394)$$

$\phi_{bi}$  denotes the built-in potential of P-N junction and is defined as follows

$$\phi_{bi} = \frac{1}{\beta} \ln \left( \frac{N_{subc} \cdot N_{depm}}{n_i^2} \right) \quad (395)$$

and  $V_{ds,res}$  denotes the effective potential at the drain side in the resistor part and is defined as follows

$$V_{ds,res} = \frac{V_{ds}}{\left[ 1 + \left( \frac{V_{ds}}{V_{ds,sat}} \right)^{\Delta} \right]^{\frac{1}{\Delta}}} \quad (396)$$

where  $\Delta$  is the same as that for the accumulation, and

$$V_{ds,sat} = DEP_{vdsef2} \cdot \left[ V'_G + DEP_{vdsef1} + \frac{qN_{depm}\epsilon_{Si}}{C_{ox}^2} \right] \left\{ 1 - \sqrt{1 + 2 \frac{C_{ox}^2}{qN_{depm}\epsilon_{Si}} \left( V'_G + DEP_{vdsef1} - \frac{1}{\beta} - V_{bs} \right)} \right\} \quad (397)$$

where

$$DEP_{vdsef1} = \mathbf{DEPVDSF1} \quad (398)$$

$$DEP_{vdsef2} = \mathbf{DEPVDSF2} \quad (399)$$

The high field carrier mobility in the n layer is written as

$$\mu_{leak,res} = \frac{\mu_{0leak,res}}{\left( 1 + \left( \frac{\mu_{0leak,res}E_y}{DEP_{vmax}} \right)^{\mathbf{DEPBB}} \right)^{\frac{1}{\mathbf{DEPBB}}}} \quad (400)$$

where

$$E_y = \frac{V_{ds,res}}{L_{ch}} \quad (401)$$

$$\frac{1}{\mu_{0leak,res}} = \frac{1}{\mu_{CB}} + \frac{1}{\mu_{PH}} \quad (402)$$

$$\mu_{PH} = \frac{DEP_{muephonon}}{E_{eff} \mathbf{DEPMUEPHO}} \quad (403)$$

$$\mu_{CB} = DEP_{mue0} + DEP_{mue1} \cdot \frac{-Q_{leak,resistor0}}{q \cdot 10^{11}} \quad (404)$$

$$E_{eff} = \frac{-Q_{leak,resistor0}}{\epsilon_{Si}} \cdot \frac{1}{1 + (\phi_{SL} - \phi_{S0}) \cdot N_{invde}} \quad (405)$$

$$(406)$$

$$\mu_{leak,back} = \frac{\mu_{0leak,back}}{\left( 1 + \left( \frac{\mu_{0leak,back}E_y}{DEP_{vmax}} \right)^{\mathbf{DEPBB}} \right)^{\frac{1}{\mathbf{DEPBB}}}} \quad (407)$$

$$E_y = \frac{V_{ds,res}}{L_{ch}} \quad (408)$$

$$\frac{1}{\mu_{0leak,back}} = \frac{1}{\mu_{CB}} + \frac{1}{\mu_{PH}} \quad (409)$$

$$\mu_{PH} = \frac{DEP_{muephonon}}{E_{eff} \text{DEPMUEPH0}} \quad (410)$$

$$\mu_{CB} = DEP_{mueback} + DEP_{mueback1} \cdot \frac{-Q_{leak,back0}}{q \cdot 10^{11}} \quad (411)$$

$$E_{eff} = \frac{-Q_{leak,back0}}{\varepsilon_{Si}} \cdot \frac{1}{1 + (\phi_{SL} - \phi_{S0}) \cdot N_{invde}} \quad (412)$$

$DEP_{mue0}$ ,  $DEP_{mue1}$ ,  $DEP_{mueback}$ ,  $DEP_{mueback1}$ ,  $N_{invde}$  and  $DEP_{vmax}$  are

$$DEP_{mue0} = \text{DEPMUE0} \quad (413)$$

$$DEP_{mue1} = \text{DEPMUE1} \quad (414)$$

$$DEP_{mueback} = \text{DEPMUEBACK0} \quad (415)$$

$$DEP_{mueback1} = \text{DEPMUEBACK1} \quad (416)$$

$$DEP_{vmax} = \text{DEPVMAX} \cdot \left( 1 + \frac{\text{DEPVMAXL}}{(L_{gate} \cdot 10^6)^{\text{DEPVMAXLP}}} \right) \quad (417)$$

$$N_{invde} = \text{NINVND} \cdot \left( 1 + \frac{\text{NINVNDW}}{(W_{gate} \cdot 10^6)^{\text{NINVNDWP}}} \right) \quad (418)$$

## 25.2 CODEP=2 : old model

In the depletion mode MOSFET model, the quasi-Fermi potential( $V_{ds,eff}$ ) for the majority carrier is written in the same way as that of the minority carrier.

$$V_{ds,eff} = \frac{V_{ds}}{\left[ 1 + \left( \frac{V_{ds}}{V_{ds,sat}} \right)^\Delta \right]^{\frac{1}{\Delta}}} \quad (419)$$

where

**CODDLT=0 :**

$$\Delta = \frac{\text{DDLTMAX} \cdot T1}{\text{DDLTMAX} + T1} + 1 \quad (420)$$

$$T1 = \text{DDLTSLP} \cdot L_{gate} \cdot 10^6 + \text{DDLTICT} \quad (421)$$

**CODDLT=1 (defualt) :**

$$\Delta = \frac{\text{DDLTMAX} \cdot T1}{\text{DDLTMAX} + T1} + \text{DDLTICT} \quad (422)$$

$$T1 = \text{DDLTSLP} \cdot L_{\text{gate}} \cdot 10^6 \quad (423)$$

$$V_{\text{ds,sat}} = \left[ V'_G + \frac{qN_{\text{depm}}\epsilon_{\text{Si}}}{C_{\text{ox}}^2} \left\{ 1 - \sqrt{1 + 2 \frac{C_{\text{ox}}^2}{qN_{\text{depm}}\epsilon_{\text{Si}}} \{V'_G\}} \right\} \right] \quad (424)$$

The total drain current  $I_{\text{ds}}$  is written as follows

$$I_{\text{ds}} = \frac{W_{\text{eff,nf}}}{L_{\text{ch}}} \cdot \frac{1}{\beta} (\mu \cdot I_{\text{dd}}) + I_{\text{ds,res}} \quad (425)$$

where the accumulation current flowing at the surface is written as

$$I_{\text{dd}} = -\beta \frac{(Q_{\text{n}0} + Q_{\text{n}l})}{2} \cdot (\phi_{\text{SL}} - \phi_{\text{S}0}) \quad (426)$$

$Q_{\text{n}0}$  and  $Q_{\text{n}l}$  denote the accumulation charge in the n layer at the source side and the drain side, respectively. The threshold voltage shift  $\Delta V_{\text{th}}$  due to the short-channel effect is modified by eliminating  $V_{\text{bs}}$  from the depletion width equation (see Eq. (32)) as

$$W_d = \sqrt{\frac{2\epsilon_{\text{Si}}(2\Phi_B)}{qN_{\text{dep}}}} \quad (427)$$

In the same way as for the inversion carrier the carrier mobility model for the accumulation current is written as

$$\mu = \frac{\mu_0}{\left( 1 + \left( \frac{\mu_0 E_y}{V_{\text{max}}} \right)^{\frac{BB}{BB}} \right)^{\frac{1}{BB}}} \quad (428)$$

$$\frac{1}{\mu_0} = \frac{1}{\mu_{\text{CB}}} + \frac{1}{\mu_{\text{PH}}} + \frac{1}{\mu_{\text{SR}}} \quad (429)$$

$$\mu_{\text{SR}} = \frac{\text{MUESR1}}{E_{\text{eff}}^{M_{\text{uesurface}}}} \quad (430)$$

$$\mu_{\text{PH}} = \frac{M_{\text{uephonon}}}{E_{\text{eff}}^{\text{MUEPH0}}} \quad (431)$$

$$\mu_{\text{CB}} = \text{MUECB0} + \text{MUECB1} \cdot \frac{-Q_{\text{n}0}}{q \cdot 10^{11}} \quad (432)$$

$$E_{\text{eff}} = \frac{\left( \frac{\text{NINV}}{\epsilon_{\text{Si}}} \right) \cdot (-Q_{\text{n}0})}{1 + (\phi_{\text{SL}} - \phi_{\text{S}0}) \cdot N_{\text{invde}}} \quad (433)$$

The resistor current is written as

$$I_{\text{ds,res}} = q \cdot N_{\text{depm}} \cdot \mu_{\text{leak,res}} \cdot \frac{W_{\text{res}} \cdot W_{\text{eff}}}{L_{\text{eff}}} V_{\text{ds,res}} \quad (434)$$

$$W_{\text{res}} = \mathbf{TNDEP} \cdot (1 - \mathbf{TNDEPV} \cdot V_{\text{ds}}) - W_s - W_b \quad (435)$$

$$W_b = \sqrt{\frac{2\epsilon_{\text{Si}}\epsilon_0 N_{\text{subc}}}{qN_{\text{depm}}(N_{\text{depm}} + N_{\text{subc}})} \cdot (\phi_{\text{bi}} - V_{\text{bs}})} \quad (436)$$

$$W_s = \sqrt{\frac{2\epsilon_{\text{Si}}\epsilon_0}{q \cdot N_{\text{depm}}} (-\phi_{\text{res}})} \quad (437)$$

where  $\phi_{\text{res}}$  is the surface potential calculated separately from the accumulation current, and  $N_{\text{depm}}$  is the impurity concentration of the n layer.  $N_{\text{subc}}$  is defined in Eq. in (92), and  $\phi_{\text{bi}}$  denotes the built-in potential of P-N junction and is defined as follows.

$$\phi_{\text{bi}} = \frac{1}{\beta} \ln \left( \frac{N_{\text{subc}} \cdot N_{\text{depm}}}{n_i^2} \right) \quad (438)$$

The effective potential at the drain side in the resistor part  $V_{\text{ds,res}}$  is defined as follows.

$$V_{\text{ds,res}} = \frac{V_{\text{ds}}}{\left[ 1 + \left( \frac{V_{\text{ds}}}{V_{\text{ds,sat}}} \right)^{\mathbf{DEPDDLT}} \right]^{\frac{1}{\mathbf{DEPDDLT}}}} \quad (439)$$

where

$$V_{\text{ds,sat}} = V'_G + \frac{qN_{\text{depm}}\epsilon_{\text{Si}}}{C_{\text{ox}}^2} \left\{ 1 - \sqrt{1 + 2 \frac{C_{\text{ox}}^2}{qN_{\text{depm}}\epsilon_{\text{Si}}} \left\{ V'_G - \mathbf{DEPVSATR} \cdot \left( V_{\text{bs}} + \frac{1}{\beta} \right) \right\}} \right\} \quad (440)$$

$$\mu_{\text{leak,res}} = \frac{\mu_{0\text{leak,res}}}{\left( 1 + \left( \frac{\mu_{0\text{leak,res}} E_y}{DEP_{\text{vmax}}} \right)^{\mathbf{DEPB}} \right)^{\frac{1}{\mathbf{DEPB}}}} \quad (441)$$

$$E_y = \frac{V_{\text{ds,res}}}{L_{\text{ch}}} \quad (442)$$

$$\frac{1}{\mu_{0\text{leak,res}}} = \frac{1}{\mu_{\text{CB}}} + \frac{1}{\mu_{\text{RES}}} \quad (443)$$

$$\mu_{\text{CB}} = DEP_{\text{mue0}} \quad (444)$$

$$\mu_{\text{RES}} = \frac{DEP_{\text{mue2}}}{E_{\text{eff}}^{\mathbf{DEPMUEA1}}} \quad (445)$$

$$E_{\text{eff}} = \frac{V_{\text{gs}} - V_{\text{bs}}}{T_{\text{dep}}} \quad (446)$$

$$DEP_{\text{vmax}} = \frac{\mathbf{DEPVMAX}}{1.8 + 0.4(T/\mathbf{TNOM}) + 0.1(T/\mathbf{TNOM})^2 - \mathbf{DEPV TMP} \cdot (1 - T/\mathbf{TNOM})} \quad (447)$$

$$DEP_{\text{mue0}} = \frac{\mathbf{DEPMUE0}}{\left( \frac{T}{T_{\text{nom}}} \right)^{\mathbf{DEPMUE0TMP}}} \quad (448)$$

$$DEP_{\text{mue2}} = \frac{\mathbf{DEPMUE2}}{\left( \frac{T}{T_{\text{nom}}} \right)^{\mathbf{DEPMUE2TMP}}} \quad (449)$$

**DEPVFBC** is the flat-band voltage of the resistor part for calculating  $\phi_{\text{res}}$ .

**DEPSUBSL** is a fitting parameter for adjusting sub-threshold slope for the resistor current.

The fitting parameter **DEPVGPSL** is introduced to achieve smooth transition from the depletion to the accumulation condition. If a minimum occurs for  $g_m$  at the transition point, adjust **DEPVGPSL** from zero.

## 25.3 CODEP=3 : new model

The drain current  $I_{\text{ds}}$  consists of the accumulation-mode current  $I_{\text{ds,acc}}$  which flows near the surface, and the resistor current  $I_{\text{ds,res}}$  which flows beneath the surface as

$$I_{\text{ds}} = I_{\text{ds,acc}} + I_{\text{ds,res}} \quad (450)$$

The resistor current  $I_{\text{ds,res}}$  is subdivided into  $I_{\text{res}}$  and  $I_{\text{res,leak}}$ .

$$I_{\text{ds,res}} = I_{\text{res}} + I_{\text{res,leak}} \quad (451)$$

where  $I_{\text{res}}$  represents the current flowing the neutral part of the resistor region, and  $I_{\text{leak}}$  represents the leakage current flowing the resistor region in thanks to carrier injection at the source side even when the neutral part of the resistor region vanishes due to depletion at a biased condition.

### 25.3.1 Accumulation-mode current $I_{\text{ds,acc}}$

In the depletion mode MOSFET model, the quasi-Fermi potential( $V_{\text{ds,eff}}$ ) for the majority carrier is written in the same way as that of the minority carrier.

$$V_{\text{ds,eff}} = \frac{V_{\text{ds}}}{\left[1 + \left(\frac{V_{\text{ds}}}{V_{\text{ds,sat}}}\right)^{\Delta}\right]^{\frac{1}{\Delta}}} \quad (452)$$

where

**CODDLT=0** :

$$\Delta = \frac{\text{DDLTMAX} \cdot T1}{\text{DDLTMAX} + T1} + 1 \quad (453)$$

$$T1 = \text{DDLTSLP} \cdot (L_{\text{gate}}/10^{-6}) + \text{DDLTICT} \quad (454)$$

**CODDLT=1** (defualt) :

$$\Delta = \frac{\text{DDLTMAX} \cdot T1}{\text{DDLTMAX} + T1} + \text{DDLTICT} \quad (455)$$

$$T1 = \text{DDLTSLP} \cdot (L_{\text{gate}}/10^{-6}) \quad (456)$$

The effective saturation voltage  $V_{ds,sat}$  is determined iteratively through a solution of the following set of equations:

$$C_{ox} \cdot (V'_G - \phi_{vsat} + \mathbf{DEPVSAT}) + Q_{sat} = 0 \quad (457)$$

$$Q_{sat} = -\sqrt{\frac{2q\mathbf{NDEPM}\varepsilon_{si}}{\beta}} \sqrt{\exp(-\beta\phi_{vsat}) + \beta\phi_{vsat} - 1} \quad (458)$$

$$V_{ds,sat} = -\phi_{vsat} \quad (459)$$

The total drain current  $I_{ds}$  is written as follows

$$I_{ds} = \frac{W_{eff}}{L_{eff}} \cdot \mathbf{NF} \cdot \frac{1}{\beta} (\mu \cdot I_{dd}) + I_{ds,res} \quad (460)$$

where  $L_{eff}$  is the effective channel length that accounts for the channel-length modulation (CLM).

In the above equation, the first term represents the accumulation current flowing at the surface and  $I_{dd}$  is written as

$$I_{dd} = -\beta \frac{(Q_{n0} + Q_{nl})}{2} \cdot (\phi_{SL} - \phi_{S0}) \quad (461)$$

$Q_{n0}$  and  $Q_{nl}$  denote the accumulation charge in the buried layer at the source side and the drain side, respectively. The threshold voltage shift  $\Delta V_{th}$  due to the short-channel effect is modified by eliminating  $V_{bs}$  from the depletion width equation (see Eq. (32)) as

$$W_d = \sqrt{\frac{2\epsilon_{Si}(2\Phi_B)}{q \cdot \mathbf{NDEPM}}} \quad (462)$$

In the same way as for the inversion carrier the carrier mobility model for the accumulation current is written as

$$\mu = \frac{\mu_0}{\left(1 + \left(\frac{\mu_0 E_y}{V_{max}}\right)^{\frac{1}{BB}}\right)^{\frac{1}{BB}}} \quad (463)$$

$$\frac{1}{\mu_0} = \frac{1}{\mu_{CB}} + \frac{1}{\mu_{PH}} + \frac{1}{\mu_{SR}} \quad (464)$$

$$\mu_{SR} = \frac{\mathbf{MUESR1}}{E_{eff} M_{uesurface}} \quad (465)$$

$$\mu_{PH} = \frac{M_{uephonon}}{E_{eff} \mathbf{MUEPHO}} \quad (466)$$

$$\mu_{CB} = \mathbf{MUECB0} + \mathbf{MUECB1} \cdot \frac{-Q_{n0}}{q \cdot 10^{11}} \cdot \{1 + (\phi_{SL} - \phi_{S0}) \cdot N_{invd}\} \quad (467)$$

$$E_{eff} = \frac{\left(\frac{\mathbf{NINV}}{\epsilon_{Si}}\right) \cdot (-Q_{n0})}{1 + (\phi_{SL} - \phi_{S0}) \cdot N_{invde}} \quad (468)$$

where  $\phi_{S0}$  and  $\phi_{SL}$  are the surface potential solutions for  $I_{acc}$ , and  $\phi_{b0}$  is the potential for the resistor region (Fig. 27).  $V_{max}$  is the saturation velocity given in Eq. (83).

Some prefactors consider the device size scaling as

$$M_{uephonon} = \text{MUEPH1} \cdot \left( 1 + \frac{\text{MUEPHL}}{(L_{gate}/10^{-6})^{\text{MUEPLP}}} \right) \cdot \left( 1 + \frac{\text{MUEPHW}}{(W_{gate}/10^{-6})^{\text{MUEPWP}}} \right) \cdot \left( 1 + \frac{\text{MUEPHS}}{((L_{gate}/10^{-6})(W_{gate}/10^{-6}))^{\text{MUEPSP}}} \right) \quad (469)$$

$$M_{uesurface} = \text{MUESR0} \cdot \left( 1 + \frac{\text{MUESRL}}{(L_{gate}/10^{-6})^{\text{MUESLP}}} \right) \cdot \left( 1 + \frac{\text{MUESRW}}{(W_{gate}/10^{-6})^{\text{MUESWP}}} \right) \quad (470)$$

$$N_{invde} = \text{NINVDE} \cdot \left( 1 + \frac{\text{NINVDL}}{(L_{gate}/10^{-6})^{\text{NINVDLP}}} \right) \cdot \left( 1 + \frac{\text{NINVDW}}{(W_{gate}/10^{-6})^{\text{NINVDWP}}} \right) \quad (471)$$

where  $(L_{gate}/10^{-6})$  and  $(W_{gate}/10^{-6})$  or equivalently,  $(L_{gate} \cdot 10^6)$  and  $(W_{gate} \cdot 10^6)$  intend normalization to a unitless quantity, the magnitude of which stays around the unity ( $=1$ ).

### 25.3.2 Resistor current $I_{ds,res}$

To recap, the resistor current is written as

$$I_{ds,res} = I_{res} + I_{res,leak} \quad (472)$$

In the following subsections, each component is described.

#### i) $I_{res}$

The resistor current in the neutral region is written as

$$I_{res} = q \cdot \text{NF} \cdot N_{res} \cdot \mu_{res} \cdot W_{res} \cdot W_{eff} \cdot E_{dri} \quad (473)$$

where  $q$  is the elementary charge,  $N_{res}$  is the effective carrier density for the neutral region,  $\mu_{res}$  is the effective mobility,  $W_{res}$  is the width for the neutral region,  $W_{eff}$  is the effective gate width, and  $E_{dri}$  is the effective electric field strength between the source and the drain within the resistor region. Further descriptions for these quantities follow below.

The effective electric field strength  $E_{dri}$  is expressed together with the quasi-Fermi potential difference

between source and drain,  $V_{ds,res}$ , as

$$E_{dri} = \frac{V_{ds,res}}{L'_{\text{eff}} + \text{DEPRDRDL1}} \quad (474)$$

$$V_{ds,res} = \begin{cases} V_{ds} & (\text{COVDSRES} = -1; \text{ compatible to HiSIM2 3.0.0's CODEP=3}) \\ \frac{V_{ds}}{\left[ 1 + \left( \frac{V_{ds}}{V_{ds,sat,res}} \right)^{\frac{1}{\text{DEPDDLT}}} \right]^{\frac{1}{\text{DEPDDLT}}}} & (\text{COVDSRES} = 3) \end{cases} \quad (475)$$

where  $L'_{\text{eff}}$  is the effective channel length without the channel-length modulation.

$V_{ds,sat,res}$  is the effective saturation voltage, or quasi-fermi saturation voltage, obtained analytically or iteratively according to the choice of **COVDSRES**.

$$V_{ds,sat,res} = \begin{cases} \frac{1}{2} ((V'_{g,res} - DEP_{\text{leak}}) + \ln(\cosh(V'_{g,res} - DEP_{\text{leak}})) + \ln(2)) + DEP_{\text{leak}} & (\text{COVDSRES} = 2 \text{ (default)}) \\ \ln(1 + \exp(V'_{g,res} - DEP_{\text{leak}})) + DEP_{\text{leak}} & (\text{COVDSRES} = 3) \end{cases}$$

where  $DEP_{\text{leak}}$  sets a floor of  $V_{dsat}$  for  $I_{ds,res}$

In the other cases,  $V_{ds,sat,res}$  is obtained by solving the following set of equations iteratively:

$$-C_{\text{ox}} \cdot (V_{G',res} - \phi_{\text{res}}) + Q_{\text{res}} = 0 \quad (476)$$

$$Q_{\text{res}} = \sqrt{\frac{2q \cdot \text{NDEPM} \cdot \varepsilon_{\text{si}}}{\beta}} \sqrt{\exp(\beta\phi_{\text{res}}) - \beta\phi_{\text{res}} - 1} \quad (477)$$

$$V_{ds,sat,res} = \phi_{\text{res}} (\geq 0) \quad (478)$$

where  $V_{G',res}$  is an effective gate voltage as

$$V_{G',res} = V'_G - \text{DEPDVFBC} \quad (479)$$

The effective carrier concentration for  $I_{\text{res}}$  is

$$N_{\text{res}} = \text{NDEPM} \cdot \left( 1 + \text{DEPCAR} \cdot E_{\text{dri}} \cdot \left( 1 - \frac{1}{1 + \mu_{0,\text{res}} \cdot \frac{E_{\text{dri}}}{DEP_{\text{vmax},res}}} \right) \right) \quad (480)$$

where  $\mu_{0,\text{res}}$  represents the low-field mobility for  $I_{\text{res}}$ .

The width of the neutral region is expressed as

$$W_{\text{res}} = \text{TNDEP} - W_s - W_b \quad (481)$$

$$W_s = \sqrt{\frac{2\epsilon_{\text{Si}}\epsilon_0}{q \cdot \text{NDEPM}} (-\phi_{\text{res}})} \quad (482)$$

$$W_b = \sqrt{\frac{2\epsilon_{\text{Si}}\epsilon_0 N_{\text{subc}}}{q \cdot \text{NDEPM} \cdot (\text{NDEPM} + N_{\text{subc}})} \cdot (\phi_{\text{bi}} - V_{\text{bs}})} \quad (483)$$

where  $W_s$  and  $W_b$  represent the depletion layer thickness on the surface side, and the depletion layer thickness across the pn junction between the buried layer (resistor) and the substrate, respectively.  $\phi_{bi}$  denotes the built-in potential of p/n junction and is defined as follows.

$$\phi_{bi} = \frac{1}{\beta} \ln \left( \frac{N_{subc} \cdot \mathbf{NDEPM}}{n_i^2} \right) \quad (484)$$

where  $N_{subc}$  is defined elsewhere in Eq. (92).  $\phi_{res}$  represents the surface potential calculated by solving the Poisson equation with the modified effective gate voltage  $V_{gp,res}$

$$V_{G',res} = V'_G - \mathbf{DEPDVFBC} \quad (485)$$

where the model parameter **DEPDVFBC** is introduced for fitting capability.

The resistor mobility  $\mu_{res}$  for  $I_{res}$  is modeled as

$$\mu_{res} = \frac{\mu_{0,res}}{\left( 1 + \left( \frac{\mu_{0,res} \cdot E_{dri}}{DEP_{vmax}} \right)^{\frac{1}{DEPBB}} \right)^{\frac{1}{DEPBB}}} \quad (486)$$

where

$$E_{dri} = \frac{V_{ds,res}}{L'_{eff} - \mathbf{DEPRDRDL2}} \quad (487)$$

where  $L'_{eff}$  is the effective channel length without channel length reduction due to CLM.

The low-field resistor mobility  $\mu_{0,res}$  for  $I_{res}$  is modeled as

$$\frac{1}{\mu_{0,res}} = \frac{1}{\mu_{CB,res}} + \frac{1}{\mu_{PH,res}} \quad (488)$$

where

$$\mu_{PH,res} = \frac{DEP_{muephonon,res}}{E_{eff,res} - \mathbf{DEPMUEPH0}} \quad (489)$$

$$\mu_{CB,res} = DEP_{mue0,res} + DEP_{mue1,res} \cdot \frac{-Q_{resistor}}{q \cdot 10^{10}} \cdot \{1 + V_{ds,res} \cdot N_{invdC,res}\} \quad (490)$$

$$Q_{resistor} = -q \cdot \mathbf{NDEPM} \cdot (\mathbf{TNDEP} - W_s - W_b) \quad (491)$$

The effective field for mobility evalutation is written as

$$E_{eff,res} = \frac{Q_{resistor}}{\varepsilon_{si}} \cdot \frac{1}{1 + V_{ds,res} \cdot N_{invdH,res}} \quad (492)$$

$DEP_{mue0,res}$ ,  $DEP_{mue1,res}$ ,  $DEP_{vmax}$ , and  $N_{invd,res}$  are

$$DEP_{mue0,res} = \mathbf{DEPMUE0} \cdot \left( 1 + \frac{\mathbf{DEPMUEOL}}{(L_{gate}/10^{-6})\mathbf{DEPMUEOLP}} \right) \quad (493)$$

$$DEP_{mue1,res} = \mathbf{DEPMUE1} \cdot \left( 1 + \frac{\mathbf{DEPMUE1L}}{(L_{gate}/10^{-6})\mathbf{DEPMUE1LP}} \right) \quad (494)$$

$$DEP_{vmax,res} = \mathbf{DEPVMAX} \cdot \left( 1 + \frac{\mathbf{DEPVMAXL}}{(L_{gate}/10^{-6})\mathbf{DEPVMAXLP}} \right) \quad (495)$$

$$\begin{aligned} N_{invdC,res} &= \mathbf{DEPNINVDC} \cdot \left( 1 + \frac{\mathbf{DEPNINVDL}}{(L_{gate}/10^{-6})\mathbf{DEPNINVDLP}} \right) \cdot \\ &\quad \left( 1 + \frac{\mathbf{DEPNINVDW}}{(W_{gate}/10^{-6})\mathbf{DEPNINVDWDP}} \right) \end{aligned} \quad (496)$$

$$\begin{aligned} N_{invdH,res} &= \mathbf{DEPNINVDH} \cdot \left( 1 + \frac{\mathbf{DEPNINVDL}}{(L_{gate}/10^{-6})\mathbf{DEPNINVDLP}} \right) \cdot \\ &\quad \left( 1 + \frac{\mathbf{DEPNINVDW}}{(W_{gate}/10^{-6})\mathbf{DEPNINVDWDP}} \right) \end{aligned} \quad (497)$$

Temperature dependence can be considered in  $DEP_{muephonon,res}$ ,  $DEP_{mue0,res}$ , and  $DEP_{vmax,res}$ , apart from the gate length dependence as follows:

$$DEP_{muephonon,res} = \frac{\mathbf{DEPMUEPH1}}{\left(\frac{T}{T_{nom}}\right)^{\mathbf{DEPMUETMP}}} \quad (498)$$

$$DEP_{mue0,res} = \frac{\mathbf{DEPMUE0}}{\left(\frac{T}{T_{nom}}\right)^{\mathbf{DEPMUE0TMP}}} \quad (499)$$

$$DEP_{vmax} = \frac{\mathbf{DEPVMAX}}{1.8 + 0.4(T/\mathbf{TNOM}) + 0.1(T/\mathbf{TNOM})^2 - \mathbf{DEPV TMP} \cdot (T/\mathbf{TNOM}) - 1} \quad (500)$$

## ii) $I_{res,leak}$

The leakage current for the resistor region is expressed as

$$I_{res,leak} = \mathbf{NF} \cdot W_{res,leak} \cdot \mathbf{DEPJLEAK} \cdot \left( \frac{W_{eff}}{L_{eff}} \right)^{DEP_{WLP}} \cdot \left( \frac{V_{ds,res0}^3}{V_{ds,res0}^3 + 0.0005} \right) \quad (501)$$

where  $W_{res,leak}$  and  $W_{eff}$  represent the width of the neutral region, and the effective gate width, respectively. **DEPJLEAK** is a model parameter for the leakage current.  $DEP_{WLP}$  is a parameter that includes temperature dependence

$$DEP_{WLP} = \mathbf{DEPWLP} + \mathbf{DEPWLP} \cdot \left( 1 - \frac{\mathbf{TEMP}}{\mathbf{TNOM}} \right) \quad (502)$$

$V_{ds,res0}$  is the upper-limited  $V_{ds,res}$  which reaches asymptotically **DEPLEAK** as  $V_{ds,res}$  increases.

The width of the neutral region for  $I_{res,leak}$  is expressed as

$$W_{res,leak} = \mathbf{TNDEP} - W_{s,leak} - W_{b,leak} \quad (503)$$

$$W_{b,leak} = \sqrt{\frac{2\epsilon_{Si}\epsilon_0 N_{subc}}{q\mathbf{NDEPM}(\mathbf{NDEPM} + N_{subc})} \cdot (\phi_{bi} - V_{bs})} \quad (504)$$

$$W_{s,leak} = \sqrt{\frac{2\epsilon_{Si}\epsilon_0}{q \cdot N_{depm}} (-\phi_{res,leak})} \quad (505)$$

where  $W_{s,\text{leak}}$  and  $W_{b,\text{leak}}$  represent the depletion layer thickness on the surface side, and the depletion layer thickness across the pn junction between the buried layer (resistor) and the substrate, respectively.  $\phi_{\text{res},\text{leak}}$  represents the surface potential calculated by solving iteratively the Poisson equation with the effective gate voltage

$$V_{G',\text{leak}} = (\mathbf{VFBC} + \mathbf{DEPDVFBC}) - 3 \quad (506)$$

where “-3” determines the gate voltage at which pure generation-recombination leakage current is expected. An additional parameter **DEPVLEAK** can be used for the adjustment of  $V_{bs}$  dependence of this leakage current.

### 25.3.3 Channel Length Modulation (CLM)

The channel-length modulation model (see Chapter 11) is introduced with three model parameters (**CLM1**, **CLM2**, **CLM3**), describing the weakened gate control under the saturation condition. For the depletion model, **CLM5** and **CLM6** can be used to adjust  $I_{ds}$  gradual increase under the saturation condition.

For accumulation-mode current  $I_{ds,\text{acc}}$ , the effective channel length in this section takes the CLM effects into account as

$$L_{\text{eff}} - \Delta L \quad (507)$$

where  $L_{\text{eff}}$  represents the effective channel length (Section 3, Eq. (5)) and  $\Delta L$  represents the channel length reduction (Section 11, Eqs. (85)—(87)) due to this effect. For resistor current  $I_{ds,\text{res}}$ , the channel length reduction due to CLM is excluded.

### 25.3.4 Smoothing parameters

**DEPQF**: smoothing  $V_{ds,\text{sat}}$  to zero.

**DEPSUBSL**: adjust subthreshold slope of  $I_{\text{res}}$ .

**DEPSUBSL0**: adjust  $V_{bs}$  dependence of subthreshold slope of  $I_{\text{res}}$ .

**DEPVGP SL**: modify  $V_{gp,\text{res}}$  to suppress a gm peak of  $I_{\text{res}}$  when it is created.

**DEPFDPD**: for better fitting to  $C_{gg}$  vs.  $V_{gs}$  around  $V_{gs} = V_{fb}$ .

**DEPPS**: smoothe accumulation charge to zero

**DEPQFRES**: smoothe  $V_{ds,\text{sat},\text{res}}$  to zero.

The HiSIM model parameters introduced in section 25 are summarized in Table 26.

Table 25: HiSIM model parameters introduced in section 25 of this manual.

<b>CODEP</b>	COMMON model flag to select the depletion model
<b>NDEPM</b>	impurity concentration of the surface layer
<b>NDEPML</b>	$L_{\text{gate}}$ dependence of impurity concentration of the surface N <sup>-</sup> layer
<b>NDEPMLP</b>	$L_{\text{gate}}$ dependence of impurity concentration of the surface N <sup>-</sup> layer thickness of the surface layer
<b>TNDEP</b>	Coulomb scattering in the resistor region
<b>DEPMUE0</b>	saturation velocity in the resistor region
<b>DEPVMAX</b>	high-field-mobility degradation in the resistor region
<b>DEPB</b>	temperature dependence of the phonon scattering in the resistor region
<b>DEPMUETMP</b>	temperature dependence of DEPVMAX
<b>DEPVTMP</b>	temperature dependence of DEP <sub>mue0</sub>
<b>DEPMUE0TMP</b>	temperature dependence of DEP <sub>mue0</sub>
<b>DEPETA</b>	<b>CODEP=1</b>
<b>DEPVDSEF1</b>	$V_{\text{ds}}$ dependence of the threshold voltage shift
<b>DEPVDSEF1L</b>	effective drain potential coefficient-1 in the resistor region
<b>DEPVDSEF1LP</b>	$L_{\text{gate}}$ dependence of the effective drain potential coefficient-1
<b>DEPVDSEF2</b>	$L_{\text{gate}}$ dependence of the effective drain potential coefficient-1 effective drain potential coefficient-2 in the resistor region
<b>DEPVDSEF2L</b>	$L_{\text{gate}}$ dependence of the effective drain potential coefficient-2
<b>DEPVDSEF2LP</b>	$L_{\text{gate}}$ dependence of the effective drain potential coefficient-2 Coulomb scattering in the back region
<b>DEPMUEBACK0</b>	$L_{\text{gate}}$ dependence of the Coulomb scattering in the back region
<b>DEPMUEBACK0L</b>	$L_{\text{gate}}$ dependence of the Coulomb scattering in the back region
<b>DEPMUEBACK1</b>	Coulomb scattering in the back region
<b>DEPMUEBACK1L</b>	$L_{\text{gate}}$ dependence of the Phonon scattering in the back region
<b>DEPMUEBACK1LP</b>	$L_{\text{gate}}$ dependence of the Phonon scattering in the back region leakage current coefficient
<b>DEPLEAK</b>	$L_{\text{gate}}$ dependence of leakage current coefficient
<b>DEPLEAKL</b>	$L_{\text{gate}}$ dependence of leakage current coefficient
<b>DEPLEAKLP</b>	leakage current coefficient
<b>DEPMUE1</b>	Coulomb scattering in the resistor region
<b>DEPMUEPH0</b>	Phonon scattering in the resistor region
<b>DEPMUEPH1</b>	Phonon scattering in the resistor region
<b>TNDEPV</b>	<b>CODEP=2</b>
<b>DEPMUEA1</b>	$V_{\text{ds}}$ dependence of the surface N <sup>-</sup> layer thickness
<b>DEPMUE2</b>	Modification of $\mu_{\text{res}}$
<b>DEPDLT</b>	Coulomb scattering of the resistor part
<b>DEPVSA</b>	smoothing coefficient for $V_{\text{ds},\text{res}}$
<b>DEPMUE2TMP</b>	$V_{\text{bs}}$ dependence of $V_{\text{ds},\text{sat}}$ of the resistor part
<b>DEPLEAKL</b>	temperature dependence of DEP <sub>mue2</sub>
<b>DEPLEAKLP</b>	$L_{\text{gate}}$ dependence of leakage current coefficient
<b>DEPVFB</b>	$L_{\text{gate}}$ dependence of leakage current coefficient
<b>DEPSUBL</b>	flat-band voltage of the resistor part
<b>DEPGPSL</b>	factor of the sub-threshold slope
<b>DEPLEAK</b>	smoothing of $g_b$ at $V_{\text{fb}}$

Table 26: HiSIM model parameters introduced in section 25 of this manual.

<b>COVDSRES</b>	<b>CODEP=3</b>
<b>DEPCAR</b>	equation selector for quasi-fermi saturation voltage for the resistor region
<b>DEPRDRDL1</b>	high field injection in the resistor region
<b>DEPRDRDL2</b>	pinch-off length in the resistor region
<b>DEPQF</b>	pinch-off length in the resistor region
<b>DEPQFRES</b>	smoothing of $V_{ds,sat}$ to zero for dep/accum transition
<b>DEPFDPD</b>	smoothing of $V_{ds,sat,res}$ to zero for dep/accum transition in the resistor region
<b>DEPPS</b>	smoothing for FD/PD transition
<b>DEPNINVDC</b>	smoothing for $\phi_S - \phi_f$
<b>DEPNINVDH</b>	Modification of $V_{dse}$ dependence on $E_{eff}$ (for $M_{u,res}$ 's Coulomb mobility)
<b>DEPRBR</b>	Modification of $V_{dse}$ dependence on $E_{eff}$ (for $M_{u,res}$ 's phonon mobility)
<b>DEPMUE1</b>	parameter for resistance effect along substrate (for minority carrier)
<b>DEPMUE1L</b>	Coulomb scattering in the resistor region ( <i>common with CODEP=1</i> )
<b>DEPMUE1LP</b>	$L_{gate}$ dependence of the Phonon scattering in the resistor region
<b>DEPMUEPH0</b>	$L_{gate}$ dependence of the Phonon scattering in the resistor region
<b>DEPMUEPH1</b>	Phonon scattering in the resistor region ( <i>common with CODEP=1</i> )
<b>DEPDVFBC</b>	Phonon scattering in the resistor region ( <i>common with CODEP=1</i> )
<b>DEPSUBSL</b>	ajustment parameter for the gate effective voltage of the resistor part
<b>DEPSUBSL0</b>	factor of the sub-threshold slope ( <i>common with CODEP=2</i> )
<b>DEPVGPSL</b>	factor of the sub-threshold slope
<b>DEPJLEAK</b>	smoothing of $V'_G$ for the resistor region
<b>DEPWLP</b>	towards $V_{fb}$ from depletion bias region ( <i>common with CODEP=2</i> )
<b>DEPVLEAK</b>	leakage current parameter for $J_{ds,leak}$
<b>DEPLEAK</b>	geometrical scaling exponent for the leakage current
	Controls the strength of $V_{bs}$ dependence in the resistor leakage current
	Quasi-Fermi saturation voltage for the resistor region ( <b>COVDSRES=3</b> )

Table 27: Model Comparison

	<b>CODEP=1</b>	<b>CODEP=2</b>	<b>CODEP=3</b>
Structural parameters	<b>NDEPM, NDEPML, NDEPMLP TNDEP</b>		
Accumulation current Quasi-Fermi Mobility Short-channel effects	drift+diffusion	drift	
	same as minority	modified	
	same as minority		
	<b>DEPETA</b>	-	-
Resistor current Effective gate voltage Explicit bias dependence Quasi-Fermi  Leak current Mobility Low-field mobility  High-field mobility  High-field injection	two terms	one term	two terms
	-	<b>DEPVFBC</b>	<b>DEPDVFBC</b>
	-	<b>TNDEPV</b>	
	<b>DEPVDSEF1</b>	-	-
	<b>DEPVDSEF2</b>	-	-
	-	<b>DEPDDLT</b>	
	-	<b>DEPVSATR</b>	-
	<b>DEPLEAK</b>		
	-	-	<b>DEPJLEAK</b>
	<b>DEPMUEPH0</b>	-	<b>DEPMUEPH0</b>
CLM	<b>DEPMUEPH1</b>	-	<b>DEPMUEPH1</b>
	<b>DEPMUE1</b>	-	<b>DEPMUE1</b>
	<b>DEPMUE0</b> <b>DEPMUE0TMP</b> <b>DEPMUETMP</b> <b>DEPV TMP</b>		
	<b>DEPMUEBACK0</b>	-	-
	<b>DEPMUEBACK1</b>	-	-
	-	<b>DEPMUEA1</b>	-
	-	<b>DEPMUE2</b>	-
	-	<b>DEPMUE2TMP</b>	-
	-	-	<b>DEPNINVDC</b>
	-	-	<b>DEPNINVDH</b>
Smoothing parameters	-	-	<b>DEPRBR</b>
	-	<b>DEPB B</b> <b>DEPV MAX</b>	
	-	-	<b>DEPRDRDL2</b>
	-	-	<b>DEPCAR</b>
const(0.3) const(2.0) const(0.12) const(0.05)	-	<b>DEPSUBSL</b> -	
	-	-	<b>DEPSUBSL0</b>
	<b>DEPV GPSL</b>		
	const(1.0)	<b>DEPQF</b>	
	const(4.0)	<b>DEPQFRES</b>	
	const(0.2)	<b>DEPFDPD</b>	
	const(0.05)	<b>DEPPS</b>	

## 26 Aging Model

In power devices, aging occurs in two different places: (a) The channel region and (b) The drift region.

### 26.1 (a) The channel region

Two aging models are considered:

- (I) **the hot electron induced aging:** HC Aging
- (II) **the N(P)BTI aging:** N(P)BTI Aging

The HC aging is mostly responsible for nMOSFET and the N(P)BTI aging is for pMOSFET. The models are valid for simulating under both DC and transient conditions. Therefore, here the HC model is described for nMOSFET and the NBTI model is for pMOSFET. Both models can be activated at the same time.

To invoke the models, the following parameters should be set:

- **CODEG=1** (for stress simulation)
  1. HC Aging model: **COISUB=1** and **TRAPGC1MAX > 0** should be set.
  2. N(P)BTI model: **TRAPA > 0**
- **CODEG=0** (for post-stress simulation or normal simulation)
  1. HC Aging model: **COISUB=1** and **TRAPGC1MAX > 0** should be set.
  2. N(P)BTI model: **TRAPDVTH > 0**

Calculation flow is presented at the end of this subsection.

#### 26.1.1 (I) HC Aging Model

Origin of the aging is modeled as the trap-density increase, which is included precisely in the Poisson equation solved iteratively [58]

$$\nabla^2 \phi = -\frac{q}{\epsilon_{Si}} (p - n + N_D - N_A - N_{tA}) \quad (508)$$

where  $p$ ,  $n$ ,  $N_D$  and  $N_A$  are the hole density, the electron density, the donor and the acceptor density, respectively. The trap density is denoted by  $N_{tA}$ .

Two trap density distributions are considered, the shallow and the deep level, where the deep trap level is considered to be responsible for the aging. Thus  $N_{tA}$  is the sum of the two densities

$$N_{tA} = N_{tA1} + N_{tA2} \quad (509)$$

where the analytical trap density is obtained after integrating the density with energy as [59, 60]

$$N_{tA,n} = N_{0,n} \exp \left( \frac{E_f - E_c}{E_{s,n}} \right) \quad (510)$$

where  $E_f$  is the Fermi energy and  $E_c$  is the conduction band edge energy. The gradient of the trap density distribution as a function of energy is described by  $E_{s,n}$ . The subscript  $n$  (1 or 2) denotes the different trap levels. In modeling, the trap density at the band edge ( $=g_{c,n}$ ) and the trap gradient ( $=E_{s,n}$ ) are varied according to the stress time.

The shallow trap level, which is independent of time, is written with model parameters **TRAPGC2** and **TRAPES2** as

$$N_{0,2} = \mathbf{TRAPGC2} \cdot \mathbf{TRAPES2} \frac{\frac{kT}{\mathbf{TRAPES2}}}{\sin \frac{kT}{\mathbf{TRAPES2}}} \quad (511)$$

The deep trap level is written as

$$N_{0,1}(t) = g_{c1,\text{deg}} \cdot E_{s1,\text{deg}} \frac{\frac{kT}{E_{s1,\text{deg}}}}{\sin \frac{kT}{E_{s1,\text{deg}}}} < N_{0,\text{limit}} \quad (512)$$

where  $g_{c1,\text{deg}}$ ,  $E_{s1,\text{deg}}$  and  $N_{0,\text{limit}}$  are written as

$$g_{c1,\text{deg}} = \mathbf{TRAPGC1} + \frac{\mathbf{TRAPGC1MAX}}{gc,\text{time1}} \exp \left[ -\frac{1}{2} \left( \frac{gc,\text{time} - gc,\text{time2}}{gc,\text{time1}} \right)^2 \right] \quad (513)$$

$$gc,\text{time} = \ln (I_{\text{sub}}' \cdot \mathbf{DEGTIME}/W) \quad (514)$$

$$gc,\text{time1} = \ln (I_{\text{sub}}' \cdot \mathbf{TRAPGCTIME1}/W) \quad (515)$$

$$gc,\text{time2} = \ln (I_{\text{sub}}' \cdot \mathbf{TRAPGCTIME2}/W) \quad (516)$$

$$E_{s1,\text{deg}} = \mathbf{TRAPES1} + \frac{\mathbf{TRAPES1MAX}}{es1,\text{time1}} \exp \left[ -\frac{1}{2} \left( \frac{es1,\text{time} - es1,\text{time2}}{es1,\text{time1}} \right)^2 \right] \quad (517)$$

$$es1,\text{time1} = \ln (I_{\text{sub}}' \cdot \mathbf{TRAPESTIME1}/W) \quad (518)$$

$$es1,\text{time2} = \ln (I_{\text{sub}}' \cdot \mathbf{TRAPESTIME2}/W) \quad (519)$$

$$N_{0,\text{limit}} = \mathbf{TRAPGCLIM} \cdot \mathbf{TRAPESLIM} \frac{\frac{kT}{\mathbf{TRAPESLIM}}}{\sin \frac{kT}{\mathbf{TRAPESLIM}}} \quad (520)$$

where **TRAPGC1, 2, LIM** and **TRAPES1, 2, LIM** are model parameters for the deep and the shallow trap densities. The time at which observable aging starts is determined by the model parameters **TRAPGCTIME1** and **TRAPESTIME1**, and the time at which aging enhancement ends is determined by **TRAPGCTIME2** and **TRAPESTIME2**. **DEGTIME** determines the aging time to be predicted.

$I_{\text{sub}}'$  is determined as

a) DC simulation

$$I_{\text{sub}}' = I_{\text{sub}} \quad (521)$$

b) Circuit simulation

$$I_{\text{sub}}' = \frac{\sum^{\mathbf{DEGTIME0}} I_{\text{sub}}}{\mathbf{DEGTIME0}} \quad (522)$$

For the  $V_{ds}$  dependence, the model parameter **TRAPLX** is introduced as

$$N_{tA} = N_{tA} \cdot \exp\left(-\frac{V_{dseff} - \phi_{SL} + \phi_{S0}}{\mathbf{TRAPLX}}\right) \quad (523)$$

The mobility degradation due to the trapped carriers is considered. In the effective electric field of its original formulation (Eq. (71)) as

$$E_{eff0} = E_{eff0} + \frac{\mathbf{TRAPN}}{\epsilon_{Si}} \cdot Q_{trap} \cdot f(\phi_S) \quad (524)$$

where  $Q_{trap}$  is the integrated trap density along the vertical direction. **TRAPN** is a fitting parameter in the same way as **NDEP** and **NINV**.

In addition to the trap density  $N_{tA}$  the model eliminating the midgap density can be activated by the Flag **CODEGES0**, realizing unoccupied midgap density with two model parameters **TRAPGC0** and **TRAPES0**.

**DEGTIME** determines the aging time to be predicted the device aging. In principle this is not model parameter but to be determined from outside. To distinguish the aging simulation under the DC condition for parameter extraction and the circuit simulation, the Flag **CODEGSTEP** must be determined.

### 26.1.2 (II) N(P)BTI Aging Model: Carrier trapping at interface

The hole trapping at Si/oxide interface of the NBTI is considered and modeled as the threshold voltage shift  $\delta V_{th,trap}$  as [61]

$$\delta V_{th,trap} = \mathbf{TRAPA} \cdot \exp(\mathbf{TRAPB} \cdot E_{ox}) \cdot \left[1 - \exp\left(-\frac{t_s}{\mathbf{TRAPBTI}}\right)\right] \quad (525)$$

$$E_{ox} = \frac{V_{Gon} - \delta V_{th,trap} - \phi_S}{T_{ox}} \quad (526)$$

$$t_s = T_{cycle} \cdot \mathbf{DEGTIME} \quad (527)$$

where  $\phi_S$  is fixed to  $2\Phi_B$  (Eq. (33)) giving the threshold voltage condition, and  $T_{cycle}$  is calculated by integrating the stress time during circuit operation for **DEGTIME0** long.  $V_{Gon}$  is averaged  $V'_G$  under the switching-on condition.

The mobility degradation due to the trapped carriers is considered in the effective electric field in the same way for the HC effect (Eq. (524)) as

$$E_{eff0} = E_{eff0} + \frac{\mathbf{TRAPP} \cdot \Delta V_{th,trap}}{T_{ox}} \cdot f(\phi_S) \quad (528)$$

where **TRAPP** is a fitting parameter.

The present implementation focuses on long-term aging, and no trap emission is included.

## 26.2 (b) The drift region

If  $V_{gs}$  and  $V_{ds}$  are high, the electric field increase in the drift region, especially at the STI corner, becomes very high. As the result, the impact ionization occurs. This causes a modification of the potential distribution. Modeling is done by modifying the internal node potential, which causes the carrier density change.

$$N_{\text{drift}} = \text{NOVER} \left\{ 1 + \text{RDRCAR} \left( \frac{V_{\text{ddp}}}{L_{\text{drift}} - \text{RDRDL2}} \right) \left( 1 - \frac{1}{1 + \frac{\mu_{\text{drift0}}}{V_{\text{max,drift}}} \cdot \frac{V_{\text{ddp}}}{L_{\text{drift}}}} \right) \right\} \\ + \left( \text{RDRQOVER} \frac{-Q'_{\text{over}}}{q} \right) \\ + \text{NOVER} \cdot D_{\text{vddp}} \quad (529)$$

For the  $V_{ds}$  dependence, the model parameter **TRAPDLX** is introduced as

$$D_{\text{vddp}} = D_{\text{vddp,deg}} \cdot \exp \left( -\frac{V_{\text{dseff}} - \phi_{\text{SL}} + \phi_{\text{S0}}}{\text{TRAPDLX}} \right) \quad (530)$$

$$D_{\text{vddp,deg}} = \text{TRAPDVDDP} + \frac{\text{TRAPD1MAX}}{time1} \exp \left[ -\frac{1}{2} \left( \frac{time - time2}{time1} \right)^2 \right] \quad (531)$$

$$time = \ln (I_{\text{ds}}' \cdot \text{DEGTIME}/W) \quad (532)$$

$$time1 = \ln (I_{\text{ds}}' \cdot \text{TRAPDTIME1}/W) \quad (533)$$

$$time2 = \ln (I_{\text{ds}}' \cdot \text{TRAPDTIME2}/W) \quad (534)$$

where **TRAPDVDDP** and **TRAPD1MAX** are a model parameter. The time at which observable aging starts is determined by the model parameter **TRAPDTIME1** and the time at which aging enhancement ends is determined by **TRAPDTIME2**.

$I_{\text{ds}}'$  is determined as

a) DC simulation

$$I_{\text{ds}}' = I_{\text{ds}} \quad (535)$$

b) Circuit simulation

$$I_{\text{ds}}' = \frac{\sum^{\text{DEGTIME0}} I_{\text{ds}}}{\text{DEGTIME0}} \quad (536)$$

The HiSIM model parameters introduced in section 26 are summarized in Table 28.

Table 28: HiSIM model parameters introduced in section 26 of this manual.

<b>DEGTIME</b>	Aging Conditions: These are in principle no model parameters. Please refer simulator definition
<b>DEGTIME0</b>	stress duration circuit simulation duration
<b>TRAPTAUCAP</b>	HC Aging Model
<b>TRAPLX</b>	time constant of trap caputre
<b>TRAPGC1</b>	Vds dependence of deep trap
<b>TRAPGC1MAX</b>	deep trap density
<b>TRAPGCTIME1</b>	time dependent deep trap
<b>TRAPGCTIME2</b>	aging start time
<b>TRAPGCLIM</b>	aging saturation time
<b>TRAPESLIM</b>	limit of trap density
<b>TRAPES1</b>	limit of trap density gradient
<b>TRAPES1MAX</b>	deep trap density gradient
<b>TRAPESTIME1</b>	time dependent deep trap density gradient
<b>TRAPESTIME2</b>	aging start time
<b>TRAPN</b>	aging saturate time
<b>TRAPGC2</b>	mobility degradation due to traps
<b>TRAPES2</b>	shallow trap density
<b>TRAPGC0</b>	shallow trap density coefficient
<b>TRAPES0</b>	midgap trap density
<b>TRAPD1MAX</b>	midgap trap density gradient
<b>TRAPDTIME1</b>	time dependent drift-region trap density gradient
<b>TRAPDTIME2</b>	aging start time
<b>TRAPDLX</b>	aging saturate time
<b>TRAPDVDDP</b>	Vds dependence of trap in the drift region
	time dependent the carrier type accumulated in the drift region
<b>TRAPA</b>	N(P)BTI Aging Model
<b>TRAPB</b>	coeffcient of existing interface trap density
<b>TRAPP</b>	coeffcient of existing interface trap density
<b>TRAPBTI</b>	coeffcient of BTI trap for Eeff
	coeffcient of existing interface trap density
<b>CODEG</b>	Flags
<b>CODEGSTEP</b>	set to 1 for aging simulation
	set to 0 for aging for DC and set to 1 for circuit aging

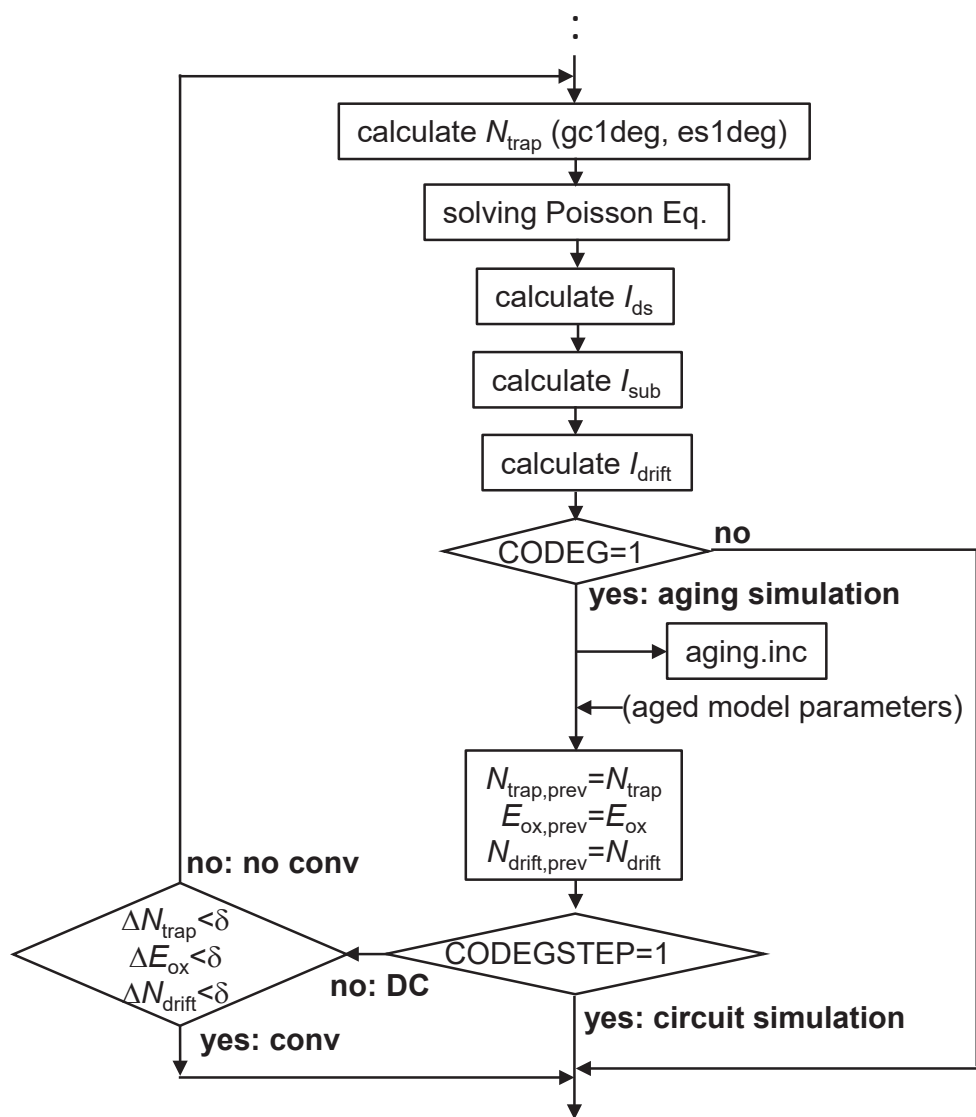


Fig. 28: Calculation Flow for aging.

## 27 Binning Model

The binning option is introduced to secure enough accuracy of model calculation results, even though the effects observed are not modeled yet. The binning method is the same as that used in BSIM3/4

$$Bin\_HiSIM\_model\_parameter = \mathbf{HiSIM\_model\_parameter} + \frac{\mathbf{P1}}{L_{\text{bin}}} + \frac{\mathbf{P2}}{W_{\text{bin}}} + \frac{\mathbf{P3}}{L_{\text{bin}} W_{\text{bin}}} \quad (537)$$

where **P1**, **P2**, and **P3** are model parameters for **L HiSIM\_model\_parameter**,

**W HiSIM\_model\_parameter**, and **L · W HiSIM\_model\_parameter**, respectively, and

$$L_{\text{bin}} = (L_{\text{gate}} \cdot 10^6)^{\mathbf{LBINN}} \quad (538)$$

$$W_{\text{bin}} = (W_{\text{gate}} \cdot 10^6)^{\mathbf{WBINN}} \quad (539)$$

The HiSIM model parameters introduced in section 27 are summarized in Table 29.

Table 29: HiSIM model parameters introduced in section 27 of this manual.

<b>LBINN</b>	power of $L_{\text{drawn}}$ function
<b>WBINN</b>	power of $W_{\text{drawn}}$ function
<b>LMAX</b>	maximum length of $L_{\text{drawn}}$ valid
<b>LMIN</b>	minimum length of $L_{\text{drawn}}$ valid
<b>WMAX</b>	maximum length of $W_{\text{drawn}}$ valid
<b>WMIN</b>	minimum length of $W_{\text{drawn}}$ valid

The model parameters which are effectively binned and which should not be used for binning are summarized in Table 30.

Table 30: HiSIM model parameters to be used for the binning option.

parameter	recommended	usable	not be used
basic	<b>NSUBC VFBC</b>		<b>TOX, KAPPA, XLD LL, LLD, LLN, XWD WL, WLD, WLN, VBI MUEPH0, MUESR0 MUEPHL, MUEPLP MUEPHS, MUEPSP MUESRL, MUESLP MUEPHW, MUEPWP MUESRW, MUESWP VOVERP BB PARL2, LP LPEXT</b>
mobility	MUECB0 MUECB1 MUEPH1 MUESR1	NINV NDEP	<b>SCP21, SCP22, BS1, BS2 PGD2, PGD4 CLM5, CLM6 QME1, QME2, QME3 RSH, RSHG RBPB, RBPD, RBPS</b>
short-channel & pocket	<b>NSUBP</b>	<b>VMAX</b>  <b>SC1, SC2, SC3 SCP1, SCP2, SCP3 NPEXT PGD1 CLM1, CLM2, CLM3</b>	<b>VOVER</b>  <b>PARL2, LP LPEXT SCP21, SCP22, BS1, BS2 PGD2, PGD4 CLM5, CLM6 QME1, QME2, QME3 RSH, RSHG RBPB, RBPD, RBPS</b>
poly-depletion CLM QME resistance			
$W_{\text{gate}}$ depnd. small size temperature		<b>RTH0 WFC, WVTH0 WL2 EG0 BGTMP1, BGTMP2 VTMP, MUETMP VDIFFJD, VDIFFJS</b>	<b>NSUBPW, NSUBPWP WL2P TNOM EGIG IGTEMP2, IGTEMP3</b>
STI	<b>WSTI, VTHSTI NSTI SCSTI1, SCSTI2</b>		<b>WL1, WL1P</b>
overlap	<b>VFBOVER NOVER</b>	<b>CGSO, CGDO, CGBO NOVERS, CVDSOVER</b>	
$I_{\text{sub}}$	<b>SUB1</b>	<b>SUB2, SVDS SVBS, SVGS IBPC1, IBPC2</b>	<b>SUB1L, SUB1LP, SUB2L SLG, SVGSL, SVGSLP SVGSW, SVGSWP, SLGL SLGLP, SVBSL, SVBSLP</b>
$I_{\text{gate}}$	<b>GLEAK1, GLEAK2 GLEAK3</b>	<b>GLEAK6</b>	<b>GLEAK4, GLEAK5 GLEAK7 GLKSD3</b>
$I_{\text{gs}}/I_{\text{gd}}$ $I_{\text{gb}}$ $I_{\text{GIDL}}$ junction	<b>GLKSD1, GLKSD2 GLKB1, GLKB2</b>		
noise	<b>NFTRP, NFALP</b>	<b>GIDL1, GIDL2</b>	
LOD	<b>NSUBPSTI1 NSUBPSTI2 NSUBPSTI3 MUESTI1 MUESTI2 MUESTI3</b>	<b>JS0D, JS0SWD, NJD, CISBKD JS0S, JS0SWS, NJS, CISBKS FALPH</b>	<b>CIT</b>
others		<b>FN1, FN2, FN3, FVBS POWRAT RD, RD22, RD23, RD24 RDICT1, RDOV13, RDSP1 RDVB, RDVD, RDVG11, RS SUB1SNP, SUB2SNP, SVDSSNP</b>	

## 28 Exclusion of Modeled Effects and Model Flags

1. To exclude specific modeled effects, following parameter settings should be chosen:

Short-Channel Effect	<b>SC1 = SC2 = SC3 = 0</b>
Reverse-Short-Channel Effect	<b>LP = 0</b>
Quantum-Mechanical Effect	<b>QME1 = QME3 = 0</b>
Poly-Depletion Effect	<b>PGD1 = PGD2 = 0</b>
Channel-Length Modulation	<b>CLM1 = CLM2 = CLM3 = 0</b>
Narrow-Channel Effect	<b>WFC = MUEPHW = WL1 = 0</b>
Small-Size Effect	<b>WL2 = 0</b>

Following flags are prepared to select required model options.

2. Selection for asymmetrical (LDMOS) or HV-MOS structure is done:

**COSYM** = 0: LDMOS (default)

**COSYM** = 1: symmetrical/asymmetrical HV-MOS

3. Selection for  $R_{\text{drift}}$  model:

**CORDRIFT** = 0: old model provided for earlier versions of HiSIM\_HV 1.

**CORDRIFT** = 1: new model (default).

4. Drift region resistances (**CORDRIFT** = 1(default) only)

**CORS** = 0 (default): no resistance on the source side will be included.

**CORS** = 1: the source-side resistance will be included.

**CORD** = 0: no resistance on the drain side will be included.

**CORD** = 1 (default): the drain-side resistance will be included.

5. Contact resistances  $R_s$  and  $R_d$  are included (for **CORDRIFT** = 0 only):

**CORSRD** = 0: no

**CORSRD** = 1 & **RS/RD** ≠ 0: yes, as internal resistance nodes

**CORSRD** = 2 & **RD** ≠ 0: yes, analytical description

**CORSRD** = 3 & **RD** ≠ 0: yes, both internal nodes and analytical description (default)

**CORSRD** = -1 & **RS/RD** ≠ 0: yes, as external resistance nodes

6. Overlap charges/capacitances are added to intrinsic ones:

**COADOV** = 0: no

**COADOV** = 1: yes (default)

7. Bias dependent overlap capacitance model is selected at drain side:

**COOVL\_P** = 0: constant overlap capacitance

**COOVL\_P** = 1: yes (default) including constant values as option

8. Bias dependent overlap capacitance model is selected at source side:

**COOVL\_P\_S** = 0: constant overlap capacitance (default)

**COOVL\_P\_S** = 1: yes including constant values as option

9. Method for calculating potential in overlap region is selected:

**COQOVSM** = 0: analytical equation excluding inversion charge

**COQOVSM** = 1: iterative solution (default)

**COQOVSM** = 2: analytical equation including inversion charge

10. Self-Heating Effect is considered:

**COSELFHEAT** = 0: no (default)

**COSELFHEAT** = 1: yes, power clipping (up to version 2.3.0)

**COSELFHEAT** = 2: yes, temperature clipping (new)

11. Substrate current  $I_{\text{sub}}$  is calculated:

**COISUB** = 0: no (default)

**COISUB** = 1: yes

12. Gate current  $I_{\text{gate}}$  is calculated:

**COIIGS** = 0: no (default)

**COIIGS** = 1: yes

13. GIDL current  $I_{\text{GIDL}}$  is calculated:

**COGIDL** = 0: no (default)

**COGIDL** = 1: yes

14. STI leakage current  $I_{\text{ds,STI}}$  is calculated:

**COISTI** = 0: no (default)

**COISTI** = 1: yes

CAUTION: This model is not supported yet in the depletion mode model.

15. Non-quasi-static (NQS) mode is invoked:

**CONQS** = 0: no (default)

**CONQS** = 1: yes

A separate flag for NQS effects on overlap charge is available.

**CONQSOV** = 0: off (default)

**CONQSOV** = 1: on

16. Gate-contact resistance is included:

**CORG** = 0: no (default)

**CORG** = 1: yes

17. Substrate resistance network is invoked:

**CORBNET** = 0: no (default)

**CORBNET** = 1: yes

18.  $1/f$  noise is calculated:

**COFLICK** = 0: no (default)

**COFLICK** = 1: yes

19. Thermal noise is calculated:

**COTHRML** = 0: no (default)

**COTHRML** = 1: yes

CAUTION: This model is not supported yet in the depletion mode model.

20. Induced gate and cross correlation noise are calculated:

**COIGN** = 0 || **COTHRML** = 0: no (default)

**COIGN** = 1 & **COTHRML** = 1: yes

CAUTION: This model is not supported yet in the depletion mode model.

21. Previous  $\phi_S$  is used for the iteration:

**COPPRV** = 0: no

**COPPRV** = 1: yes (default)

22. Parameter variations for the DFM support is considered:

**CODFM** = 0: no (default)

**CODFM** = 1: yes

23. Previous Ids is used for calculating source/drain resistance effect ( $R_s$  and/or  $R_d \neq 0$ ): This flag is inactivated.

**COIPRV** = 0: no (default)

**COIPRV** = 1: yes

24. Selection for temperature dependence of models:

	$R_{d0,temp}$	$R_{dvd,temp}$	$V_{max}$	$N_{invd}$
<b>COTEMP</b> = 0:	$T$	$T0$	$T0$	$T0$ :default & backward compatible
<b>COTEMP</b> = 1:	$T0$	$T0$	$T0$	$T0$
<b>COTEMP</b> = 2:	$T$	$T$	$T$	$T$
<b>COTEMP</b> = 3:	$T$	$T$	$T0$	$T0$

where  $T$  includes the temperature increase by the self-heating effect and  $T0$  is without.

25. Selection for the 5th node:

**COSUBNODE** = 0: the 5th node is the thermal nodel (default).

**COSUBNODE** = 1: the 5th node is the  $V_{sub}$  node.

26. Selection for output message whether model parameter is within recommendend range:

**COERRREP** = 0: no message is given.

**COERRREP** = 1: range check result is given (default).

27. Selection for the depletion mode model:

**CODEP** = 0: conventional HVMOS/LDMOS model (default).

**CODEP** = 1: 2.20 old depletion mode HVMOS/LDMOS model.

**CODEP** = 2: 2.30 old depletion mode HVMOS/LDMOS model.

**CODEP** = 3: 2.40 new depletion mode HVMOS/LDMOS model.

28. Selection for the  $V_{ds,sat}$  model :

**CODDLT** = 0: previous  $V_{ds,sat}$  model.  
**CODDLT** = 1: new  $V_{ds,sat}$  model (default).

29. Hard breakdown (avalanche breakdown) is calculated:

**COHBD** = 0: no (default)  
**COHBD** = 1 or -1: yes

30. Snapback is calculated:

**COSNP** = 0: no (default)  
**COSNP** = 1: yes; **CORBNET**=1 and **COISUB**=1 should be also specified.

31. Diode connection:

**CODIO**=0: All three diode components (bottom area, STI sidewall and gate sidewall) connect the outer branches (sb,s) or (db,d). (default)  
**CODIO**=1: Gate-sidewall peripheral component connects the inner branches (bp,sp) or (bp,dp) and remaining components connect the outer branches (sb,s) or (db,d).

31b. Reverse recovery in diodes:

**CORECOVERY** = 0: no (default)  
**CORECOVERY** = 1: yes

32. Selection for the aging model:

**CODEG** = 0: no (default)  
**CODEG** = 1: yes  
**COFIXAG** = 0: same as 2.4.0 and 2.4.1 (default)  
**COFIXAG** = 1: bugfix applied.

33. Selection for simulation step in the aging model:

**CODEGSTEP** = 0: circuit (default)  
**CODEGSTEP** = 1: DC stress simulation

34. Selection for realizing unoccupied midgap density:

**CODEGES0** = 0: no (default)  
**CODEGES0** = 1: yes

35. Selection for bias-dependent overlap length (section 16.3)

**COOVJUNC** = 0: using  $\phi_{s,over}$  (default; original implementation)  
**COOVJUNC** = 1: using  $V_{db}$  (more reasonable implementation)

36. Selection for capacitance due to trench gate (section 16.5)

**COTRENCH** = 0: no (default)  
**COTRENCH** = 1: yes

37. Selection for punch-through model:

**COPT** = 0: no (default)  
**COPT** = 1: punchthrough effects

**COPSP**T = 0: analytical solution (for deep punchthrough effect)

**COPSP**T = 1: iterative solution (for deep punchthrough effect)

Note. Analytical equations are used for shallow punchthrough effect.

Non positive **MUPT** deactivates shallow punchthrough effect.

## 29 List of Instance Parameters

Partly the same instance-parameter names and their definitions as in the BSIM3/4 models are adopted for the convenience of HiSIM users. The HiSIM Research Group wishes to acknowledge the UC Berkeley BSIM Research Group for the introduction of these instance parameters.

<b>L</b>	gate length ( $L_{gate}$ ) default: $\mathbf{L} = 2\mu m$
<b>W</b>	gate width ( $W_{gate}$ ) default: $\mathbf{W} = 5\mu m$ ** Diode **
<b>AD</b>	area of drain junction
<b>AS</b>	area of source junction
<b>PD</b>	perimeter of drain junction
<b>PS</b>	perimeter of source junction ** Source/Drain Resistance **
<b>NRS</b>	number of source squares
<b>NRD</b>	number of drain squares ** Gate Resistance **
<b>XGW</b>	distance from the gate contact to the channel edge
<b>XGL</b>	offset of the gate length
<b>NF</b>	number of gate fingers
<b>M</b>	multiplication factor
<b>NGCON</b>	number of gate contacts ** Substrate Network **
<b>RBPB</b>	substrate resistance network
<b>RBPD</b>	substrate resistance network
<b>RBPS</b>	substrate resistance network ** Length of Diffusion **
<b>SA</b>	length of diffusion between gate and STI
<b>SB</b>	length of diffusion between gate and STI
<b>SD</b>	length of diffusion between gate and gate ** Temperature **
<b>DTEMP</b>	device temperature change ** Design for Manufacturability **
<b>NSUBCDFM</b>	substrate impurity concentration ** Substrate Current **
<b>SUBLD1</b>	substrate current induced in $L_{drift}$ (inactivated)
<b>SUBLD2</b>	substrate current induced in $L_{drift}$ (inactivated) ** Resistance **
<b>LDRIFT1</b>	length of lightly doped drift region (default: 0)
<b>LDRIFT2</b>	length of heavily doped drift region (default: $1 \mu m$ )
<b>LDRIFT1S</b>	length of lightly doped drift region in source side (default: 0)
<b>LDRIFT2S</b>	length of heavily doped drift region in source side (default: $1 \mu m$ ) ** Overlap **
<b>LOVER</b>	length of overlap region in source side for LDMOS
<b>LOVERLD</b>	length of overlap region in drain side
<b>LOVERS</b>	length of overlap region in source side for HVMOS
<b>COSELFHEAT</b>	flag to switch on the self-heating effect
<b>COSUBNODE</b>	flag for selection of the 5th node

<b>NPEXT</b>	maximum concentration of pocket tail
<b>FALPH</b>	power of $f$ describing deviation of $1/f$
<b>RS</b>	source-contact resistance of LDD region
<b>RD</b>	drain-contact resistance of LDD region
<b>RD22</b>	$V_{bs}$ dependence of <b>RD</b> for <b>CORSRD</b> =2,3
<b>RD23</b>	modification of <b>RD</b> for <b>CORSRD</b> =2,3
<b>RD24</b>	$V_{gs}$ dependence of <b>RD</b> for <b>CORSRD</b> =2,3
<b>RDVG11</b>	$V_{gs}$ dependence of <b>RD</b> for <b>CORSRD</b> =1,3
<b>RDICT1</b>	<b>LDRFIT1</b> dependence of resistance for <b>CORSRD</b> =1,3
<b>RDOV13</b>	alternative $L_{over}$ dependence model for <b>CORSRD</b>
<b>RDSL1</b>	<b>LDRFIT1</b> dependence of resistance for <b>CORSRD</b> =1,3
<b>RDVB</b>	$V_{bs}$ dependence of <b>RD</b> for <b>CORSRD</b> =1,3
<b>RDVD</b>	$V_{ds}$ dependence of <b>RD</b> for <b>CORSRD</b> =1,3
<b>RTH0</b>	thermal resistance
<b>VOVER</b>	velocity overshoot effect
<b>CGBO</b>	gate-to-bulk overlap capacitance
<b>CVDSOVER</b>	modification of the $C_{gg}$ peak for $V_{ds} \neq 0$
<b>POWRAT</b>	thermal dissipation

## 30 Default Parameters and Limits of the Parameter Values

The maximum and minimum limits of the model parameter are recommended values. These values may be violated in some specific cases. "default" in remarks means that the default value is preferable.

Parameter	Unit	Min	Max	Default	Remarks
<b>VERSION</b>		2.20	2.40	2.40	
<b>TOX</b>	[m]			7n	
<b>XL</b>	[m]			0	
<b>XW</b>	[m]			0	
<b>XLD</b>	[m]	0	50n	0	
<b>XWD</b>	[m]	-100n	300n	0	
<b>XWDLD</b>	[m]			0	given if $\neq$ <b>XWD</b>
<b>XWDC</b>	[m]	-500n	500n	0	given if $\neq$ <b>XWD</b>
<b>TPOLY</b>	[m]			200n	
<b>LL</b>	[m <sup>LLN+1</sup> ]			0	
<b>LLD</b>	[m]			0	
<b>LLN</b>	[—]			0	
<b>WL</b>	[m <sup>WLN+1</sup> ]			0	
<b>WLD</b>	[m]			0	
<b>WLN</b>	[—]			0	
<b>NSUBC</b>	[cm <sup>-3</sup> ]	$1 \times 10^{16}$	$1 \times 10^{19}$	$3 \times 10^{17}$	<b>CODEP=0</b>
		$1 \times 10^{16}$	$1 \times 10^{19}$	$5 \times 10^{16}$	<b>CODEP=1,2,3</b>
<b>NSUBP</b>	[cm <sup>-3</sup> ]	$1 \times 10^{16}$	$1 \times 10^{19}$	$1 \times 10^{18}$	<b>CODEP=0</b>
		$1 \times 10^{16}$	$1 \times 10^{19}$	$1 \times 10^{17}$	<b>CODEP=1,2,3</b>
<b>DDRIFT</b>	[m]			$1.0 \times 10^{-6}$	
<b>NSUBSUB</b>	[cm <sup>-3</sup> ]			$1.0 \times 10^{15}$	required for $V_{sub,s}$ dependence
<b>LP</b>	[m]	0	300n	15n	<b>CODEP=0</b>
		0	300n	0n	<b>CODEP=1,2,3</b>
<b>*NPEXT</b>	[cm <sup>-3</sup> ]	$1 \times 10^{16}$	$1 \times 10^{18}$	$5 \times 10^{17}$	
<b>*LPEXT</b>	[m]	$1 \times 10^{-50}$	$1 \times 10^{-5}$	$1 \times 10^{-50}$	
<b>VFBC</b>	[V]	-1.2	0.0	-1.0	<b>CODEP=0</b>
		-1.2	0.8	-0.2	<b>CODEP=1,2,3</b>
<b>VBI</b>	[V]	1.0	1.2	1.1	
<b>KAPPA</b>	[—]			3.9	
<b>EG0</b>	[eV]	1.0	1.3	1.1785	
<b>BGTMPI</b>	[eV K <sup>-1</sup> ]	$50\mu$	$1000\mu$	$90.25\mu$	default
<b>BGTMPII</b>	[eV K <sup>-2</sup> ]	$-1\mu$	$1\mu$	$0.1\mu$	
<b>TNOM</b>	[°C]	22	32	27	
<b>VMAX</b>	[cm s <sup>-1</sup> ]	1MEG	20MEG	10MEG	
<b>VMAXT1</b>	[cm (sK) <sup>-1</sup> ]			0	
<b>VMAXT2</b>	[cm (sK <sup>2</sup> ) <sup>-1</sup> ]			0	
<b>VOVER</b>	[m VOVERP]	0	4.0	0.3	
<b>VOVERP</b>	[—]	0	2.0	0.3	
<b>*VTMP</b>	[—]	-2.0	1.0	0	
<b>QME1</b>	[Vm]	0	1n	0	
<b>QME2</b>	[V]	1.0	3.0	2.0	
<b>QME3</b>	[m]	0	500p	0	
<b>PGD1</b>	[V]	0	30m	0	
<b>PGD2</b>	[V]	0	1.5	1.0	
<b>*PGD4</b>	[—]	0	3.0	0	
<b>PARL2</b>	[m]	0	50n	10n	
<b>SC1</b>	[—]	0	10	0	
<b>SC2</b>	[V <sup>-1</sup> ]	0	1	0	

Parameter	Unit	Min	Max	Default	Remarks
*SC3	[V <sup>-1</sup> m]	0	20μ	0	
* * SC4	[1/V]	0		0	
SCP1	[—]	0	10	0	
SCP2	[V <sup>-1</sup> ]	0	1	0	
*SCP3	[V <sup>-1</sup> m]	0	200n	0	
*SCP21	[V]	0	5.0	0	
*SCP22	[V <sup>4</sup> ]	0	0	0	reset to zero
*BS1	[V <sup>2</sup> ]	0	0.05	0	
*BS2	[V]	0.5	1.0	0.9	
*PTL	[V]	0		0	
*PTLP	[—]			1.0	
*PTP	[—]	3.0	4.0	3.5	
*PT2	[V <sup>-1</sup> ]	0		0	
*PT4	[V <sup>-2</sup> ]	0		0	
*PT4P	[—]	0		1	
*GDL	[—]	0	0.22	0	
*GDLP	[—]			0	
*GDLD	[m]			0	
NJUNC	[1/cm <sup>3</sup> ]			10 <sup>20</sup>	
XJPT	m			3×10 <sup>-8</sup>	
MUPT	m <sup>2</sup> /V/s			0	
VFBPT	V			0	
PSLIMPT	V			0	
MUECB0	[cm <sup>2</sup> V <sup>-1</sup> s <sup>-1</sup> ]	100	100k	1k	
MUECB1	[cm <sup>2</sup> V <sup>-1</sup> s <sup>-1</sup> ]	5	10k	100	
MUEPH0	[—]	0.25	0.35	0.3	default
MUEPH1	[cm <sup>2</sup> V <sup>-1</sup> s <sup>-1</sup> (V cm <sup>-1</sup> ) <sup>MUEPH0</sup> ]	2k	30k	20k (nMOS) 9k(pMOS)	
MUEEFB	[V <sup>-1</sup> ]			0.0	
MUETMP	[—]	0.5	2.5	1.5	
*MUEPHL	[—]			0	
*MUEPLP	[—]			1.0	
MUESR0	[—]	1.8	2.2	2.0	default <b>CODEP=0</b> <b>CODEP=1,2,3</b>
MUESR1	[cm <sup>2</sup> V <sup>-1</sup> s <sup>-1</sup> (V cm <sup>-1</sup> ) <sup>MUESR0</sup> ]	1×10 <sup>14</sup>	1×10 <sup>16</sup>	6×10 <sup>14</sup>	
		1×10 <sup>14</sup>	1×10 <sup>16</sup>	5×10 <sup>15</sup>	
*MUESRL	[—]			0	
*MUESLP	[—]			1.0	
NDEP	[—]	0	1.0	1.0	
*NDEPL	[—]			0	
*NDEPLP	[—]			1.0	
NINV	[—]	0	1.0	0.5	
NINVD	[1/V]	0		0.0	
NINVDW	[—]	0		0.0	
NINVDWP	[—]	0		1.0	
NINVDT1	[1/K]	0		0.0	
NINVDT2	[1/K <sup>2</sup> ]	0		0.0	
BB	[—]			2.0(nMOS) 1.0(pMOS)	
WFC	[F m <sup>-1</sup> ]	-5.0×10 <sup>-15</sup>	1×10 <sup>-6</sup>	0	
*WVTH0	[V]			0	
*NSUBCW	[—]			0	
*NSUBCWP	[—]			1	
*NSUBP0	[cm <sup>-3</sup> ]			0	
*NSUBWP	[—]			1.0	

Parameter	Unit	Min	Max	Default	Remarks
*MUEPHW	[ ]			0	possibly negative
*MUEPWP	[ ]			1.0	
*MUESRW	[ ]			0	possibly positive
*MUESWP	[ ]			1.0	
*VTHSTI	[V]			0	
VDSTI	[ ]			0	
SCSTI1	[ ]			0	
SCSTI2	[V <sup>-1</sup> ]			0	
NSTI	[cm <sup>-3</sup> ]		1×10 <sup>16</sup>	1×10 <sup>19</sup>	5×10 <sup>17</sup>
WSTI	[m]			0	
WSTIL	[ ]			0	
WSTILP	[ ]			1.0	
WSTIW	[ ]			0	
WSTIWP	[ ]			1.0	
WL1	[ ]			0	
WL1P	[ ]			1.0	
NSUBPSTI1	[m]			0	
NSUBPSTI2	[ ]			0	
NSUBPSTI3	[ ]			1.0	
MUESTI1	[m]			0	
MUESTI2	[ ]			0	
MUESTI3	[ ]			1.0	
WL2	[V]			0	
WL2P	[ ]			1.0	
*MUEPHS	[ ]			0	
*MUEPSP	[ ]			1.0	
*VOVERS	[ ]			0	
*VOVERSP	[ ]			0	
CLM1	[ ]	0.01	1.0	0.05	CODEP=0,3
CLM2	[ ]	1.0	4.0	2.0	CODEP=0,3
CLM3	[ ]	0.5	5.0	1.0	CODEP=0,3
CLM5	[ ]	0	2.0	1.0	CODEP=0,3
CLM6	[ ]	0	20.0	0	CODEP=0,3
SUB1	[V <sup>-1</sup> ]			10	
SUB1L	[m <sup>SUB1LP</sup> ]			2.5×10 <sup>-3</sup>	
SUB1LP	[ ]			1.0	
SUB2	[V]			25.0	
SUB2L	[m]	0	1.0	2×10 <sup>-6</sup>	
SUBTMP	[1/T]	0	5×10 <sup>-3</sup>	0	
SVDS	[ ]			0.8	
SLG	[m]			3×10 <sup>-8</sup>	
SLGL	[m <sup>SLGLP</sup> ]			0	
SLGLP	[ ]			1.0	
SVBS	[ ]			0.5	
SVBSL	[m <sup>SVBSLP</sup> ]			0	
SVBSLP	[ ]			1.0	
SVGS	[ ]			0.8	
SVGSL	[m <sup>SVGSLP</sup> ]			0	
SVGSLP	[ ]			1.0	
SVGSW	[m <sup>SVGSWP</sup> ]			0	
SVGSWP	[ ]			1.0	
IBPC1	[VA <sup>-1</sup> ]	0	1.0×10 <sup>12</sup>	0	
IBPC1L	[ ]			0	
IBPC1LP	[ ]			1.0	
IBPC2	[V <sup>-1</sup> ]	0	1.0×10 <sup>12</sup>	0	

Parameter	Unit	Min	Max	Default	Remarks
<b>SUBLD1</b>	[V <sup>-1</sup> ]			0	
<b>SUBLD1L</b>	[μm <sup>SUBLD1LP</sup> ]			0	
<b>SUBLD1LP</b>	[—]			1.0	
<b>SUBLD2</b>	[mV <sup>-1</sup> ]			0	
<b>XPDV</b>	[—]	0		0	
<b>XPVDTH</b>	[—]	0		0	
<b>XPVDTHG</b>	[—]	-1	1	0	
<b>MPHDFM</b>	[—]	-3	3	-0.3	
<b>SAREF</b>	[m]			1.0×10 <sup>-6</sup>	
<b>SBREF</b>	[m]			1.0×10 <sup>-6</sup>	
<b>GLEAK1</b>	[V <sup>-3/2</sup> s <sup>-1</sup> ]			50	
<b>GLEAK2</b>	[V <sup>-1/2</sup> cm <sup>-1</sup> ]			10MEG	
<b>GLEAK3</b>	[—]			60×10 <sup>-3</sup>	
<b>GLEAK4</b>	[m <sup>-1</sup> ]			4.0	
* <b>GLEAK5</b>	[V m <sup>-1</sup> ]			7.5×10 <sup>3</sup>	
* <b>GLEAK6</b>	[V]			250×10 <sup>-3</sup>	
* <b>GLEAK7</b>	[m <sup>2</sup> ]			1×10 <sup>-6</sup>	
* <b>EGIG</b>	[V]			0.0	
* <b>IGTEMP2</b>	[VK]			0	
* <b>IGTEMP3</b>	[VK <sup>2</sup> ]			0	
<b>GLKSD1</b>	[A m V <sup>-2</sup> ]			1×10 <sup>-15</sup>	
<b>GLKSD2</b>	[V <sup>-1</sup> m <sup>-1</sup> ]			1×10 <sup>3</sup>	
<b>GLKSD3</b>	[m <sup>-1</sup> ]			-1×10 <sup>3</sup>	
<b>GLKB1</b>	[A V <sup>-2</sup> m <sup>-2</sup> ]			5×10 <sup>-16</sup>	
<b>GLKB2</b>	[m V <sup>-1</sup> ]			1.0	
<b>GLKB3</b>	[V]			0	
<b>GLPART1</b>	[—]	0	1.0	0.5	
<b>FN1</b>	[V <sup>-1.5</sup> . m <sup>2</sup> ]			50	
<b>FN2</b>	[V <sup>-0.5</sup> . m <sup>-1</sup> ]			170×10 <sup>-6</sup>	
<b>FN3</b>	[V]			0	
<b>FVBS</b>	[—]			12×10 <sup>-3</sup>	
<b>GIDL1</b>	[V <sup>-3/2</sup> s <sup>-1</sup> m]			2.0	
<b>GIDL2</b>	[V <sup>-0.5</sup> m <sup>-1</sup> ]			3×10 <sup>7</sup>	
<b>GIDL3</b>	[—]			0.9	
* <b>GIDL4</b>	[V]			0	
* <b>GIDL5</b>	[—]			0.2	
<b>VBSMIN</b>	[V]				no more required
<b>VGSMIN</b>	[V]			-100(nMOS)	fixed
				100(pMOS)	fixed
<b>VZADD0</b>	[V]			0.01	fixed
<b>PZADD0</b>	[V]			0.005	fixed
<b>DDLTMAX</b>	[—]	1	10	10	
<b>DDLTSLP</b>	[μm <sup>-1</sup> ]	0	20	10	
<b>DDLTICT</b>	[—]	-3	20	0	
<b>JS0</b>	[A m <sup>-2</sup> ]			0.5×10 <sup>-6</sup>	
<b>JS0D</b>	[A m <sup>-2</sup> ]			<b>JS0</b>	
<b>JS0S</b>	[A m <sup>-2</sup> ]			<b>JS0</b>	
<b>JS0SW</b>	[A m <sup>-1</sup> ]			0	
<b>JS0SWD</b>	[A m <sup>-1</sup> ]			<b>JS0SW</b>	
<b>JS0SWS</b>	[A m <sup>-1</sup> ]			<b>JS0SW</b>	
<b>JS0SWG</b>	[A m <sup>-1</sup> ]			0	CODIO=1
<b>JS0SWGD</b>	[A m <sup>-1</sup> ]			<b>JS0SWG</b>	CODIO=1
<b>JS0SWGS</b>	[A m <sup>-1</sup> ]			<b>JS0SWG</b>	CODIO=1
<b>NJ</b>	[—]			1.0	
<b>NJD</b>	[—]			<b>NJ</b>	

Parameter	Unit	Min	Max	Default	Remarks
NJS	[ ]			NJ	
NJSW	[ ]			1.0	
NJSWD	[ ]			NJSW	
NJSWS	[ ]			NJSW	
NJSWG	[ ]			1.0	
NJSWGD	[ ]			NJSWG	
NJSWGS	[ ]			NJSWG	
XTI	[ ]			2.0	
XTID	[ ]			XTI	
XTIS	[ ]			XTI	
XTI2	[ ]			0	
XTI2D	[ ]			XTI	
XTI2S	[ ]			XTI	
DIVX	[V <sup>-1</sup> ]			0	
DIVXD	[V <sup>-1</sup> ]			DIVX	
DIVXS	[V <sup>-1</sup> ]			DIVX	
CTEMP	[ ]			0	
CISB	[ ]			0	
CISBD	[ ]			CISB	
CISBS	[ ]			CISB	
CISBK	[A]			0	
CISBKD	[A]			CISBK	
CISBKS	[A]			CISBK	
CVB	[ ]	-0.1	0.2	0	
CVBD	[ ]	-0.1	0.2	CVB	
CVBS	[ ]	-0.1	0.2	CVB	
CJ	[F m <sup>-2</sup> ]			5×10 <sup>-4</sup>	
CJD	[F m <sup>-2</sup> ]			CJ	
CJS	[F m <sup>-2</sup> ]			CJ	
CJSW	[F m <sup>-1</sup> ]			5×10 <sup>-10</sup>	
CJSWD	[F m <sup>-1</sup> ]			CJSW	
CJSWS	[F m <sup>-1</sup> ]			CJSW	
CJSWG	[F m <sup>-1</sup> ]			5×10 <sup>-10</sup>	
CJSWGD	[F m <sup>-1</sup> ]			CJSWG	
CJSWGS	[F m <sup>-1</sup> ]			CJSWG	
MJ	[ ]			0.5	
MJD	[ ]			MJ	
MJS	[ ]			MJ	
MJSW	[ ]			0.33	
MJSWD	[ ]			MJSW	
MJSWS	[ ]			MJSW	
MJSWG	[ ]			0.33	
MJSWGD	[ ]			MJSWG	
MJSWGS	[ ]			MJSWG	
PB	[V]			1.0	
PBD	[V]			PB	
PBS	[V]			PB	
PBSW	[V]			1.0	
PBSWD	[V]			PBSW	
PBSWS	[V]			PBSW	
PBSWG	[V]			1.0	
PBSWGD	[V]			PBSWG	
PBSWGS	[V]			PBSWG	
VDIFFJ	[V]			0.6×10 <sup>-3</sup>	
VDIFFJD	[V]			VDIFFJ	

Parameter	Unit	Min	Max	Default	Remarks
<b>VDIFFJS</b>	[V]			<b>VDIFFJ</b>	
<b>TCJBD</b>	[K <sup>-1</sup> ]			0	
<b>TCJBDSW</b>	[K <sup>-1</sup> ]			0	
<b>TCJBDSWG</b>	[K <sup>-1</sup> ]			0	
<b>TCJBS</b>	[K <sup>-1</sup> ]			0	
<b>TCJBSSW</b>	[K <sup>-1</sup> ]			0	
<b>TCJBSSWG</b>	[K <sup>-1</sup> ]			0	
<b>TPBBD</b>	[V K <sup>-1</sup> ]			0	
<b>TPBBDSW</b>	[V K <sup>-1</sup> ]			0	
<b>TPBBDSWG</b>	[V K <sup>-1</sup> ]			0	
<b>TPBBS</b>	[V K <sup>-1</sup> ]			0	
<b>TPBBSSW</b>	[V K <sup>-1</sup> ]			0	
<b>TPBBSSWG</b>	[V K <sup>-1</sup> ]			0	
<b>NDIBOT</b>	[cm <sup>-3</sup> ]			1e16	Doping of drift reg.
<b>INJ1</b>	[ <sup>-</sup> ]			1.0	For carrier density
<b>INJ2</b>	[ <sup>-</sup> ]			10.0	For carrier density
<b>NQS</b>	[s]			5 × 10 <sup>-9</sup>	Carr. delay time
<b>TAU</b>	[s]			2 × 10 <sup>-7</sup>	Carr. lifetime
<b>WI</b>	[m]			5 × 10 <sup>-6</sup>	Length of drift reg.
<b>DEPNQS</b>	[s]			0.0	Depletion delay
<b>TAUT</b>	[ <sup>-</sup> ]			0.0	Temp. co. lifetime
<b>INJT</b>	[ <sup>-</sup> ]			0.0	Temp. co. carr.
<b>HBDA</b>				0.0	<b>COHBD=1</b>
<b>HBDB</b>				0.0	<b>COHBD=1</b>
<b>HBDC</b>				100.0	<b>COHBD=1</b>
<b>HBDF</b>				1.0	<b>COHBD=1</b>
<b>HBDCTMP</b>				0.0	<b>COHBD=1</b>
<b>SUB1SNP</b>	[1/V]			<b>SUB1</b>	<b>COSNP=1</b>
<b>SUB2SNP</b>	[V]			0.6 × <b>SUB2</b>	<b>COSNP=1</b>
<b>SVDSSNP</b>	[ <sup>-</sup> ]			<b>SVDS</b>	<b>COSNP=1</b>
<b>NFALP</b>	[cm s]			1 × 10 <sup>-19</sup>	
<b>NFTRP</b>	[V <sup>-1</sup> ]			1 × 10 <sup>10</sup>	
*CIT	[F cm <sup>-2</sup> ]			0	
<b>FALPH</b>	[sm <sup>3</sup> ]			1.0	
<b>DLY1</b>	[s]			100 × 10 <sup>-12</sup>	
<b>DLY2</b>	[m <sup>2</sup> ]			0.7	
<b>DLY3</b>	[Ωm <sup>2</sup> ]			0.8 × 10 <sup>-6</sup>	
<b>DLYOV</b>	[1/A]			0.8 × 10 <sup>-4</sup>	
<b>XQY</b>	[m]	10n	50n	0	
<b>XQY1</b>	[F · μm <sup>XQY2-1</sup> ]	0		0	
<b>XQY2</b>	[ <sup>-</sup> ]	0		2	
<b>OVSLP</b>	[mV <sup>-1</sup> ]			2.1 × 10 <sup>-7</sup>	
<b>OVMAG</b>	[V]			0.6	
<b>CGSO</b>	[F m <sup>-1</sup> ]	0	100nm × C <sub>ox</sub>		to be set by user
<b>CGDO</b>	[F m <sup>-1</sup> ]	0	100nm × C <sub>ox</sub>		to be set by user
<b>CGBO</b>	[F m <sup>-1</sup> ]	0		0	
<b>RS</b>	[Ωm]	0	0.01	0	
<b>RD</b>	[Ωm]	0	0.1	0	
<b>RSH</b>	[V A <sup>-1</sup> square]	0	500	0	
<b>RSHG</b>	[V A <sup>-1</sup> square]	0	100	0	
<b>GBMIN</b>	[ <sup>-</sup> ]			1 × 10 <sup>-12</sup>	for circuit simulation
<b>GDSLEAK</b>	[ <sup>-</sup> ]			0	for circuit simulation

Parameter	Unit	Min	Max	Default	Remarks
<b>RBPB</b>	[ $\Omega$ ]			50	
<b>RBPD</b>	[ $\Omega$ ]			50	
<b>RBPS</b>	[ $\Omega$ ]			50	
<b>RTH0</b>	[Kcm/W]	0	10	0.1	
<b>RTHTEMP1</b>	[m/W]	-1	1	0	
<b>RTHTEMP2</b>	[m/W/K]	-1	1	0	
<b>CTH0</b>	[Ws/(Kcm)]			$1 \times 10^{-7}$	
<b>RTH0L</b>	[—]	-100	100	0	
<b>RTH0LP</b>	[—]	-10	10	1	
<b>RTH0W</b>	[—]	-100	100	0	
<b>RTH0WP</b>	[—]	-10	10	1	
<b>RTH0NF</b>	[—]	-5	5	0	
<b>POWRAT</b>	[—]	0	1.0	1.0	
<b>PRACTEMP1</b>	[1/K]	-1	1	0	
<b>PRACTEMP2</b>	[1/K <sup>2</sup> ]	-1	1	0	
<b>SHEMAX</b>	[K]	300	900	500	
<b>SHEMAXDLT</b>	[—]	0		0.1	
<b>XLDLD</b>	[m]	0		$1 \times 10^{-6}$	reset to <b>XLDLD</b> $\geq 0$
<b>LOVERLD</b>	[m]	0		$1.0 \times 10^{-6}$	
<b>LOVERS</b>	[m]	0		30n	
<b>LOVER</b>	[m]	0		30n	
<b>NOVER</b>	[cm <sup>-3</sup> ]			$3 \times 10^{16}$	
<b>NOVERS</b>	[cm <sup>-3</sup> ]			$1.0 \times 10^{17}$	
<b>VFBOVER</b>	[V]	-1.2	1	0.5	
<b>QOVADD</b>	[F/m <sup>2</sup> ]			0	
<b>QOVJUNC</b>	[—]	-1	50	0	
<b>CVDSOVER</b>	[—]	0	1.0	0	(COTRENCH=0)
<b>LDRIFT1</b>	[m]	0		$1.0 \times 10^{-6}$	
<b>LDRIFT2</b>	[m]	0		$1.0 \times 10^{-6}$	
<b>WTRENCH</b>	[m]	0		$0.2 \times 10^{-6}$	(COTRENCH=1)
<b>OLMDLT</b>	[—]	0	100	5	(COTRENCH=1)
<b>TOXB</b>	[m]			<b>TOX</b>	(COTRENCH=1)
<b>**CORDRIFT=1**</b>					
<b>RDRDL1</b>	[m]			0	
<b>RDRDL2</b>	[m]			0	
<b>DRRCX</b>	[—]	0	1	0	reset within the range
<b>DRRCAR</b>	[mV <sup>-1</sup> ]	0	50n	100n	
<b>RDRDJUNC</b>	[m]			$1.0 \times 10^{-6}$	
<b>RDRBB</b>	[—]			1.0	
<b>RDRBBS</b>	[—]			1.0	
<b>RDRMUE</b>	[cm <sup>2</sup> (V · s) <sup>-1</sup> ]	100	3000	1000	
<b>RDRMUES</b>	[cm <sup>2</sup> (V · s) <sup>-1</sup> ]	100	3000	1000	
<b>RDRMUEL</b>	[—]			0	
<b>RDRMUEL</b>	[—]			1	
<b>RDRBBTMRP</b>	[1/K]			0	
<b>RDRMUETMRP</b>	[—]	0.0	2.0	0	
<b>RDRVMAX</b>	[cm s <sup>-1</sup> ]	1MEG	100MEG	30MEG	
<b>RDRVMAXS</b>	[cm s <sup>-1</sup> ]	1MEG	100MEG	30MEG	
<b>RDRVMAXL</b>	[—]			0	
<b>RDRVMAXLP</b>	[—]			1	
<b>RDRVMAXW</b>	[—]			0	
<b>RDRVMAXWP</b>	[—]			1	
<b>RDRV TMP</b>	[—]	-2.0	1.0	0	

Parameter	Unit	Min	Max	Default	Remarks
<b>RDRQOVER</b>	[1/cm]	0	$1 \times 10^7$	$1 \times 10^5$	
<b>**CORDRIFT=0**</b>					
RDVG11	[]	0	$V_{ds,max}/30$	0	CORSRD=1,3
RDVG12	[V <sup>-1</sup> ]	0	$V_{ds,max}$	100	CORSRD=1,3
RDVD	[Ωcm/V]	0	2.0	$7.0 \times 10^{-2}$	CORSRD=1,3
RDVB	[V <sup>-1</sup> ]	0	2.0	0	CORSRD=1,3
RDS	[μm <sup>RDSP</sup> ]	-100	100	0	CORSRD=1,3
RDSP	[—]	-10	10	1	CORSRD=1,3
RDVDL	[μm <sup>-RDVDLP</sup> ]	-100	100	0	CORSRD=1,3
RDVDLP	[—]	-10	10	1	CORSRD=1,3
RDVDS	[μm <sup>RDVDSP</sup> ]	-100	100	0	CORSRD=1,3
RDVDSP	[—]	-10	10	1	CORSRD=1,3
RD20	[—]	0	30	0	CORSRD=2,3
RD21	[—]	0	1.0	1.0	CORSRD=2,3
RD22	[Ω m/V <sup>RD22D+1</sup> ]	-5.0	0	0	CORSRD=2,3
RD22D	[—]	0	2.0	0	CORSRD=2,3
RD23	[Ω m/V <sup>RD21</sup> ]	0	2.0	0.005	CORSRD=2,3
RD23L	[μm <sup>-RD23LP</sup> ]	-100	100	0	CORSRD=2,3
RD23LP	[—]	-10	10	1	CORSRD=2,3
RD23S	[μm <sup>RD23SP+1</sup> ]	-100	100	0	CORSRD=2,3
RD23SP	[—]	-10	10	1	CORSRD=2,3
RD24	[Ωm/V <sup>RD21+1</sup> ]	0	0.1	0	CORSRD=2,3
RD25	[V]	0	$V_{gs,max}$	0	CORSRD=2,3
RDOV11	[—]	0	10	0	CORSRD=1,3
RDOV12	[—]	0	2	1.0	CORSRD=1,3
RDOV13	[—]	0	1.0	1.0	CORSRD=1,3
RDSLPI	[—]	-10	10	0	CORSRD=1,3
RDICT1	[—]	-10	10	1.0	CORSRD=1,3
RDSLPI	[—]	-10	10	1	CORSRD=1,3
RDICT2	[—]	-10	10	0	CORSRD=1,3
RDTEMP1	[Ωcm/K]	-0.1	2	0	
RDTEMP2	[Ωcm/K <sup>2</sup> ]	$-1.0 \times 10^{-3}$	$1.0 \times 10^{-3}$	0	
RDVDTEMP1	[Ωcm V <sup>-1</sup> K <sup>-1</sup> ]	-0.1	1.0	0	
RDVDTEMP2	[Ωcm V <sup>-1</sup> K <sup>-2</sup> ]	$-1.0 \times 10^{-3}$	$1.0 \times 10^{-3}$	0	
RDVDSUB	[—]			0.3	
RDVSUB	[—]			1.0	
VBISUB	[—]			0.7	
Depletion mode					
<b>**CODEP=1,2,3**</b>					
NDEPM	[cm <sup>-3</sup> ]	$5 \times 10^{15}$	$1 \times 10^{18}$	$1 \times 10^{17}$ $4 \times 10^{16}$	(CODEP=1,2) (CODEP=3)
NDEPML	[—]			0	
NDEPMLP	[—]			1	
TNDEP	[m]	10n	100n	200n 300n	(CODEP=1,2) (CODEP=3)
DEPMUE0	[cm <sup>2</sup> V <sup>-1</sup> s <sup>-1</sup> ]	1	1e5	1000	(CODEP=1,2)
		1	1e10	$1 \times 10^8$	(CODEP=3)
DEPMUE0L	[—]			0	
DEPMUE0LP	[—]			1	
DEPMUE1	[cm <sup>2</sup> V <sup>-1</sup> s <sup>-1</sup> ]			0 100	(CODEP=1,2) (CODEP=3)
DEPMUE1L	[—]			0	
DEPMUE1LP	[—]			1	
DEPMUEPH0	[—]			0.3	(CODEP=1,2)
				0	(CODEP=3)

Parameter	Unit	Min	Max	Default	Remarks
<b>DEPMUEPH1</b>	[cm <sup>2</sup> V <sup>-1</sup> s <sup>-1</sup> ]	1 100	1e5 2e9	5 × 10 <sup>3</sup> 400	(CODEP=1,2) (CODEP=3)
<b>DEPVMAX</b>	[cm/s]			3 × 10 <sup>7</sup> 1 × 10 <sup>7</sup>	(CODEP=1,2) (CODEP=3)
<b>DEPVMAXL</b>	[—]			0	
<b>DEPVMAXLP</b>	[—]			1	
<b>DEPBB</b>	[—]	0.01		1 2	(CODEP=1,2) (CODEP=3)
<b>DEPMUETMP</b>	[—]			1.5	
<b>DEPVTMP</b>	[—]			0.0	
<b>DEPLEAK</b>	[V]	0 0	5 5	0.5 0.1	(CODEP=1,2) (CODEP=3)
<b>DEPLEAKL</b>	[—]			0	
<b>DEPLEAKLP</b>	[—]			1	
<b>**CODEP=3**</b>					
<b>DEPDVFBC</b>	[V]			0.1	CODEP=3
<b>DEPRBR</b>	[—]	0	1	1	CODEP=3
<b>DEPJLEAK</b>	[A/m <sup>2</sup> ]	0		0	CODEP=3
<b>DEPWLP</b>	[—]			0	CODEP=3
<b>DEPPB0</b>	[V]	0	0.5	0.5	Compatible to HiSIM2
<b>DEPNINVDC</b>	[1/V]			100	Use 0.0 initially in parameter extraction
<b>DEPNINVDH</b>	[1/V]			10	Use 0.0 initially in parameter extraction
<b>DEPNINVDL</b>	[—]			0	CODEP=3
<b>DEPNINVDLP</b>	[—]			0	CODEP=3
<b>DEPNINVDW</b>	[—]			0	CODEP=3
<b>DEPNINVDWP</b>	[—]			0	CODEP=3
<b>DEPNINVDT1</b>	[—]			0	CODEP=3
<b>DEPNINVDT2</b>	[—]			0	CODEP=3
<b>DEPCAR</b>	[m/V]			0	CODEP=3
<b>DEPRDRDL1</b>	[m]			0.0	CODEP=3
<b>DEPRDRDL2</b>	[m]			0.0	CODEP=3
<b>DEPSUBSL0</b>	[—]	10n		<b>DEPSUBL</b>	CODEP=3
<b>DEPQF</b>	[V]	10n	8	0.01	CODEP=3
<b>DEPQFRES</b>	[V]	10n	8	0.05	CODEP=3
<b>DEPFDPD</b>	[V]	10n	4	0.2	CODEP=3
<b>DEPPS</b>	[V]			0.01	CODEP=3
<b>DEPVSAATA</b>	[V]			0.0	CODEP=3
<b>**CODEP=2,3**</b>					
<b>TNDEPV</b>	[V <sup>-1</sup> ]			0.0	
<b>DEPMUE2</b>	[cm <sup>2</sup> V <sup>-1</sup> s <sup>-1</sup> ]	0		10 <sup>3</sup>	
<b>DEPDDLT</b>	[—]			3.0 1.0	(CODEP=2) (CODEP=3)
<b>DEPSUBL</b>	[—]	10n		2.0	
<b>DEPMUE0TMP</b>	[—]			0.0	
<b>DEPVGPSL</b>	[V]	0		0.0 0.2	(CODEP=2) (CODEP=3)
<b>** CODEP=2**</b>					
<b>DEPVFBC</b>	[V]			-0.2	CODEP=2
<b>DEPMUEA1</b>	[—]			0.0	CODEP=2
<b>DEPVSATR</b>	[—]			0	CODEP=2
<b>DEPMUE2TMP</b>	[—]			0.0	CODEP=2
<b>**CODEP=1,2**</b>					
<b>DEPVDFEF1</b>	[V]			2.0	CODEP=1,2

Parameter	Unit	Min	Max	Default	Remarks
DEPVDSEF1L	[—]			0	CODEP=1,2
DEPVDSEF1LP	[—]			1	CODEP=1,2
DEPVDSEF2	[—]	0.1	4.0	0.5	CODEP=1,2
DEPVDSEF2L	[—]			0	CODEP=1,2
DEPVDSEF2LP	[—]			1	CODEP=1,2
**CODEP=1**					
DEPETA	[V <sup>-1</sup> ]			0	CODEP=1
DEPMUEBACK0	[cm <sup>2</sup> V <sup>-1</sup> s <sup>-1</sup> ]	1	1e5	100	CODEP=1
DEPMUEBACK0L	[—]			0	CODEP=1
DEPMUEBACK0LP	[—]			1	CODEP=1
DEPMUEBACK1	[cm <sup>2</sup> V <sup>-1</sup> s <sup>-1</sup> ]			0	CODEP=1
DEPMUEBACK1L	[—]			0	CODEP=1
DEPMUEBACK1LP	[—]			1	CODEP=1
Aging model parameter					
DEGTIME	[s]			0.0	CODEG=1
TRAPTAUCAP	[s]			10 <sup>-6</sup>	CODEG=1
TRAPLX	[V]			1	CODEG=1
TRAPGC1	[cm <sup>-3</sup> eV <sup>-1</sup> ]			10 <sup>15</sup>	CODEG=1
TRAPGC1MAX	[cm <sup>-3</sup> eV <sup>-1</sup> ]			5×10 <sup>19</sup>	CODEG=1
TRAPGCTIME1	[s]			30	CODEG=1
TRAPGCTIME2	[s]			10 <sup>8</sup>	CODEG=1
TRAPGCLIM	[s]			10 <sup>18</sup>	CODEG=1
TRAPESLIM	[s]			5	CODEG=1
TRAPES1	[eV]			0.2	CODEG=1
TRAPES1MAX	[eV]			1	CODEG=1
TRAPESTIME1	[s]			100	CODEG=1
TRAPESTIME2	[s]			10 <sup>8</sup>	CODEG=1
TRAPGC2	[cm <sup>-3</sup> eV <sup>-1</sup> ]			5×10 <sup>13</sup>	CODEG=1
TRAPES2	[eV]			0.03	CODEG=1
TRAPTEMP1	[1/K]			0	CODEG=1
TRAPTEMP2	[1/K <sup>2</sup> ]			0	CODEG=1
TRAPN	[—]			1.0	CODEG=1
TRAPP	[—]			1.0	CODEG=1
TRAPD1MAX	[cm <sup>-3</sup> eV <sup>-1</sup> ]			30	Drift region CODEG=1
TRAPDTIME1	[s]			1000	CODEG=1
TRAPDTIME2	[s]			2×10 <sup>10</sup>	CODEG=1
TRAPDLX	[—]			1	CODEG=1
TRAPDVDDP	[—]			0	

# 31 Overview of the Parameter-Extraction Procedure

## 31.1 General MOSFET Part

In HiSIM, device characteristics are strongly dependent on basic device parameter values, such as the impurity concentration and the oxide thickness. Therefore, the parameter-value extraction has to be repeated with measured characteristics of different devices in a specific sequence until extracted parameter values reproduce all device characteristics consistently and reliably. To achieve reliable results, it is recommended to start with initial parameter values according to the recommendations listed in the table below. Since some of the model parameters such as  $T_{ox}$  are difficult to extract, they are expected to be determined directly by dedicated measurements. Threshold voltage measurements allow to derive a rough extraction for the model parameters referred to as “basic device parameters”. The parameters identified with the symbol “\*\*” in the Model Parameter Table are initially fixed to zero.

Determined by dedicated measurements (not changed during extraction procedure) are used	Default values listed in the section 30 initially for the groups of parameters listed below
<b>TOX</b>	basic device parameters (not listed on left side) gate leakage GIDL source/bulk and drain/bulk diodes noise subthreshold swing non-quasi-static model overlap capacitances

The sequence of device selection for the parameter extraction is recommended in 4 steps

1. Long-Channel Devices
2. Short-Channel Devices
3. Long-Narrow Devices
4. Short-Narrow Devices

Prior to the extraction, a rough extraction with measured  $V_{th} - L_{gate}$  characteristics is recommended to get rough idea about parameter values. These parameters are usually important giving strong influence on accuracy of the total parameter extraction. The parameter extraction of the general MOSFET part is summarized in the following Table.

## 31.2 HiSIM\_HV Specific Part

Model parameters are categorized into two parts: (1) general MOSFET related parameters and (2) the HiSIM\_HV specific parameters. The HiSIM\_HV specific model parameters are extracted after the extraction of the intrinsic MOSFET part. Recommended extraction procedure is to perform first (1) and then (2). Thus the parameter extraction is done in the following sequence:

1. rough extraction of the MOSFET parameters with measured  $V_{th} - L_{gate}$
2. fine extraction with measured subthreshold in  $I_{ds} - V_{gs}$
3. extraction of mobility parameters with  $I_{ds} - V_{gs}$  and  $I_{ds} - V_{ds}$

Table 32: Summary of the 7 steps of HiSIM's Parameter Extraction Procedure.

<b>Step 1: Initial preparation and rough extraction</b>	
1-1. Initialize all parameters to their default values	<i>TOX</i>
1-2. Use the measured gate-oxide thickness for <i>TOX</i>	<b>NSUBC, VFB, SC1, SC2</b>
1-3. Rough extraction with $V_{th}$ -dependence on $L_{gate}$ [ $V_{th} - V_{gs}$ ]	<b>SC3, NSUBP, LP, SCP1</b> <b>SCP2, SCP3</b> <b>NPEXT, LPEXT</b> <b>QME1, QME2, QME3</b> <b>PGD1, PGD2</b>
1-4. Quantum and poly-depletion effects [ $C_{gg} - V_{gs}$ ]	
<b>Step 2: Extraction with long and wide transistors</b>	
2-1. Fitting of sub-threshold characteristics [ $I_{ds} - V_{gs}$ ]	<b>NSUBC, VFB, MUECB0</b> <b>MUECB1</b>
2-2. Determination of mobility parameters for low $V_{ds}$ [ $I_{ds} - V_{gs}$ ]	<b>MUEPH0, MUEPH1</b> <b>MUESR0, MUESR1</b>
2-3. Determination of mobility parameters for high $V_{ds}$ [ $I_{ds} - V_{gs}$ ]	<b>NINV, NDEP</b>
<b>Step 3: Extraction with medium/short length and large width transistors</b>	
3-1. Pocket-parameter extraction with medium length transistors [ $I_{ds} - V_{gs}$ ]	<b>NSUBP, LP</b> <b>SCP1, SCP2, SCP3</b> <b>NPEXT, LPEXT</b> <b>SC1, SC2, SC3</b> <b>PARL2, XLD</b>
3-2. Short-channel-parameter extraction with short-length transistors [ $V_{th} - L_{gate}$ ]	<b>MUEPHL, MUEPLP</b> <b>MUESRL, MUESLP</b>
3-3. Mobility-parameter refinement for low $V_d$ [ $I_{ds} - V_{gs}$ ]	<b>VMAX, VOVER, VOVERP</b>
3-4. Velocity parameter extraction for high $V_d$ [ $I_{ds} - V_{gs}$ ]	<b>CLM1, CLM2, CLM3</b>
3-5. Parameters for channel-length modulation [ $I_{ds} - V_{ds}$ ]	
3-6. Source/drain resistances [ $I_{ds} - V_{ds}$ ]	<b>RS, RD, RSH, NRS, NRD</b>
<b>Step 4: Extraction of the width dependencies for long transistors</b>	
4-1. Fitting of sub-threshold width dependencies [ $I_{ds} - V_{gs}$ ]	<b>NSUBC, NSUBCW, NSUBCWP</b> <b>WFC, XWD, WVTH0</b>
4-2. Fitting of mobility width dependencies [ $I_{ds} - V_{gs}$ ]	<b>MUEPHW, MUEPWP</b> <b>MUESRW, MUESWP</b>
<b>Step 5: Extraction of the width dependencies for short transistors</b>	
5-1. Fitting of sub-threshold dependencies [ $I_{ds} - V_{gs}$ ]	<b>NSUBP0, NSUBWP</b>
<b>Step 6: Extraction of small-geometry effects</b>	
6-1. Effective channel-length corrections	<b>WL2, WL2P</b>
6-2. Mobility and velocity [ $I_{ds} - V_{ds}$ ]	<b>MUEPHS, MUEPSP</b> <b>VOVERS</b> <b>VOVERSP</b>
<b>Step 7: Extraction of temperature dependence with long-channel transistors</b>	
7-1. Sub-threshold dependencies [ $I_{ds} - V_{gs}$ ]	<b>BGTMPI, BGTMPI2</b> <b>EG0</b>
7-2. Mobility and maximum carrier-velocity dependencies [ $I_{ds} - V_{gs}$ ]	<b>MUETMP, VTMP</b>

4. extraction of resistance parameters with  $I_{ds} - V_{gs}$  and  $I_{ds} - V_{ds}$
5. fine extraction of resistance with channel-conductance and trans-conductance
6. capacitance extraction

Agreement of the extraction results after the 3rd step is not sufficient especially in high  $V_{gs}$  region and low  $V_{ds}$  region. The 4th resistance-extraction step is focused on the region where the quasi-saturation effect is obvious. It is recommended to repeat the extraction steps from 3rd to 5th to achieve better fitting. The steps from 1st to 3rd are the same as the conventional extraction procedure.

The extraction of the resistance parameters are done after the model selection as summarized in Fig. 29.

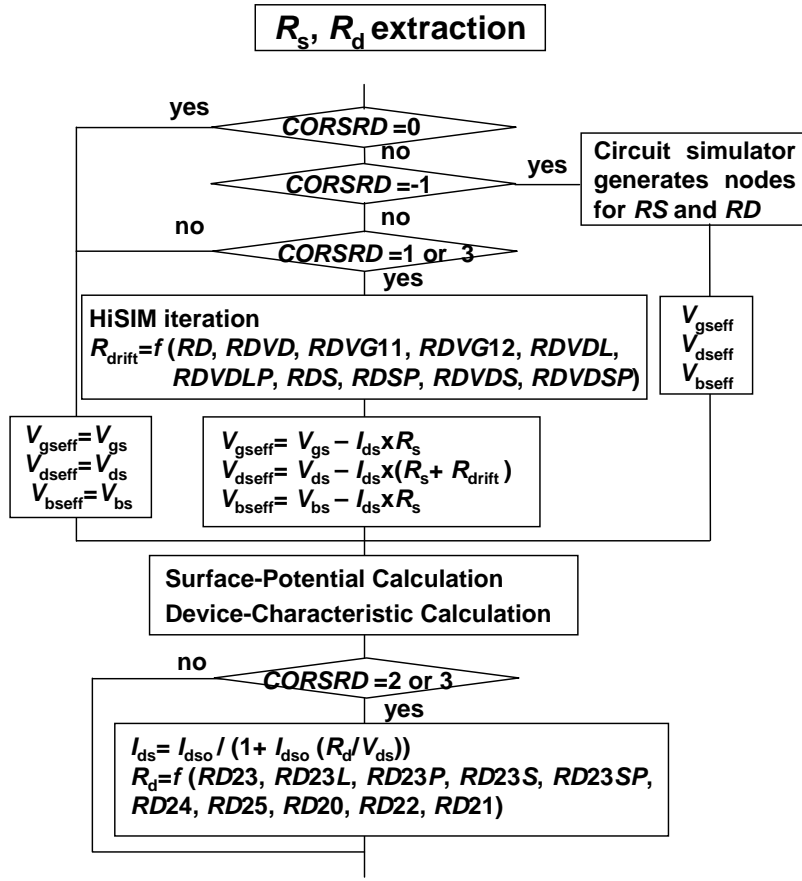


Fig. 29: Parameter extraction flow for resistance parameters. For the new resistance model (**CORDRIFT=1**) the flag **CORSRD** is no more valid but only one extraction procedure is followed, namely the "HiSIM iteration" part with the new model equations.

If the self-heating effect is activated, all device characteristics are changed drastically. Retuning of model parameters are required. These model parameters are mostly related to the mobility and resistance models. The temperature dependent parameters are extracted without the self-heating effect with temperature dependent measurements. These values are usually not necessary to be modified after activating the self-heating effect.

## References

- [1] M. Miura-Mattausch, H. J. Mattausch, and T. Ezaki, “The Physics and Modeling of MOSFETs,” *World Scientific*, 2008.
- [2] H. C. Pao and C. T. Sah, “Effects of diffusion current on characteristics of metal-oxide (insulator)-semiconductor transistors,” *Solid-State Electron.*, vol. 9, pp. 927–937, Oct. 1966.
- [3] H. J. Mattausch, M. Miyake, T. Iizuka, H. Kikuchihiara, M. Miura-Mattausch, “The Second-Generation of HiSIM\_HV Compact Models for High-Voltage MOSFETs,” *IEEE Trans. Electron Devices*, vol. 60, no. 2, pp. 653-661, Feb. 2013.
- [4] M. Yokomichi, N. Sadachika, M. Miyake, T. Kajiwara, H. J. Mattausch, and M. Miura-Mattausch, “Laterally diffused metal oxide semiconductor model for device and circuit optimization,” *Jpn. J. Appl. Phys.*, vol. 47, pp. 2560–2563, April 2008.
- [5] Y. Oritsuki, M. Yokomichi, T. Sadachika, M. Miyake, T. Kajiwara, H. Kikuchihiara, T. Yoshida, U. Feldmann, H. J. Mattausch, and M. Miura-Mattausch, “HiSIM-LDMOS/HV: A complete surface-potential-based MOSFET model for high voltage applications,” *Proc. NSTI-Nanotech*, pp. 893–896, Boston, June, 2008.
- [6] U. Feldmann, M. Miyake, T. Kajiwara, and M. Miura-Mattausch “On local handling of inner equations in compact models,” *Scientific Computing in Electrical Engineering*, Helsinki, pp. 143–150, Sept. 2008.
- [7] M. Miura-Mattausch, U. Feldmann, A. Rahm, M. Bollu, and D. Savignac, “Unified complete MOSFET model for analysis of digital and analog circuits,” *IEEE Trans. CAD/ICAS*, vol. 15, pp. 1–7, Jan. 1996.
- [8] S.-Y. Oh, D. E. Ward, and R. W. Dutton, “Transient Analysis of MOS Transistors,” *IEEE J. Solid-State Circ.*, vol. SC-15, pp. 636–643, Aug. 1980.
- [9] Y. P. Tsividis, “Operation and Modeling of the MOS Transistor,” *McGraw-Hill*, 1999.
- [10] J. R. Brews, “A charge-sheet model of the MOSFET,” *Solid-State Electron.*, vol. 21, pp. 345–355, Feb. 1978.
- [11] M. Miura-Mattausch and H. Jacobs, “Analytical model for circuit simulation with quarter micron metal oxide semiconductor field effect transistors: Subthreshold characteristics,” *Jpn. J. Appl. Phys.*, vol. 29, pp. L2279–L2282, Dec. 1990.
- [12] C. T. Sah, “Characteristics of the metal-oxide-semiconductor transistors,” *IEEE Electron Devices*, vol. ED-11, pp. 324–345, 1964.
- [13] P. M. Rousseau, S. W. Crowder, P. B. Griffin, and J. D. Plummer, “Arsenic deactivation enhanced diffusion and the reverse short-channel effect,” *IEEE Electron Device Lett.*, vol. 18, pp. 42–44, 1997.

- [14] M. Suetake, M. Miura-Mattausch, H. J. Mattausch, S. Kumashiro, N. Shigyo, S. Odanaka, and N. Nakayama, "Precise physical modeling of the reverse-short-channel effect for circuit simulation," in *Proc. SISPAD*, pp. 207–210, Sep. 1999.
- [15] M. Miura-Mattausch, M. Suetake, H. J. Mattausch, S. Kumashiro, N. Shigyo, S. Odanaka, and N. Nakayama, "Physical modeling of the reverse-short-channel effect for circuit simulation," *IEEE Electron Devices*, vol. 48, pp. 2449–2452, Oct., 2001.
- [16] S. Kumashiro, H. Sakamoto, and K. Takeuchi, "Modeling of channel boron distribution deep sub- $0.1\mu\text{m}$  n-MOSFETs," *IEICE Trans. Electro.*, vol. E82-C, June 1999.
- [17] D. Buss, "Device issues in the integration of analog/RF functions in deep submicron digital CMOS," *Tech. Digest IEDM*, pp. 423–426, 1999.
- [18] D. Kitamaru, H. Ueno, K. Morikawa, M. Tanaka, M. Miura-Mattausch, H. J. Mattausch, S. Kumashiro, T. Yamaguchi, K. Yamashita, and N. Nakayama, " $V_{\text{th}}$  model of pocket-implanted MOSFETs for circuit simulation," *Proc. SISPAD*, pp. 392–395, 2001.
- [19] H. Ueno, D. Kitamaru, K. Morikawa, M. Tanaka, M. Miura-Mattausch, H. J. Mattausch, S. Kumashiro, T. Yamaguchi, K. Yamashita, and N. Nakayama, "Impurity-Profile-Based Threshold-Voltage Model of Pocket-Implanted MOSFETs for Circuit Simulation," *IEEE Electron Devices*, vol. 49, pp. 1783–1789, Oct 2002.
- [20] M. Suetake, K. Suematsu, H. Nagakura, M. Miura-Mattausch, H. J. Mattausch, S. Kumashiro, T. Yamaguchi, S. Odanaka, and N. Nakayama, "HiSIM: A drift-diffusion-based advanced MOSFET model for circuit simulation with easy parameter extraction," *Proc. SISPAD*, pp. 261–264, 2000.
- [21] F. Stern and W. E. Howard, "Properties of semiconductor surface inversion layers in the electric quantum limit," *Phys. Rev.*, vol. 163, No. 3, pp. 816–835, 1967.
- [22] Z. Yu, R. W. Dutton, and R. A. Kiehl, "Circuit device modeling at the quantum level," *Proc. IWCE-6*, pp. 222–229, 1998.
- [23] T. Ando, A. B. Fowler, and F. Stern, "Electronic properties of two-dimensional systems," *Rev. Modern Phys.*, vol. 54, pp. 437–621, 1982.
- [24] Y. Matsumoto and Y. Uemura, "Scattering mechanism and low temperature mobility of MOS inversion layers," *Jpn. J. Appl. Phys. Suppl.*, vol. 2, Pt 2, pp. 367–370, 1974.
- [25] S. Takagi, M. Iwase, and A. Toriumi, "On the universality of inversion-layer mobility in n- and p-channel MOSFETs," *Tech. Digest IEDM*, pp. 398–401, 1988.
- [26] S. Matsumoto, K. Hisamitsu, M. Tanaka, H. Ueno, M. Miura-Mattausch, H. J. Mattausch, S. Kumashiro, T. Yamaguchi, S. Odanaka, and N. Nakayama, "Validity of the Mobility Universality for Scaled Metal-Oxide-Semiconductor Field-Effect Transistors down to 100nm Gate Length," *J. Appl. Phys.*, vol. 92, pp. 5228–5232, 2002.

- [27] D. M. Caughey and R. E. Thomas, “Carrier mobilities in Silicon empirically related to doping and field,” *Proc. IEEE*, vol. 55, pp. 2192–2193, 1967.
- [28] K. Joardar, K. K. Gullapalli, C. C. McAndrew, M. E. Burnham, and A. Wild, “An improved MOSFET model for circuit simulation,” *IEEE Trans. Electron Devices*, vol. 45, pp. 134–148, Jan. 1998.
- [29] Y. A. El-Mansy and A. R. Boothroyd, “A simple two-dimensional model of IGFET operation in the saturation region,” *IEEE Trans. Electron Devices*, vol. ED-24, pp. 241–253, 1977.
- [30] D. Navarro, T. Mizoguchi, M. Suetake, K. Hisamitsu, H. Ueno, M. Miura-Mattausch, H. J. Mattausch, S. Kumashiro, T. Yamaguchi, K. Yamashita, and N. Nakayama, “A compact model of the pinch-off region of 100nm MOSFETs based on the surface potential,” *IEICE Trans. Electron.*, vol. E88-C, No. 5, pp. 1079–1086, 2005.
- [31] G. Scott, J. Lutze, M. Rubin, F. Nouri, and M. Manley, “NMOS drive current reduction caused by transistor layout and trench isolation induced stress,” *Tech. Digest IEDM*, pp. 827–830, 1999.
- [32] M. Miura-Mattausch, “Analytical MOSFET model for quarter micron technologies,” *IEEE Trans. CAD/ICAS*, vol. 13, pp. 610–615, 1994.
- [33] F. H. Gaensslen and R. C. Jaeger, “Temperature dependent threshold behavior of depletion mode MOSFETs.” *Solid-State Electron.*, vol. 22, pp. 423–430, 1979.
- [34] *BSIM4.0.0 MOSFET Model, User’s Manual*, Department of Electrical Engineering and Computer Science, University of California, Berkeley CA, 2000.
- [35] D. Navarro, K. Hisamitsu, T. Yamaoka, M. Tanaka, H. Kawano, H. Ueno, M. Miura-Mattausch, H. J. Mattausch, S. Kumashiro, T. Yamaguchi, K. Yamashita, and N. Nakayama, “Circuit-Simulation Model of Gate-Drain- Capacitance Changes in Small-Size MOSFETs Due to High Channel-Field Gradients,” *Proc. SISPAD*, pp. 51–52, 2002.
- [36] B. J. Sheu and P.-K. Ko, “Measurement and modeling of short-channel MOS transistor gate capacitances,” *IEEE J. Solid-State Circuits*, vol. SC-22, pp. 464–472, 1987.
- [37] R. Shrivastava and K. Fitzpatrick, “A simple model for the overlap capacitance of a VLSI MOS device,” *Proc. IEEE*, vol. ED-29, pp. 1870–1875, 1982.
- [38] N. Arora, “MOSFET models for VLSI circuit simulation: theory and practice,” *Springer-Verlag*, 1993.
- [39] E. O. Kane, “Zener Tunneling in Semiconductors,” *J. Phys. Chem. Solids*, vol. 12, pp. 181–188, 1959.
- [40] Q. Ngo, D. Navarro, T. Mizoguchi, S. Hosokawa, H. Ueno, M. Miura-Mattausch, and C. Y. Yang, “Gate Current Partitioning in MOSFET Models for Circuit Simulation,” *Proc. Modeling and Simulation of Microsystems*, vol. 1.2, pp. 322–325, 2003.

- [41] R. Inagaki, K. Konno, N. Sadachika, D. Navarro, K. Machida, Q. Ngo, C. Y. Yang, T. Ezaki, H. J. Mattausch, M. Miura-Mattausch, and Y. Inoue, “A Gate–Current Model for Advanced MOSFET Technologies Implemented into HiSIM2,” *Proc. Int. 3rd Workshop on Compact Modeling*, Yokohama, Jan. 2006.
- [42] T. Yoshida, M. Miura-Mattausch, H. Ueno, H. J. Mattausch, S. Kumashiro, T. Yamaguchi, K. Yamashita, and N. Nakayama, “Conservation of symmetry at  $V_{ds} = 0$  for reliable analog simulations,” submitted for publication.
- [43] *BSIM3, version3.0 manual*, Department of Electrical Engineering and Computer Science, University of California, Berkeley CA, 1996.
- [44] S. Matsumoto, H. Ueno, S. Hosokawa, T. Kitamura, M. Miura-Mattausch, H. J. Mattausch, T. Ohguro, S. Kumashiro, T. Yamaguchi, K. Yamashita, and N. Nakayama, “ $1/f$  noise characteristics in 100nm-MOSFETs and its modeling for circuit simulation,” *IEICE Trans. Electron.*, vol. E88-C, pp. 247–254, 2005.
- [45] A. van der Ziel, “Noise in solid state devices and circuits,” New York, John Wiley
- [46] S. Hosokawa, Y. Shiraga, H. Ueno, M. Miura-Mattausch, H. J. Mattausch, T. Ohguro, S. Kumashiro, M. Taguchi, H. Masuda, and S. Miyamoto, “Origin of enhanced thermal noise for 100nm-MOSFETs,” Ext. Abs. SSDM, pp. 20–22, 2003.
- [47] S. Hosokawa, D. Navarro, M. Miura-Mattausch, H. J. Mattausch, T. Ohguro, T. Iizuka, M. Taguchi, S. Kumashiro, and S. Miyamoto, “Gate-length and drain-voltage dependence of thermal drain noise in advanced metal-oxide-semiconductor field-effect transistors,” *Appl. Phys. Lett.* 87, 092104, 2005.
- [48] M. Miura-Mattausch, H. Ueno, H. J. Mattausch, K. Morikawa, S. Itoh, A. Kobayashi, and H. Masuda, “100nm-MOSFET model for circuit simulation: Challenges and solutions,” *IEICE Trans. Electron.*, vol. E86-C, pp. 1009–1021, 2003.
- [49] T. Warabino, M. Miyake, N. Sadachika, D. Navarro, Y. Takeda, G. Suzuki, T. Ezaki, M. Miura-Mattausch, H. J. Mattausch, T. Ohguro, T. Iizuka, M. Taguchi, S. Kumashiro, and S. Miyamoto, “Analysis and compact modeling of MOSFET high-frequency noise,” *Proc. SISPAD*, pp. 158–161, 2006.
- [50] N. Nakayama, D. Navarro, M. Tanaka, H. Ueno, M. Miura-Mattausch, H. J. Mattausch, T. Ohguro, S. Kumashiro, M. Taguchi, and S. Miyamoto, “Non-quasi-static model for MOSFET based on carrier-transit delay,” *Electronics Letters*, vol. 40, pp. 276–278, 2004.
- [51] D. Navarro, N. Nakayama, K. Machida, Y. Takeda, H. Ueno, H. J. Mattausch, M. Miura-Mattausch, T. Ohguro, T. Iizuka, M. Taguchi, T. Kage, and S. Miyamoto, “Modeling of carrier transport dynamics at GHz-frequencies for RF circuit simulation,” *Proc. SISPAD*, pp. 259–262, 2004.
- [52] D. Navarro, Y. Takeda, M. Miyake, N. Nakayama, K. Machida, T. Ezaki, H. J. Mattausch, M. Miura-Mattausch, “A carrier-transit-delay-based non-quasi-static MOSFET model for circuit simulation and

- its application to harmonic distortion analysis," IEEE T. Electron Devices, vol. 53, pp. 2025–2034, 2006.
- [53] K. Machida, D. Navarro, M. Miyake, R. Inagaki, N. Sadachika, G. Suzuki, Y. Takeda, T. Ezaki, H. J. Mattausch, M. Miura-Mattausch, "Efficient NQS MOSFET Model for both Time-Domain and Frequency-Domain Analysis," Proc. SiRF, pp. 73-76, 2006.
- [54] D. Navarro, Y. Takeda, M. Miura-Mattausch, H. J. Mattausch, T. Ohguro, T. Iizuka, M. Taguchi, T. Kage, and S. Miyamoto, "On the validity of conventional MOSFET nonlinearity characterization at RF switching," IEEE Microwave and Wireless Components Lett., pp. 125-127, 2006.
- [55] T. Kajiwara, M. Miyake, N. Sadachika, H. Kikuchihara, U. Feldmann, H. J. Mattausch, and M. Miura-Mattausch, "Spatial distribution analysis of self-heating effect in high-voltage MOSFETs," to be appeared in Proc. APEC, Feb. 2009.
- [56] A. Tanaka, Y. Oritsuki, H. Kikuchihara, M. Miyake, H. J. Mattausch, M. Miura-Mattausch, Y. Liu and K. Green, "Quasi-2-dimensional compact resistor model for the drift region in high-voltage LDMOS devices," IEEE Trans. Electron Devices, vol. 58, no. 7, pp. 2072-2080, Jul. 2011.
- [57] T. Iizuka, T. Sakuda, Y. Oritsuki, A. Tanaka, M. Miyake, H. Kikuchihara, U. Feldmann, H. J. Mattausch, M. Miura-Mattausch, "Compact Modeling of Expansion Effects in LDMOS," IEICE Trans. Electron., Vol. E95-C, No. 11, pp. 1817-1823, Nov. 2012.
- [58] H. Tanoue, A. Tanaka, Y. Oodate, T. Nakahagi, C. Ma, M. Miyake, H. J. Mattausch, and M. Miura-Mattausch, "Universal Properties and Compact Modeling of Dynamic Hot-Electron Degradation in n-MOSFETs," IEEE Int. Reliability Phys. Symp., pp. CM 4.1, April 2013.
- [59] T. Leroux, "Static and Dynamic Analysis of Amorphous-Silicon Field-Effect Transistors," Solid-State Electron., vol. 29, no. 1, pp. 47-58, Jan. 1986.
- [60] S. Miyano, Y. Shimizu, T. Murakami, M. Miura-Mattausch and HiSIM Research Center, "A surface potential based Poly-Si TFT model for circuit simulation," Proc. SISPAD, pp. 373-376, September, 2008.
- [61] C. Ma, H. J. Mattausch, K. Matsuzawa, S. Yamaguchi, T. Hoshida, M. Imade, R. Koh, T. Arakawa, and M. Miura-Mattausch, "Universal NBTI Compact Model for Circuit Aging Simulation under Any Stress Conditions," IEEE Trans. Semiconductor Manufacturing, vol. 14, no. 3, pp. 818-825, 2014.
- [62] P. O. Lauritzen and C. L. Ma, "A simple diode model with reverse recovery," IEEE Trans. Power Electron., vol. 6, no. 2, pp. 188-191, Apr. 1991.
- [63] C. L. Ma, P. O. Lauritzen and J. Sigg, "Modeling of Power Diodes with the Lumped-Charge Modeling Technique," IEEE Trans. Power Electron., vol. 12, no. 3, pp. 398-405, May 1997.
- [64] J. Nakashima, M. Miyake and M. Miura-Mattausch, "Dynamic-Carrier-Distribution-Based Compact Modeling of P-i-N Diode Reverse Recovery Effects," Jpn. J. Appl. Phys., Vol. 51, No. 2, ID: 02BP06, Feb. 2012.

- [65] M. Miyake, J. Nakashima, and M. Miura-Mattausch, “Compact Modeling of the p-i-n Diode Reverse Recovery Effect Valid for both Low and High Current-Density Conditions,” IEICE Trans. Electron., Vol. E95-C, No. 10, pp. 1682-1688, Oct. 2012.